VARIABILITY OF RESIDUAL PROPERTIES IN THE COLUMBIA RIVER ESTUARY: PILOT APPLICATION OF EMERGING TECHNOLOGIES

Wendy Nicole Sommerfield
B.Sc., Pennsylvania State University, 1994

A thesis submitted to the faculty of the
Oregon Graduate Institute of Science & Technology
in partial fulfillment of the
requirements for the degree of
Master of Science
in
Environmental Science and Engineering

January 1999

The thesis "Variability of residual properties in the Columbia River estuary: pilot application on emerging technologies" by Wendy Nicole Sommerfield has been examined and approved by the following Examination Committee:

António M. Baptista, Ph.D., Thesis Advisor
Professor

David A. Jay, Ph.D.
Associate Professor

Robert L. Doneker, Ph.D.
Assistant Professor

William Fish, Ph.D.
Associate Professor, Portland State University
Adjunct Associate Professor, Oregon Graduate Institute of Science & Technology

For my parents, Bob and Sandi, my brother, Roger, and Nicholas Pearson

Acknowledgements

Initially I came to OGI with a very limited background, intent on completing the one-year master's program. Two and ¼ years later while pursuing a master's thesis, my knowledge and experiences have been broadened. Much of this is credited to my advisor, António Baptista, for exposing me to the world of numerical modeling (a world I barely knew existed) and to estuarine processes, pushing me to strive beyond my limits and broadening my scientific background in a wide range of areas. I thank António Baptista for teaching me to be a better scientist and for believing in my capabilities when I did not.

I wish to express my gratitude to the other members of my thesis committee: David Jay, Robert Doneker and William Fish for their insightful comments and suggestions to improve my thesis.

Being the "new kid" in CCALMR, I was a novice with computers. Thanks to Cole McCandlish and Paul Turner for their countless hours of computer support, and especially Ed Myers for being so patient and helpful in answering my numerous questions on just about everything. I also wish to thank Anabela Oliveira, Salil Das, Phil Pearson, Ed Myers, and Zhaoqing Yang, whose scientific contributions to my thesis helped make it possible.

I wish to thank Michelle Scherer, Jeff Darland, Ed Myers, Cole McCandlish, Phil Pearson, Anna Farrenkopf, Brian Mader, Ameer Tavakoli, Daloris Fleming, Linda Wolf and Phil Barrett for being supportive and making me laugh. Thanks to the lunch crew (you know who you are) for taking my mind off of work.

Thanks to my parents for always supporting me in my endeavors, and my brother, for being my number one fan. I survived it all due to the unconditional love and affection of Nicholas Pearson.

This material was sponsored in part by the Department of the Navy, Office of Naval Research, under Grant No. N00014-96-1-0893, the National Science Foundation, under Grant No. OCE-9412028 and the National Marine Fisheries Service of the National Oceanic and Atmospheric Administration, under Grant No. NA87FE0405. Any opinions, findings, and conclusions or recommendations expressed in this material are those of the author and do not necessarily reflect the views of the Government, the National Science Foundation and the National Marine Fisheries Service.

Table of Contents

List of Figures

List of Tables

ABSTRACT

Variability of residual properties in the Columbia River estuary: pilot application of emerging technologies

Wendy Nicole Sommerfield
Oregon Graduate Institute of Science & Technology, 1998
Supervising Professor: António M. Baptista

Nowcast-forecast systems are an emerging technology with broad potential implications on research and management of coasts and estuaries. In this thesis we begin to explore the role of nowcast-forecast systems as a scientific tool. Specifically, we use CORIE, a pilot nowcast-forecast system for the Columbia River estuary, to investigate residual properties in the estuary.

While nowcast-forecast systems are most recognized by their real-time capabilities, we focus primarily on the use of CORIE's data archival and hindcast modeling capabilities. In particular we combine the analysis of archived Acoustic Doppler Profiler (ADP) data with archived numerical simulations to characterize Eulerian residual velocities. We also use hindcast numerical simulations to characterize residence times. In this latter context, CORIE's real-time capabilities (in particular, model forecasts and real-time telemetry network) are used to support a limited drifter survey designed to evaluate model performance.

Our analysis provides useful insights on spatial and temporal variability of both residual velocities and residence times. Residual properties are river-dominated at seasonal scales, but the interaction of tides and river discharge is critical to variability at shorter scales. Residence times in the main stem of the estuary are typically of the order of a few hours to one day, which emphasizes the ecological importance of understanding variability or residual circulation at tidal and shorter scales. The two main channels in the estuary have distinctive behavior, in particular with regard to residual circulation. The Navigation channel, long and effectively designed as the main conveyor belt for freshwater, exhibits consistent ocean-ward residual velocities over most of the water column, most of the year. Land-ward residual velocities are observed primarily at the lower to mid-water layers of the deeper, shorter North channel.

Throughout this work, we found the iterative coupling between modeling and data analysis enabled by CORIE to be extremely powerful, particularly in its ability to foster scientific inquiry and merge it with practical applications. For instance, this coupling was instrumental in building confidence in our residence time analysis and, quite by serendipity, also assisted the interpretation of an U.S. Coast Guard mission. However, our modeling analysis was primarily based on two-dimensional numerical circulation and particle-tracking codes. In an estuary with complex vertical stratification, this is necessarily a significant limitation. Even if main traits shown by models were often confirmed by data, many important details of the residual dynamics of the estuary are simply not detectable with the operation CORIE models. The on-going development of operational 3D baroclinic-modeling capabilities will dramatically increase CORIE's impact as a scientific tool.

Introduction

Nowcast-forecast systems are an emerging technology with broad potential implications on research and management of coasts and estuaries. In this thesis we begin to explore the role of nowcast-forecast systems as scientific tools. Specifically, we use CORIE, a pilot nowcast-forecast system for the Columbia River estuary, to investigate residual properties in the estuary.

CORIE (Baptista et al., 1998) integrates real-time monitoring of physical properties at multiple stations with a suit of numerical models, towards the characterization of present, past and future conditions of water levels, circulation, and water properties in the Columbia River estuary and vicinity. Similar systems are being developed elsewhere (e.g., Cheng and Wilson, 1997; Vincent et al., 1997) and we anticipate that over the next decade most of the coastal continental US and its largest estuaries will be served by a nowcast-forecast network.

While nowcast-forecast systems are most recognized by their real-time capabilities, we view that as a way to seamlessly describe past, present and future conditions. Here, we focus primarily on the use of CORIE's data archival and hindcast modeling capabilities, using real-time capabilities and specialized field surveys (e.g., a drifter release) only on an as-needed basis. Specifically, we combine the analysis of archived Acoustic Doppler Profiler (ADP) data with archived numerical simulations to characterize Eulerian residual velocities. We also use hindcast numerical simulations to characterize residence times. In this latter context, CORIE's real-time capabilities (in particular, model forecasts and real-time telemetry) are used to support a limited drifter survey designed to evaluate model performance.

Our analysis of residual velocities and residence times focuses on spatial and temporal variability. Variability of instantaneous properties is an important, well recognized trait of the Columbia River dynamics. Temporal variability is driven largely

by forcings, primarily river discharges and tides. Spatial variability is constrained primarily by system topology, which features two deep channels of contrasting length and depth carved in an otherwise shallow environment. Variability of residual properties is less understood, particularly at shorter-than-seasonal scales. Given predominantly small residence times, we expect that tidal and shorter scales of variability of residual properties will be very significant to understand the ecosystem. The need to better understand residual variability at these scales was an important motivation for this work, as was the need to further understand the contrasting residual properties of the two main channels of the Columbia River estuary.

Residual properties are utilized because they integrate instantaneous velocities to quantify net transport and circulation, processes that are difficult to measure in the field but are important for understanding water quality aspects and the hydrodynamics in the estuary. While mixing and transformation also contribute to the net transport of most environmental tracers, our focus here is on advection. Therefore, our use of the term residence times should be understood throughout this work as referring primarily to "water residence times".

CORIE is a work in progress, and limitations remain in several components of the system. Many of these limitations are related to modeling, in particular the fact that operational circulation modeling (in hindcast and nowcast-forecast modes) is based on two-dimensional barotropic codes. Some are related to data, in particular with evolving quality assurance and quality control procedures. We approached this thesis mostly with the perspective of using established tools and capabilities, identifying associated limitations but recognizing that their solution is often beyond our limited work scope. There were three important exceptions:

- our retrospective analysis of the quality of the Acoustic Dopler Profile (ADP) data has directly impacted the development of supporting QA/QC tools;

- a drifter experiment in support of our residence time analysis forced the addition of drifters to the set of CORIE capabilities;
- the integration of particle-tracking models with CORIE circulation forecasts brought us closer to tools of practical applicability for search and rescue operations and for oil spill response.

Throughout this work, we found the iterative coupling between modeling and data analysis enabled by CORIE to be extremely powerful, particularly in its ability to foster scientific inquiry and merge it with practical applications. For instance, this coupling was instrumental in building confidence in our residence time analysis and, as a by-product, provided serendipity assistance to the interpretation of an actual search-and-rescue mission conducted by the U.S. Coast Guard (results not shown).

However, the modeling side of our analysis was primarily based on two-dimensional numerical circulation and particle-tracking codes. In an estuary with complex vertical stratification, this is necessarily a significant limitation. Even if main traits shown by models were often confirmed by data, many complex important details of the residual dynamics of the estuary are simply not detectable with the operational CORIE models. This work emphasizes, by default, the importance of the on-going development of operational 3D baroclinic-modeling CORIE capabilities.

This thesis is divided into seven sections including this Introduction (Section 1). Section 2 describes the Columbia River estuary and the critical factors affecting physical variability in the estuary. Sections 3 through 6 are the heart of this work. The techniques applied to the field data and model results for calculating residual properties are presented and analysis of the variability of these properties in the estuary is discussed. Section 7 presents a synthesis of our analysis and future considerations.

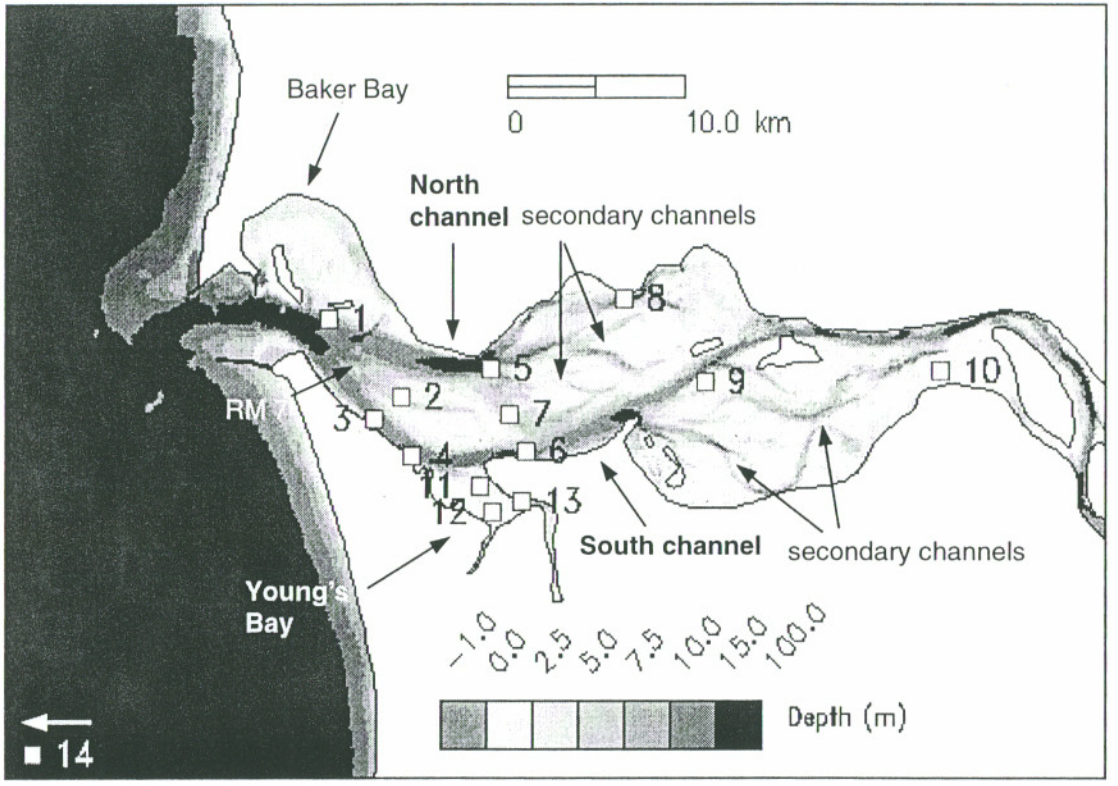

#	Station
1	Sand Island
2	Desdemona
3	Red26
4	Tansy Pt
5	Am012
6	Am169
7	Am084
8	Grays Pt
9	Rice Island
10	Woody
11	Yb101
12	Lwsck
13	Yacht
14	Ogi01

Figure 1.1. Location of CORIE stations in lower Columbia River estuary. (Pearson, 1998 personal communication)

The Columbia River Estuary

2.1 Location and Physical Characteristics[1]

The Columbia River estuary is characterized as a "river estuary", with highly variable freshwater input, ebb-dominated tidal currents and seasonal vertical stratification. It is located in the northwest region of the United States on the Pacific Coast where it feeds into the Pacific Ocean at 46°15'N and 124°5'W (Figure 2.1). The Columbia River is the largest river draining into the Pacific Ocean with an annual average flow of 7300 m^3/s. Its drainage basin covers an area of 660,000 km^2 that contains portions of seven U.S. states and British Columbia, and drains 77% of the total freshwater input between San Francisco and the Strait of Juan de Fuca. The Cascadia Range divides the drainage basin into two main sub-basins: coastal and eastern basins. The two basins have different climatic and hydrologic characteristics which affects their contribution to the freshwater input to the estuary. The coastal basin comprises only 8% of the total drainage area, yet it contributes 25% of the freshwater to the estuary. Its freshwater input is higher in winter since discharge from the tributaries (Willamette, Cowlitz and Lewis rivers) is 10 times greater from December through March. The eastern basin occupies 92% of the drainage area and contributes significantly more freshwater in spring as compared to winter. Precipitation, snowmelt and flow regulation controls the river flow (73%) from the eastern sub-basin into the estuary in the spring.

The complex bathymetry of the Columbia River estuary strongly affects water circulation patterns. Prominent bathymetric features include two main channels, several narrow channels, intertidal flats, and shallow, lateral bays in the lower region (Figure 1.1) and one main channel with many shallow areas in the upper reaches of the estuary. Upstream of river mile (RM) 7, the single channel connecting the estuary to the ocean divides into the North and South channels. The main navigation South channel is artificially maintained for navigational purposes, therefore it acts as a conveyor belt for

[1] References used in this description are Orem, 1968, CREDDP (1984) and Sherwood et al. (1990)

most of the flow from the river to the ocean. The hydrologic characteristics of the two channels differ as a result of the channelization in the river and estuary. As a result, we would expect *a priori* that the residual properties in the two channels should differ. Our analysis of residual velocities supports this premise of North-South channel contrasts (discussed in Section 6.2.1).

Transport and circulation in estuaries are governed by interactions between river discharge, tides and wind. In the Columbia River estuary, river discharge and tides are generally dominant. Dimensional analysis has shown that wind stress in narrow estuaries is only significant when the river flow and tidal forcing are weak, therefore, wind does not strongly affect the physical processes in the Columbia River estuary (Jay and Smith, 1990; see also Section 2.4). The variability of the physical processes is induced by changes occurring in the freshwater and ocean inputs, and both contributing factors vary at distinct scales in space and time. The spatial scales of physical variability in the estuary are very localized and the time scales of this variability are primarily seasonal, monthly and daily.

2.2 River Discharge

River flow variation at interannual and seasonal time scales has been documented through data collection at the Bonneville Dam, the most downstream of the main stem dams, over the past 100 years. El Niño/La Niña years (usually representative of anomalously dry and wet years, respectively) and periods of drought in the late 1980's are reflected in the hydrologic cycle[2] over the past 30 years (Figure 2.2). Seasonal variability in river flow at Bonneville Dam is attributed to the freshwater input from the eastern sub-basin. The annual cycle is divided into the high flow season of April - June and the low flow season of July - March. The highest river discharge in the spring, known as the "spring freshet", occurs during snowmelt runoff. The lowest flows occur between

[2] Data collected by the USACE, NWD is accessible through Data in Real Time (DART), a database maintained by the School of Fisheries, University of Washington

August - November when there is minimal runoff and precipitation in the form of rainfall.

In the estuary, seasonal variations are attributed to both sub-basins. The annual cycle peaks in winter from precipitation and runoff in the coastal sub-basin and peaks higher in the spring from the freshet in the eastern sub-basin. The monthly variations in the estuary are strongest in the winter and are mostly attributed to the occurrence of heavy storm events in the coastal sub-basin. Dams in the eastern sub-basin dampen its monthly variability. Sudden changes in weather patterns, like a spring storm, would not always be conveyed to the estuary.

Between 1929 and 1975, over 20 dams on the main stem of the Columbia and Snake Rivers (Figure 2.1) and over 100 dams on their tributaries have been constructed. Data collected at Bonneville Dam has been used to study how river discharge to the estuary has been affected over the last century. Sherwood et al. (1990) evaluated the effects of flood regulation on the estuary and determined the greatest changes in freshwater input occurred in the past thirty years. Specifically, seasonal variability in river discharge was greatest pre-1969 during the period prior to significant flow regulation (Figure 2.2). According to the Bonneville Dam data, the flow in spring averaged $315x10^3$ cfs and the flow in fall averaged $117x10^3$ cfs during 1960-1969, whereas the flow averaged $268x10^3$ cfs and $141x10^3$ cfs for the spring and fall, respectively, between 1990 and 1997. Also, spring peaks reached maximums of $650x10^3$ cfs pre-1969, while spring peaks in post-regulation years (post-1969) never exceeded $450x10^3$ cfs, with the exception of 1997 ($550x10^3$ cfs maximum). Although the extremes, especially the spring freshets, have been controlled in the post-regulation years, seasonal variability is pronounced, in which differences range between 100 - $500x10^3$ cfs in more recent years (the largest differences for 1997 as shown in Figure 2.3). The increasing spring freshets in recent years (Figure 2.2) suggest the trend of decreased seasonal variability may be ending. The spring freshets and associated seasonal variability should

be monitored closely in the near future to identify whether there are changing climate patterns affecting the Pacific Northwest.

Correlation analyses between atmospheric and oceanic data indicate large-scale climate patterns exist in the Pacific Northwest. This long-term climate variation consequently influences precipitation patterns, streamflow, and fish production (Mantua, 1996; Mantua et al., 1997). The term Pacific Decadal Oscillation (PDO) identifies long term sea surface temperature (SST) anomalies associated with the large-scale climate patterns (Mantua et al., 1997). Using SST anomalies as an indicator of the PDO, studies show a positive PDO between 1929-1946 and 1977-present, and a negative PDO between 1947-1976 (Mantua et al., 1997). The positive PDO signature in the Pacific Northwest is identifiable by warm winter temperatures, low precipitation and reduced snowpack. These effects, while similar to the effects of El Niño events, occur at decadal time scales. The negative PDO signature is representative of cool, wet winters, which leads to increased river discharge in much the same way as a La Niña event impacts the Pacific Northwest. The increasing spring freshets in recent years observed in the Bonneville Dam data suggest a change in positive signature. Determinations about the trend of the large-scale climate patterns can only be made by monitoring the precipitation and streamflow patterns in the coming years.

2.3 Tidal Forcings

Tides are a dominant forcing in the Columbia River estuary. Columbia River tides are predominantly semi-diurnal (Figure 2.4) and their vertical influence can extend 150 km upstream from the mouth (CREDDP, 1984). Upstream tidal propagation is complex, with strong dependence on river discharge and significant non-linearities induced by advection, finite amplitude, and friction effects (Figure 2.5). Typical of river tides, harmonic constituents exhibit strong temporal variability in both the astronomic and shallow water frequencies, largely associated with the variability of the upstream discharge. This variability is partially illustrated in Figure 2.6 by contrasting harmonic

"constants" for a low and high river discharge month. Giese and Jay (1989), using a one-dimensional harmonic model, provided a much more thorough discussion of the spatial and temporal (monthly and seasonal) variability of the tidal energetics of the Columbia River. Tidal variability at daily and subtidal scales is also important in the estuary, but is not detectable by harmonic methods. Jay and Flinchem (1997) discuss these scales of variability, based on continuous wavelet transform (CWT) methods.

2.4 Wind Stress

Wind stress affects physical processes differently outside and inside the estuary. Regional winds play a key role in driving surface currents in the coastal ocean, thereby controlling the Columbia River plume. Seasonal variability in large-scale wind patterns influences the direction of the plume, and this subsequently affects regional-scale circulation in the Pacific Ocean between Alaska and California. Wind gradients push the Columbia River plume to the north along the coast in winter, and south offshore in summer (Barnes et al., 1972). The lower density water of the plume flowing at the surface has been shown to affect baroclinic circulation in the ocean (Hickey, 1998). Seasonal variability of the large-scale atmospheric forcings also has some influence on baroclinic circulation inside the estuary. The effects are evident in the summer when strong wind stresses induce upwelling off the coast, bringing colder, saltier water from the deep ocean into the estuary.

We evaluated the importance of wind stress inside the Columbia River estuary since our analysis focuses on physical processes occurring inside the estuary. As mentioned earlier, wind has a significant effect in narrow estuaries only when the tides and river discharge are weak. We computed the surface stress and local advection terms in the x- and y-momentum equations using field data from CORIE. Calculations were performed for July of 1997, a month with low river discharge. The surface stress term caused by the wind forcing was computed using (Garratt, 1977):

$$\frac{\tau_{sx}}{\rho_o} = C_D \frac{\rho_a}{\rho_o} |W| W_x \tag{2.1}$$

$$\frac{\tau_{sy}}{\rho_o} = C_D \frac{\rho_a}{\rho_o} |W| W_y \tag{2.2}$$

where $C_D = (0.75+0.067|W|) \times 10^{-3}$, ρ_a/ρ_o is the ratio of the density of air to the density of water, W_x and W_y are wind speeds recorded from the micro-wind instrument located at station Tansy and |W| is the magnitude of the wind speed. Assuming that wind stress is distributed evenly in the vertical water column, the surface stress terms were divided by the total depth (Pugh, 1987). The total depth was computed from pressure data recorded at the same station as the wind instrument using a conversion equation that accounts for temperature and salinity (Fofonoff and Millard, Jr., 1983). Local acceleration terms, $\partial u/\partial t$ and $\partial v/\partial t$, were computed at the surface and bottom of the water column using velocity data recorded by the ADP at the same station. The results indicate the maximum wind stress is an order of magnitude less than the local acceleration in the water column in both directions and most values are two orders of magnitude smaller (Figures 2.7 - 2.8). In addition, variability in the wind stress over the month is an order of magnitude smaller than the variability of the local acceleration. We conclude that wind stress is often not a major aspect of variability. Localized effects of wind stress that would be significant primarily occur during very large storms. The infrequent occurrence of such events as compared to the dominance of river discharge and tidal forcings further suggests wind stress may be eliminated from our analysis.

Figure 2.1. Drainage basin of the Columbia River estuary. Over 100 dams are located on the main stem of the Columbia and Snake Rivers and their tributaries. The location and operator of several dams in the Columbia River basin are identified. Source: USACE.

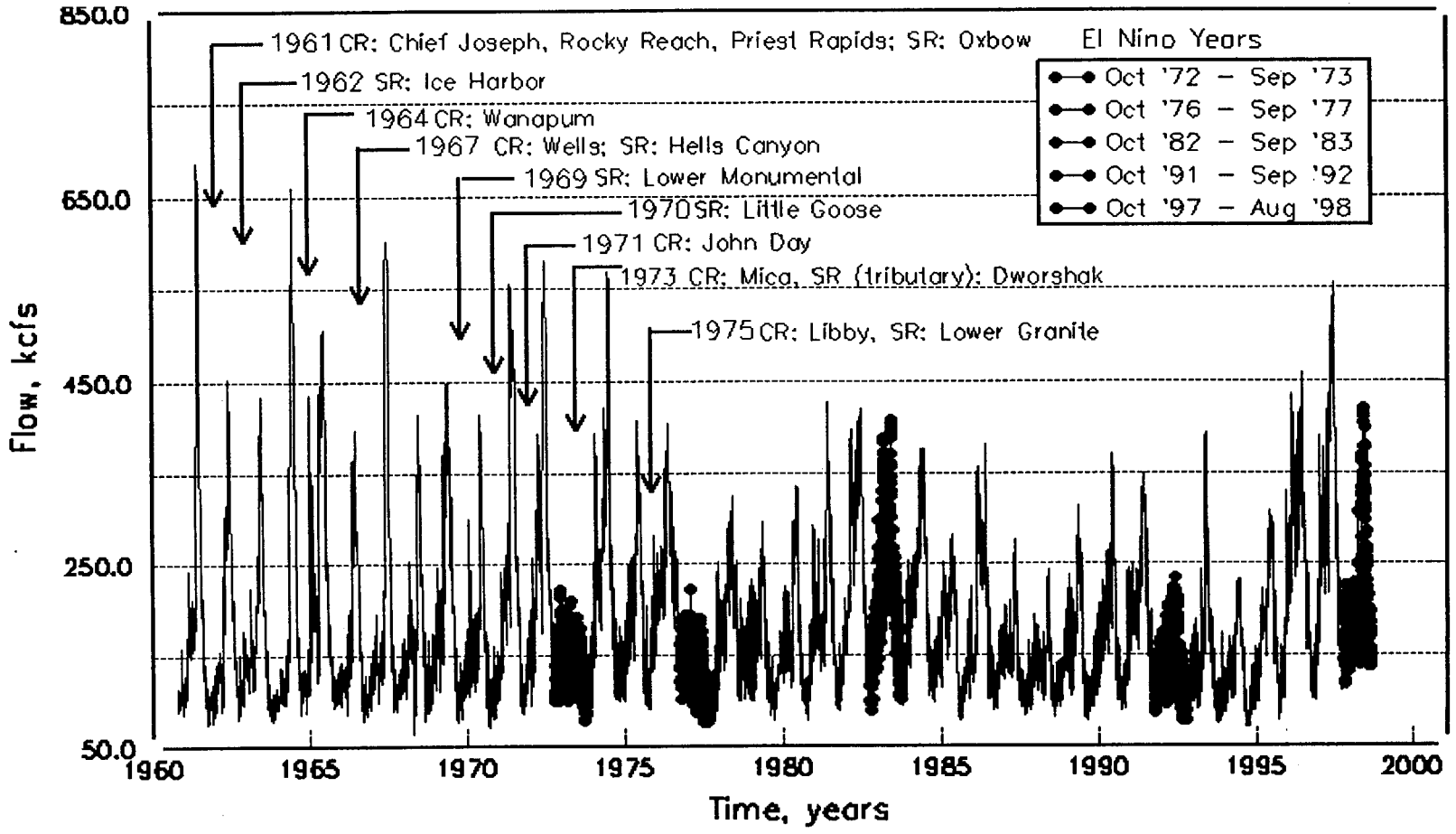

Figure 2.2. 1960-1998 river flow data for the Columbia River recorded at Bonneville Dam. Outflow data is measured by the NWD of the Army Corps of Engineers and is available in 24-hour averaged values. Arrows identify years when major dams were constructed on the Columbia River (CR), Snake River(SR) and their tributaries. The large peaks coincide with spring "freshets" caused by snowmelt. There is a general trend of decreased peaks in the spring as a result of the control structures (Sherwood et al., 1990), except for exceptionally wet years, such as 1997. The circles signify recorded El Niño years. Typically "freshets" are significantly decreased due to less snowpack from the prior winter. The 1982-83 and 1997-98 are considered two of the strongest El Niño's to date, but do not conform to the typical pattern.

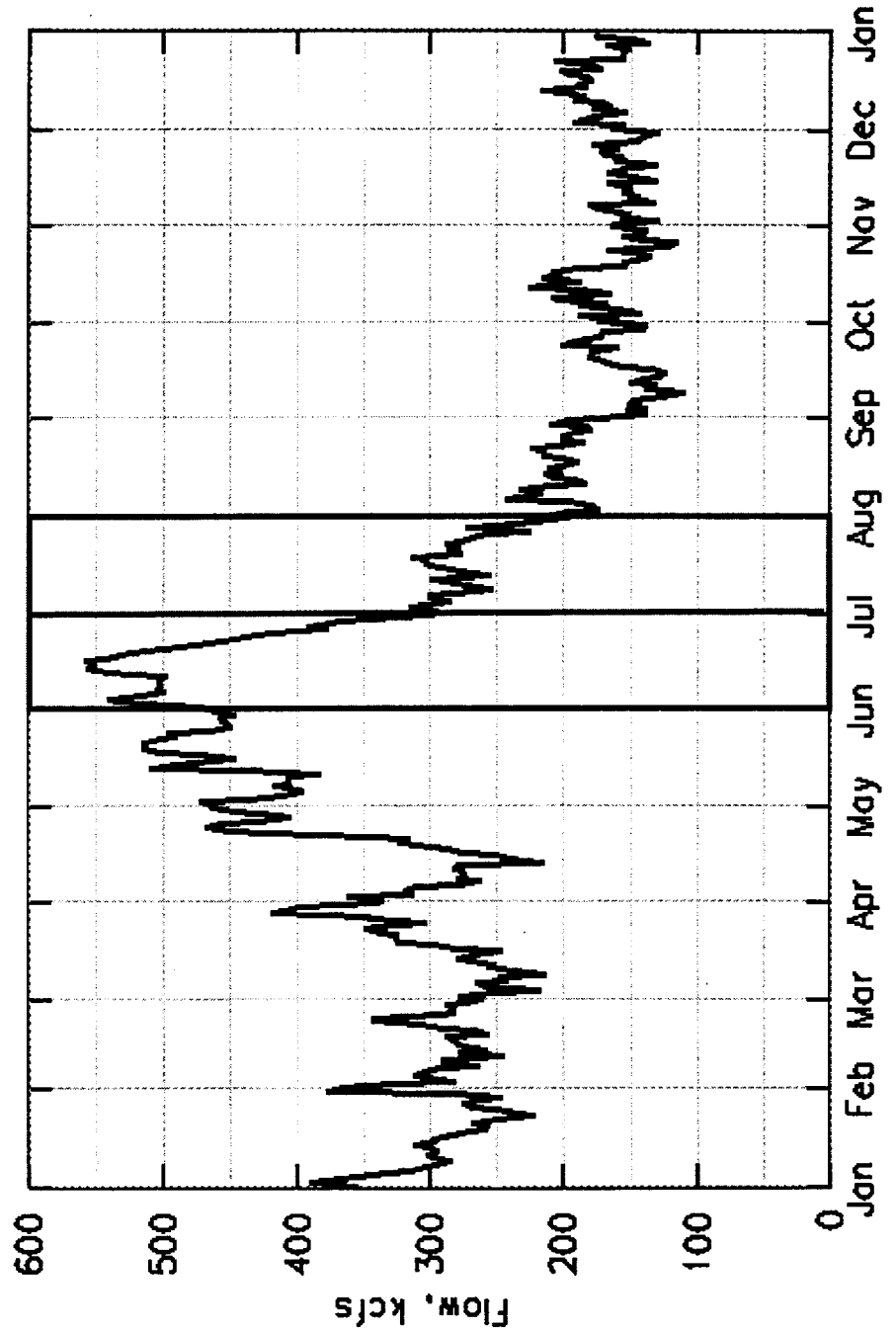

Figure 2.3. 1997 river flow data for the Columbia River (expanded from Figure 2.2). June and July are months with contrasting flow conditions used in our analysis of residual properties.

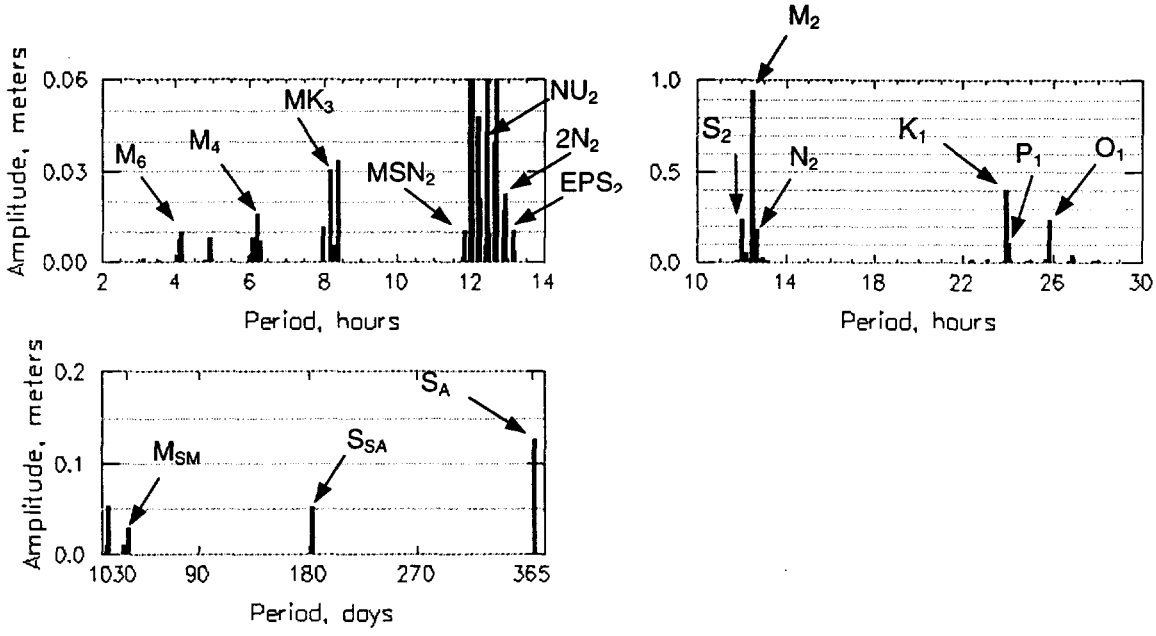

Figure 2.4. Harmonic analysis (Godin, 1972; Foreman, 1977) of observations collected by NOAA at Tongue Pt (RM 18) for a 2-year period (1/96 - 12/97). The S_{SA} and S_A are the dominant long-period constituents that contribute to the slow variation of tidal heights in the estuary. Of the high frequency tidal components, the semi-diurnal (M_2, S_2, N_2) and diurnal (e.g. K_1, O_1) constituents dominate while the non-linear components (M_6, M_4, MK_3, NU_2) have considerably smaller amplitudes in this region of strong tidal influence.

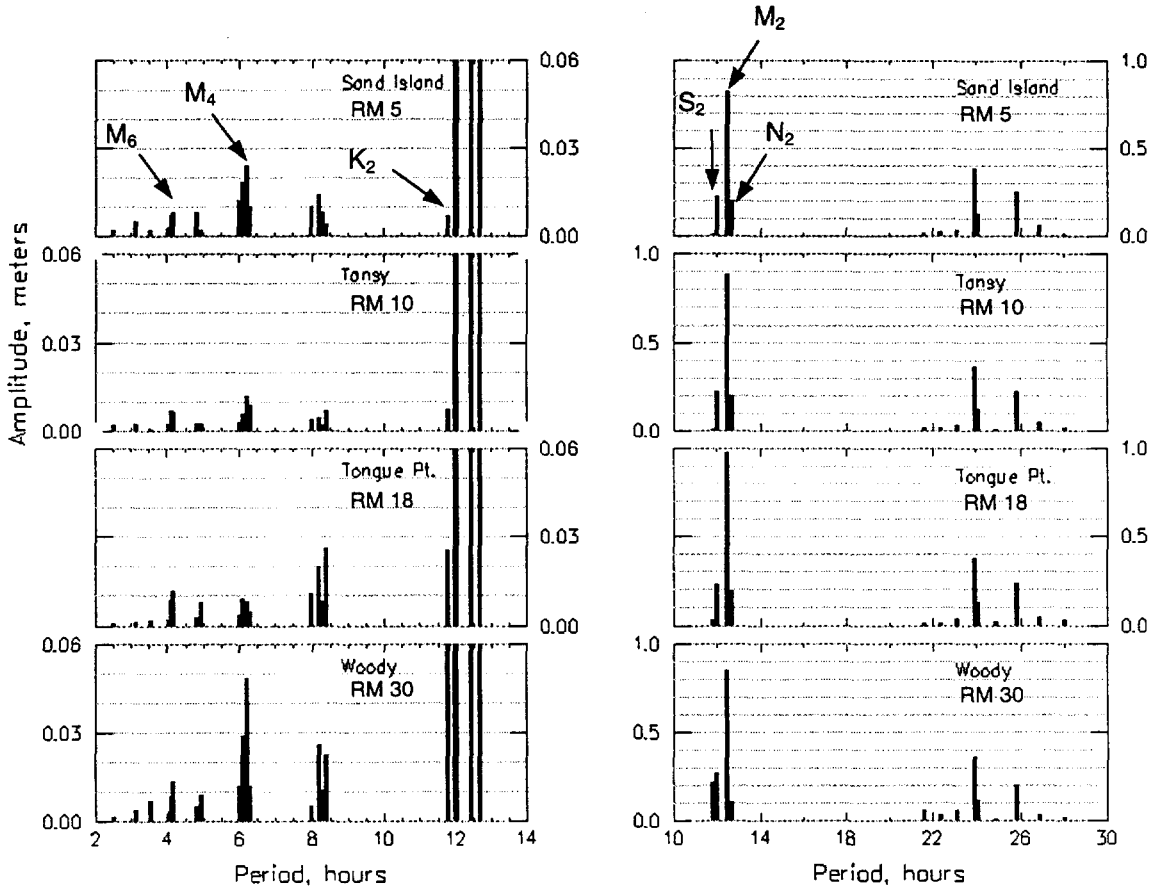

Figure 2.5. Harmonic analysis (Godin, 1972; Foreman, 1977) of observations collected by CORIE (Tongue Pt. collected by NOAA) for a low flow month. Stations are ordered from top to bottom to show propagation of a tide in the estuary. Interactions among tidal constituents and with the river flow increase with distance from the mouth. This is clearly illustrated by the increase in the amplitudes of the non-linear components (e.g. M_4 and M_6) at the expense of the astronomic components (e.g. M_2, S_2, N_2) from RM 18 to RM 30.

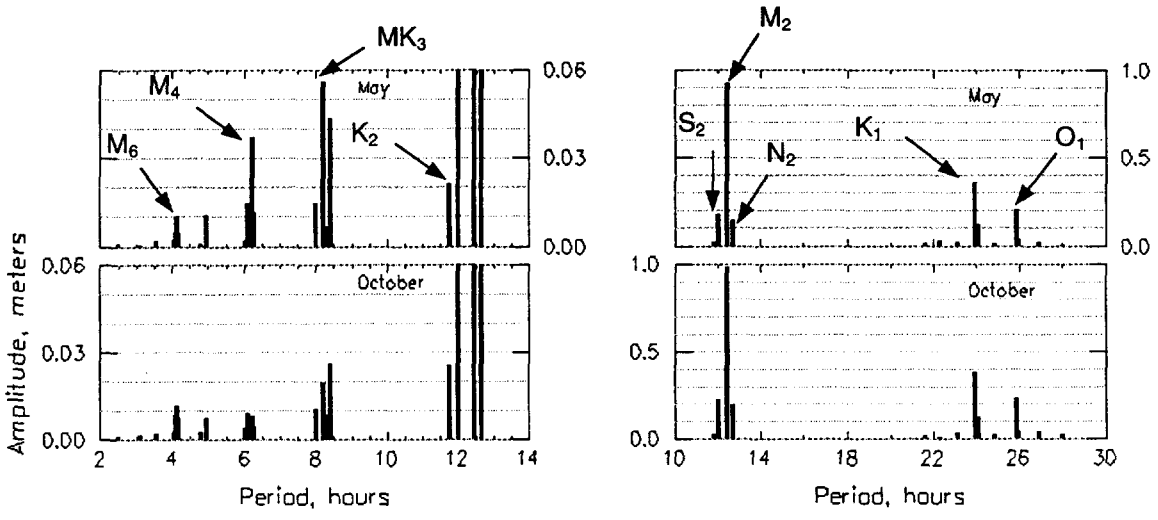

Figure 2.6. Harmonic analysis (Godin, 1972; Foreman, 1977) of observations collected by NOAA at Tongue Pt (RM 18) for a high (May) and low (October) flow month. Seasonal variability in river discharge strongly affects the generation of non-linearities in the estuary. Increased river discharge in May contributes to the decreased amplitudes of the astronomic components (M_2, S_2, N_2, K_1, O_1) and increased amplitudes of the non-linear overtides (M_4, M_6, MK_3) as compared to October. The interactions among astronomic constituents are also affected by river discharge, in which the MK_3 ($M_2 + K_1$) constituent decreases in amplitude with low river flow conditions.

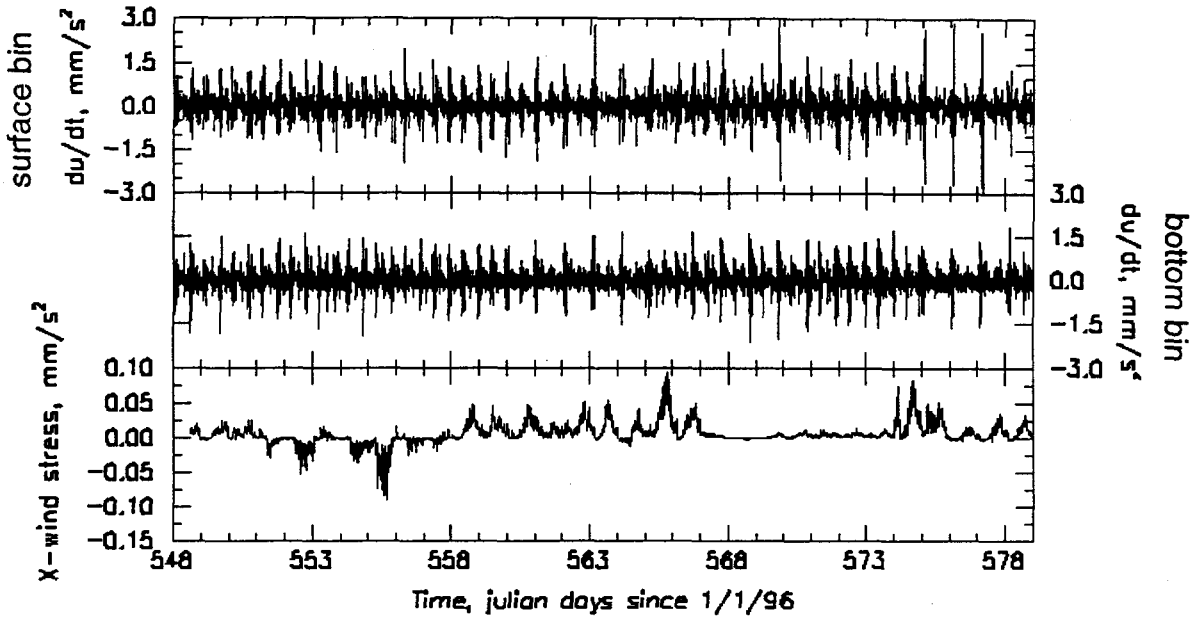

Figure 2.7. Dimensional analysis of wind stress and local acceleration in the x-direction for July 1997. Wind speeds and velocities were recorded at Tansy (station location in Figure 1.1)

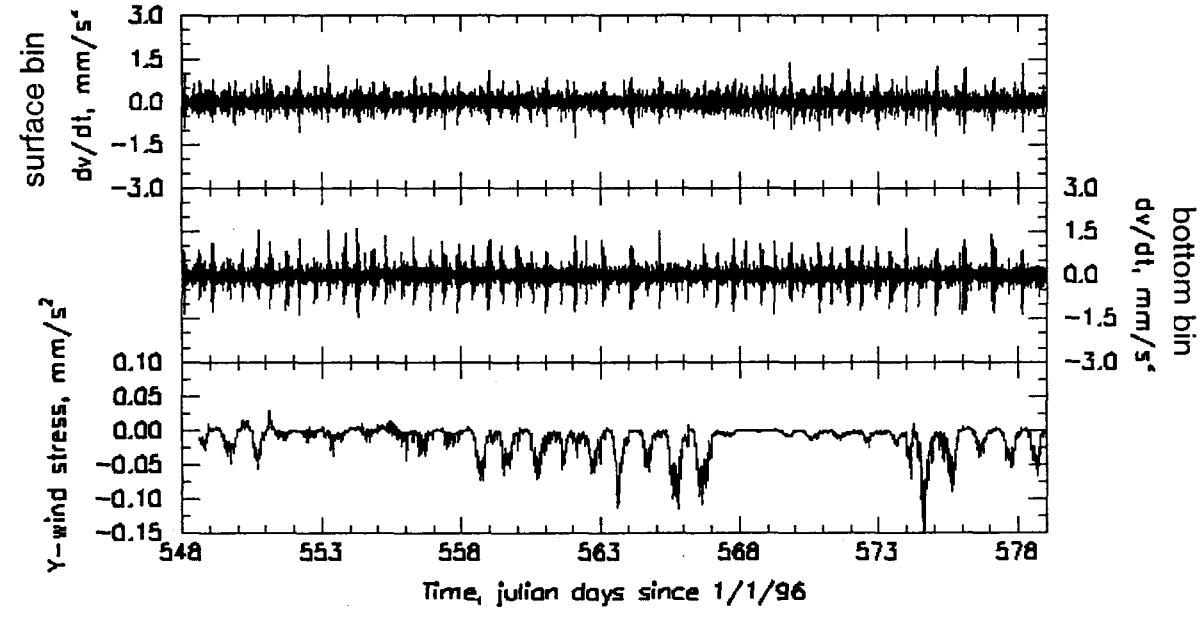

Figure 2.8. Dimensional analysis of wind stress and local acceleration in the y-direction for July 1997. Wind speeds and velocities were recorded at Tansy (station location in Figure 1.1)

Residence Times

3.1 Methods

3.1.1 Calculation of Residence Times

Residence times have been used to characterize the physical and ecological attributes of estuaries (e.g., Pilson, 1985; Jay, 1994; Oliveira and Baptista, 1997; Zimmerman, 1998) because they partially represent an estuary's ability to flush water and ecologically-relevant dissolved matter to the ocean. Traditional methods characterize residence times as a single number over an entire estuary, by balancing the volume of the estuary and its salt content against river discharge (e.g., Pilson, 1985). In an extension of this concept, box models (which locally integrate sub-regions in space and time) have been applied to well-mixed and to stratified conditions (Officer, 1980; Jay, 1994).

After a review of the various methods used to evaluate residence times in estuarine systems, Oliveira and Baptista (1997) proposed an approach that enables detailed accounting of spatial and temporal variability. This approach resorts to numerical tracking of virtual particles driven by a space-time varying flow field, thus addressing variability associated with bathymetry, river discharge and tidal forcings, within the constraints of the dimensionality and physics of the driving circulation model. A salient feature of VELA is the use of a 4^{th} order Runge-Kutta scheme with error control, resulting in a potentially high level of tracking accuracy. As illustrated via sensitivity analysis in the original application to the Tagus estuary, numerical tracking accuracy depends in a controllable way on error checking options with the tracking algorithm, but overall accuracy is limited by the physics, forcing realism and spatial and temporal resolution of the driving simulated flows.

In a diagnostic application to the Tagus estuary, Oliveira and Baptista (1997) contrasted a "single-number" approach based on salinity data and river discharge (Pilson, 1985) with their particle-tracking method. While both methods yielded similar "single-

values" after appropriate integration of the particle-based results, the particle-tracking method provided interesting insights on spatial and temporal variability. Maps and statistics of residence times computed for the Tagus estuary were not validated with field data, but were consistent with intuition and empirical evidence.

Since the complexity of physical processes in the Columbia River estuary is significant and our goal is to explore variability of the physical processes at multiple space and time scales, we employ here the same particle-tracking method and code (VELA) used by Oliveira and Baptista (1997). Utilizing the flow fields that are operationally available from CORIE (Section 3.1.2), we were limited (as were Oliveira and Baptista, for similar reasons) to conduct our residence time analysis based on a depth-averaged barotropic flow. This is a clear *a priori* limitation of the analysis, given the complex stratification regime in the Columbia River. However, results of a drifter experiment in the field (Section 4) are encouraging regarding the reasonability of the results.

3.1.2 Driving Flow Field

A two-dimensional barotropic circulation model of the Columbia River estuary (Das and Baptista, 1998, personnal communication) was utilized to generate the flow fields needed to drive particle tracking. The supporting code, ADCIRC (Luettich et al., 1991) uses a finite-element solution of the shallow water equations (generalized wave-continuity equation and primitive momentum equations) to compute surface elevations and depth-averaged velocities at the nodes of unstructured grids formed by triangular elements. The version of ADCIRC (Luettich and Westerlink, 1995) applied to the Columbia River enables wetting and drying of the tidal flats.

The finite element grid used in the numerical simulations of ADCIRC and VELA extends from Bonneville Dam to the ocean (approximate radius of 60 km from the mouth of the Columbia River) and includes the Cowlitz and Willamette rivers (Figure 3.1). The

computational grid has 30495 nodes and 54237 elements, with equivalent diameters ranging from 40 m to 20 km (Figures 3.1 and 3.2a). The North and South channels are well defined and the smaller channels connecting the lateral bays to the main channels are also well represented (Figure 3.2b). Das and Baptista forced the circulation model with tides along the open ocean boundary extracted from a regional model (Yang, personal communication), river discharge acquired from the Army Corps of Engineers for the three river boundaries and wind obtained from a NOAA buoy located off-shore.

ADCIRC simulations are available for the entire year of 1997. For a low flow month, RMS errors of elevations between the model results and CORIE data were between 0.15 - 0.25 meters (Figure 3.3)[1]. Scatter plots of velocity components (Figure 3.4) show reasonable agreement between simulated and observed depth-averaged velocity magnitudes. Directions are also well represented in the South channel (stations Red26, Tansy, Am169) but not in the North channel station (Am012). Das and Baptista have attributed the model's systematic difficulty in representing velocity direction at AM012 to uncertainties in the bathymetric data.

While it would be possible to further improve the match between model and data by doing data assimilation, we have not pursued that approach. The rationale is that data assimilation based on a two-dimensional barotropic model would try to artificially compensate for missing physics (in particular, baroclinic effects) rather than, or in addition to, optimizing the description of forcings. For the residence time calculations, reducing the present level of RMS errors seems futile compared with not having a three-dimensional baroclinic representation of the flow[2].

---

[1] More recent simulations, using ocean boundary conditions from Myers and Baptista (1998), have further reduced RMS (Figure 3.3). However, these simulations do not cover all the periods relevant to the present work.

[2] While three dimensional baroclinic models of the Columbia River have been developed within the CORIE group, they constitute on-going research (in particular regarding representation of the vertical stratification) and are not available for long enough periods to support the present work.

In addition to the model-data error bounds noted above, there are regions of the estuary where simulations should be distrusted due to topology or forcing data insufficiencies. Specifically, bathymetry is a limiting factor in Baker Bay and (as discussed earlier) in the upstream end of the North channel. Also, Youngs Bay freshwater inputs are neglected by lack of discharge information. The coastal region included in the grid of Figure 3.1 is forced only with tides, and thus can not represent continental shelf circulation.

3.1.3 Experimental Set-up for Residence Time Calculations

Residence times at (x_0, y_0, t_0) are calculated based on the length of time a particle released at location (x_0, y_0) and time t_0 stays in a pre-specified control domain representing the estuary. Maps of residence times are calculated for the estuary by following particles placed initially at every node of the finite element grid (Figure 3.1) contained in a pre-specified control volume. Here, the control volume extends from the mouth of the Columbia (external limits of the jetties) to the Bonneville Dam. June and July of 1997 were chosen for evaluation of residence times because these months provided a good contrast between high and low river flow conditions (Figure 2.3). Flow fields for these months were extracted from CORIE-archived hindcast simulations. Estuary limits were specified at the mouth and the particles were released at injection times specific for each experiment.

Oliveira and Baptista (1997) considered two contrasting interpretations of particle permanence in the evaluation of residence times. In the "re-entrant tracer" interpretation, the residence time is defined as the time it takes a particle to leave the control volume without returning later in the simulation. In the "once-through tracer" interpretation, the residence time is measured when the particle first exits the control volume, whether it will or will not return later. In this work we focus on the "once-through tracer" interpretation, for reasons discussed in Section 3.2.1.

As a part of the experimental design, we evaluated the numerical accuracy of the particle-tracking algorithm as a function of an internal error control parameter (ε) that resets internally the imposed time step, ΔT, to match a pre-imposed theoretical accuracy. Following Oliveira and Baptista (1997) we evaluated accuracy by calculating the "closure errors". The closure error is defined as the distance between the initial and final locations (x_A,y_A,t_A) and (x_A',y_A',t_A) of a particle as it is forward tracked from the present into the future to a location (x_M,y_M,t_M) and then backward tracked to the present. We ran the particle-tracking code for two periods: two days and thirty days. Using ΔT of 1 hour and a range of ε values (10^{-5}, 10^{-6} and 10^{-7} meters), closure errors were of the order of 10^{-2}, 10^{-3}, and 10^{-3} meters, respectively, for the 2-day run and consistently of 10^{-2} meters for the 30-day runs. Because closure errors are satisfactory in all cases, we set ε to 10^{-5} meters for all production runs, thus minimizing computational costs for the range of ε tested. Note that, conceivably, an even larger value of ε could have been used, with further reduced computational costs. This is an option to explore in further work, given that a map of residence times such as that shown in Figure 3.5 requires 3 hours of computational time on a Dec Alpha system.

Examining different variability scales required particle seeding strategies in space and time. To examine spatial variability of residence times, we ran month-long particle tracking simulations with particles placed at all nodes between the limits and Bonneville Dam. To examine seasonal variability in the estuary, we repeated these simulations for June and July 1997 (months of contrasting flow conditions), with particles released at approximately the same phase of the tidal cycle with similar coefficients for both months. To examine monthly variability we released four particles (located as shown in the inset of Figure 3.1) at approximately 3.1-hour (¼ of the M_2 period) intervals over a time period encompassing the spring and neap tidal cycles. Particle locations were chosen to include contrasting physical environments; a tidal flat (Desdemona Sands), South channel (two distances from the boundary) and North channel. To explore tidal variability we seed particles at all nodes in the grid at equally spaced time intervals over two tidal cycles for June 1997.

3.2 Results

Residence times were initially calculated for the once-through tracer for the entire estuary (Figure 3.5). Upstream of RM 30, residence times are on the order of weeks and in some areas outside the main channel a simulation time of one month was not long enough for the particles to cross the limits of the estuary. For the remainder of our analysis we focus on the Columbia River estuary between the mouth and RM 30. This is the most interesting region of the Columbia River for our purposes, because of strong tidal influence, strong spatial variability and complex bathymetry. Also, residence times in this region are relevant for an on-going National Science Foundation Land-Margin Ecosystem Research project on the physical and ecological characteristics of Columbia River estuarine turbidity maxima (CRETM).

Note that all the discussion is based on two-dimensional depth-averaged simulations, and should be interpreted as a broad-scale analysis. Clearly, stratification-induced trapping (e.g., in the estuarine turbidity maxima) can and will change residence times locally, in ways that the type of approach used here can not clarify until operational three-dimensional baroclinic models are available.

3.2.1 Once-through vs. Re-entrant Tracer

We reviewed earlier (Section 3.1.3) the contrasting concepts of once-through and re-entrant tracers, as they pertain to the evaluation of residence times. Our focus in this work is on once-through tracers, partly because they are the most interesting in the context of the CRETM project. Also, the driving flows are based on forcing conditions that do not require an appropriate representation of estuary-coast exchanges, which would be necessary to have confidence on residence time interpretations based on the re-entrant tracer concept. However, Oliveira and Baptista (1997) had found dramatically different results using the contrasting once-through and re-entrant tracer concepts for the Tagus

estuary. We were therefore intrigued by whether those findings would be duplicated in the Columbia River, which has a much-higher river discharge.

As a sensitivity test, we used the general procedure outlined in the experimental setup (Section 3.1.3) to compute residence times for June of 1997 using alternatively the once-through or the re-entrant tracer interpretations. Isolines of the residence times show minimal differences between the two tracers (Figures 3.6a-b), which is in striking contrast with the Tagus estuary case. Indeed, for the Tagus estuary, Oliveira and Baptista (1997) had to use histograms to characterize residence times for the re-entrant tracer scenario, because strong, chaotic local gradients of residence times made maps of residence times unreadable. Chaotic stirring at the mouth was identified as the cause of this behavior: particles originally placed at very close locations (i.e., a meter apart) would take very different paths as they exited the estuary, and would re-enter at dramatically different locations and times. In the Columbia River estuary, river dominance and perhaps flow channelization inhibits chaotic stirring and causes the particles to exit the estuary in less random tracks. Perhaps more important, ebb-dominance in the near-field plume inhibits the return of most particles when they leave the estuary.

We repeated the sensitivity test for July 1997 (a low flow month) and the isolines of residence times also showed minimal differences between the two interpretations (Figures 3.7a-b). Therefore, we conclude that both river and ebb-dominance are significant under most flow conditions in the Columbia River estuary.

3.2.2 Spatial variability

Residence times, even if typically short, exhibit strong spatial variability. Isolines of residence times for particles released during flood tide clearly show the effect of the estuarine topology (e.g., Figure 3.6a for June 1997). Indeed, residence times are 2-3 times shorter in the channels than in adjoint shallows. This is an expected trend, even if we urge caution in interpreting residence times computed for regions of the estuary (e.g., Baker

Bay and Youngs Bay) where the representation of bathymetry or local forcing is limited (see discussion in Section 3.1.2). Also, residence times may actually be longer in the lateral bays where marsh or other intertidal substrate that affects transport has not been represented by the model. Within a same type of environment, residence times tend to increase with distance from the mouth, due primarily to increased travel time and (depending on the time of release) to weaker ebb currents.

3.2.3 Temporal Variability

3.2.3.1 Seasonal Variability

Residence times exhibit seasonal variability that is attributed to seasonal changes in river flow. Maps of residence times for June and July show higher river discharge leads to residence times on the order of a few hours to one day (Figure 3.6a), whereas less river discharge leads to increased residence times of 1-2 days (Figure 3.7a). Most of the seasonal variability is observed upstream from the mouth where particles spend more time in the estuary, therefore, more influenced by variations in river flow. The mouth and region of the channels nearest to the mouth show the least seasonal variability because strong ebb currents cause the particles to leave the estuary too quickly to be affected by changes in river flow. Variability in the lateral bays is most likely not represented in the isoline maps for the reasons mentioned above (and in Section 3.1.2). Overall, the residence times are considerably short, even during low flow conditions, indicating river flow is very dominant in the estuary.

Although the maps of residence times indicate seasonal variability is mostly induced by river discharge, we wanted to further examine this relationship. Using the procedure described for the monthly time scale experiment (Section 3.1.2), residence times were computed for the four particles (locations shown in the inset of Figure 3.1) for two high and two low river flow months (May and June, July and October, respectively). (The experiment was slightly altered to release the particles at 24.8-hour intervals.)

Similar to the isoline plots for June and July of 1997, the results show that shorter residence times correspond to the increase in river discharge (Figure 3.8). However, a clear, linear relationship between river flow and residence times for each particle is not apparent. This suggests that residence times are influenced by tidal variability which is most apparent during the low flow periods (100-200x10^3 cfs). The low correlation of all the particles together represents significant diversity in residence times, caused by spatial attributes and distance from the mouth, in addition to tidal variability. Overall, the results indicate that a single residence time value would not be representative of the lower estuary under varying flow conditions.

3.2.3.2 Spring-Neap Variability

Variability of tidal heights and currents on a monthly time scale is attributed to spring and neap tides. The tidal range between flood and ebb tides in the estuary is larger during spring tides and smaller during neap tides, as shown in Figure 3.9a. The residence times of the particles released in the channels (locations in Figure 3.1) at 3.1 hour (¼ T_{M2}) intervals show no significant change with the transition from spring to neap tidal regimes (Figure 3.9b-e). Although most of the tidal exchange occurs in the channels, the smaller tidal heights and weaker currents of neap tides do not cause longer residence times, illustrating the importance of river flow in the channels during a high flow month. The particle placed between the channels exhibits monthly variability because transport over the tidal flats in dependent upon both tides and river flow. The transition from spring to neap tidal regimes causes the residence times to increase because of the weaker ebb tides during neap tidal regimes.

3.2.3.3 Tidal Variability

To examine the variability of residence times at a smaller time scale, we released particles throughout the estuary at times identified in Figure 3.10. Isolines of residence

times show the greatest variability occurs near the mouth and ocean-ward region of the channels (Figure 3.11) because the downstream region of the estuary is influenced most by the tides, the energy of which is strongest for the M_2 frequency. The least amount of variation in residence times occurs in the upstream sections of the channel because these regions are less sensitive to tidal advection since much of the M_2 tidal energy has dissipated in the estuary. The variability observed at the mouth and downstream region of the channels is caused by the direction and strength of the currents at the time of release. Although residence times are short, it clear that the characterization of temporal variability is much more important than just one number for studying the ecosystem in this region. The small changes observed in the upstream reaches are caused by the direction and strength of the currents several tidal cycles later as the particles reach the region of more dominant tidal influence.

Spatial variability in the area of tidal influence appears consistent over the eight release times. The mean residence times for the two tidal cycles (Figure 3.12) establish that residence times are smallest closest to the mouth and increase with distance from the mouth, but remain small in the channels. While June is a high flow month for which transport is river-dominated, we repeated the experiment for July and observed similar trends over the tidal cycle (Figure 3.13a). Average residence times in July were longer than in June for the same reasons discussed earlier for seasonal variability. The small standard deviations (3-6 hours) throughout most of the domain for June (Figure 3.12b) emphasize that the system is highly river dominated with tidal influence mostly affecting the mouth. In July, (Figure 3.13b) the standard deviations increase to 12 hours for most of the domain, which further indicates the influence of tidal variability is greater and extends farther upstream during a low flow month.

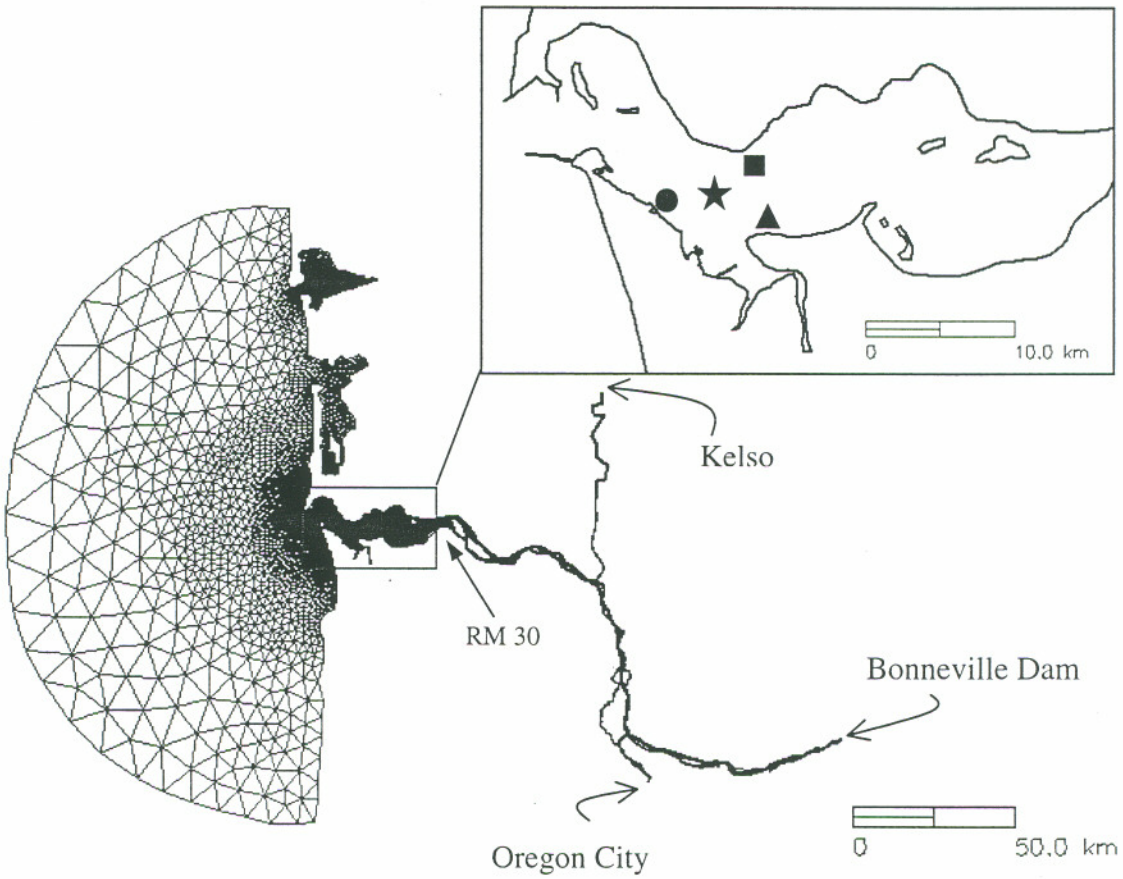

Figure 3.1. The finite element grid representing the Columbia River estuary and near ocean region from Bonneville Dam to approximately 60 km into the ocean; includes the Willamette River to Oregon City and the Cowlitz River to Kelso. (Das and Baptista, 1998). Inset shows release location of particles used in residence times analysis at the monthly time scale ■-Am012, ▲-Am169, ●-Red26, ★- between channel location.

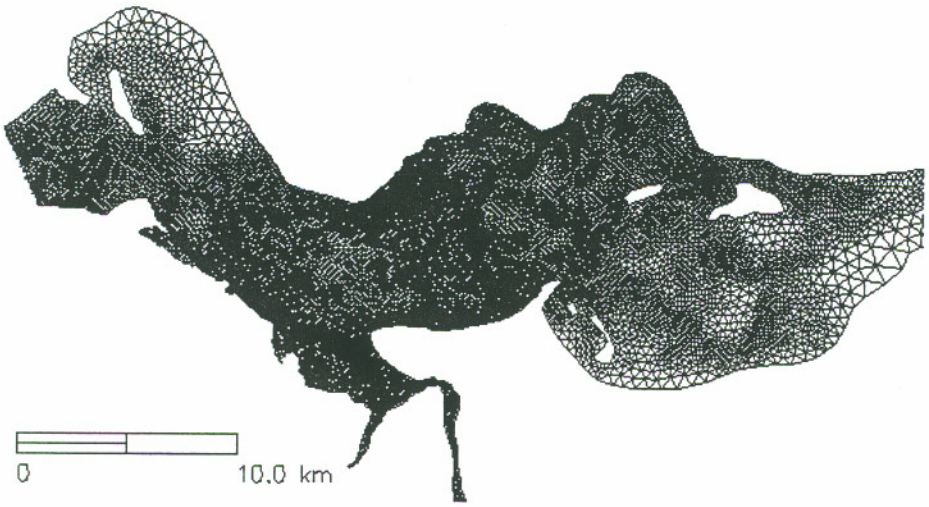

Figure 3.2a. The finite element grid cut at the estuary mouth and RM 30 showing high grid resolution in the main and secondary channels.

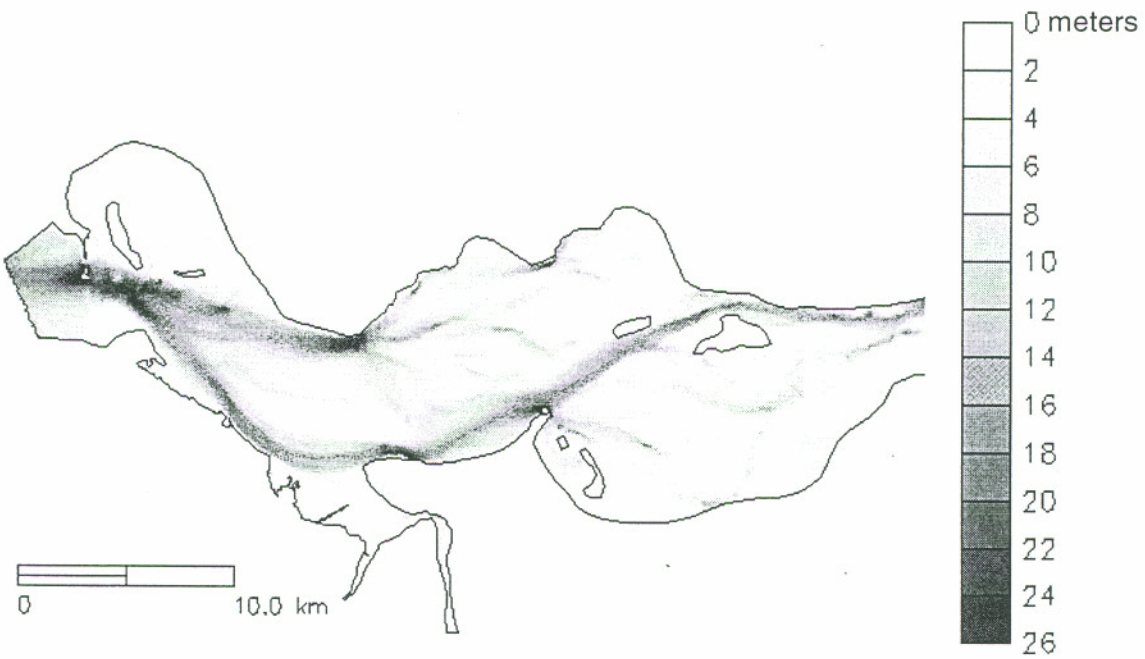

Figure 3.2b. Bathymetry of the finite element grid cut at the estuary mouth and RM 30. The main and secondary channels are well defined.

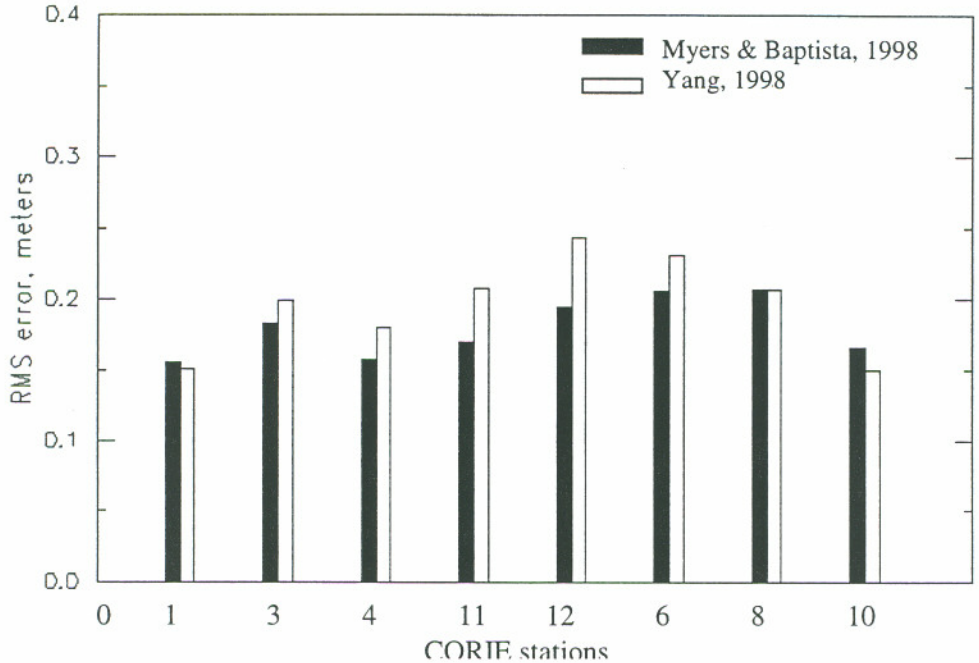

Figure 3.3. RMS errors of elevations from model results using boundary conditions from Yang (1998) and Myers & Baptista (1998). (Station locations in Figure 1.1)

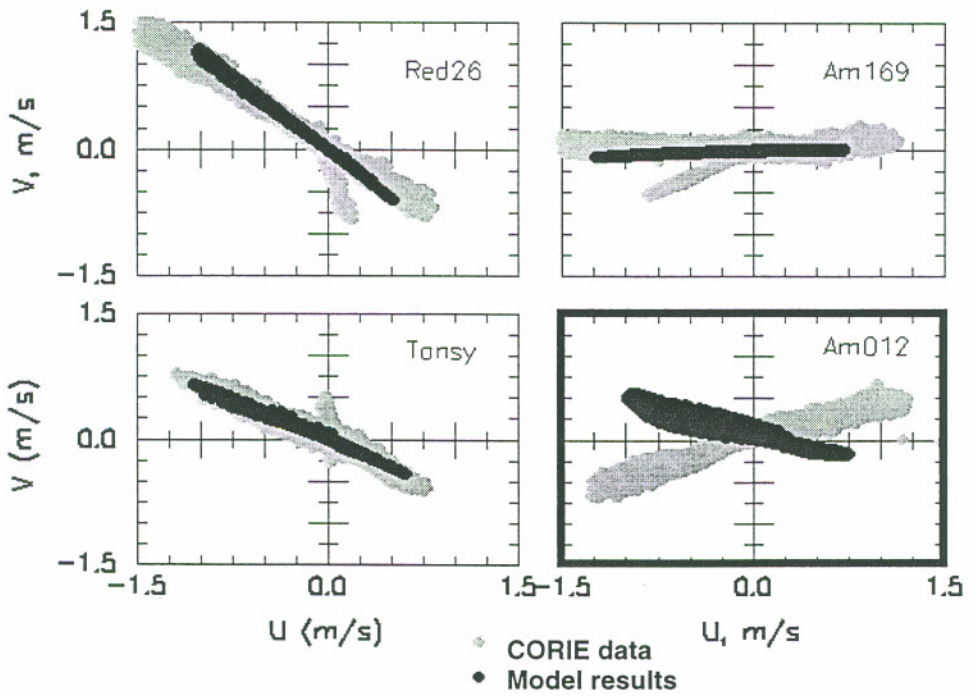

Figure 3.4. Scatter plots of *u* and *v* velocity components for model results and CORIE data. (Station locations in Figure 1.1)

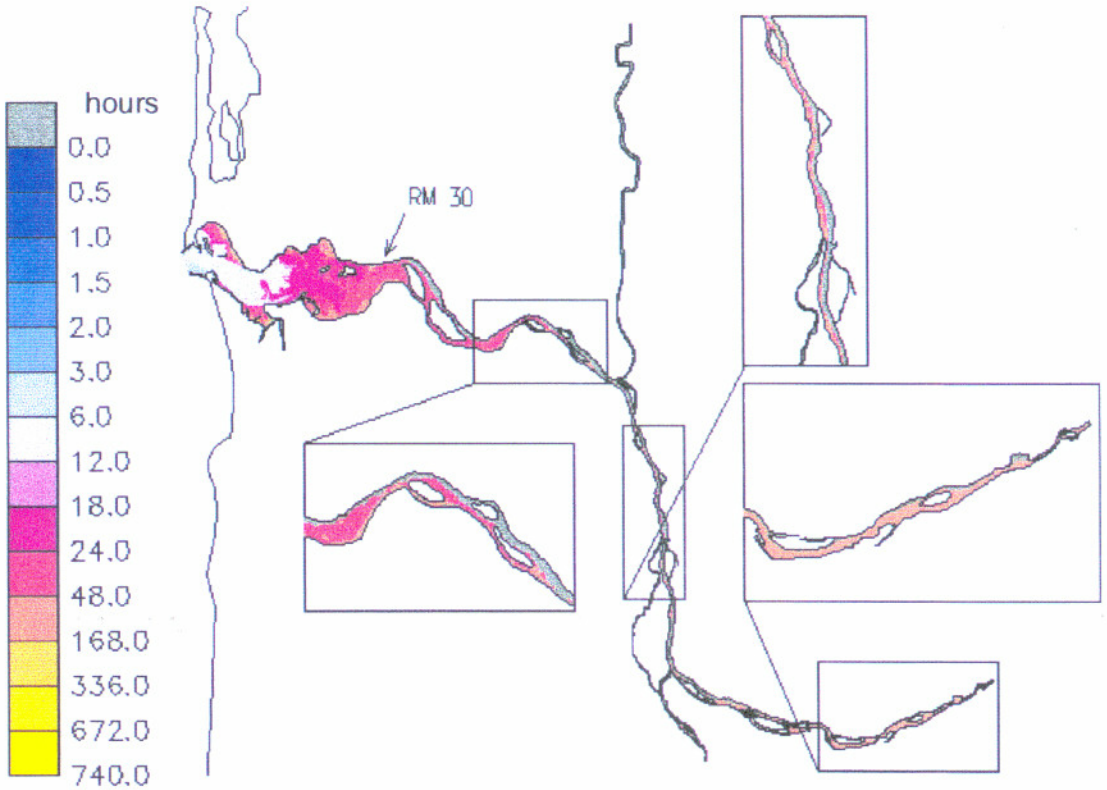

Figure 3.5. Residence times for the Columbia River estuary using the once-through tracer scenario for June 1997. Gray regions contain tracers that did not leave the estuary within the one month time period.

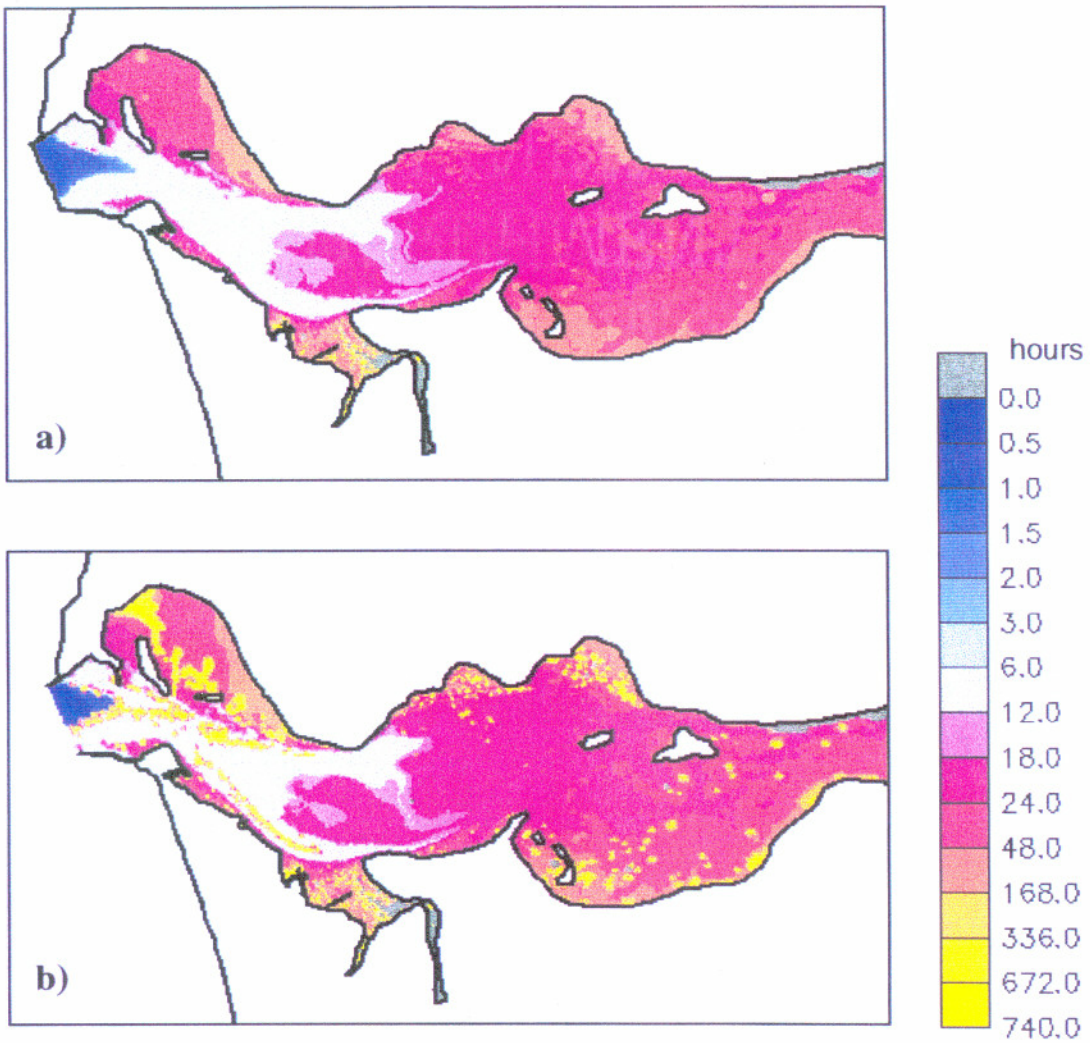

Figure 3.6. Residence times for June 1997 to RM 30 in the estuary. a) once-through scenario; b) re-entrant tracer scenario.

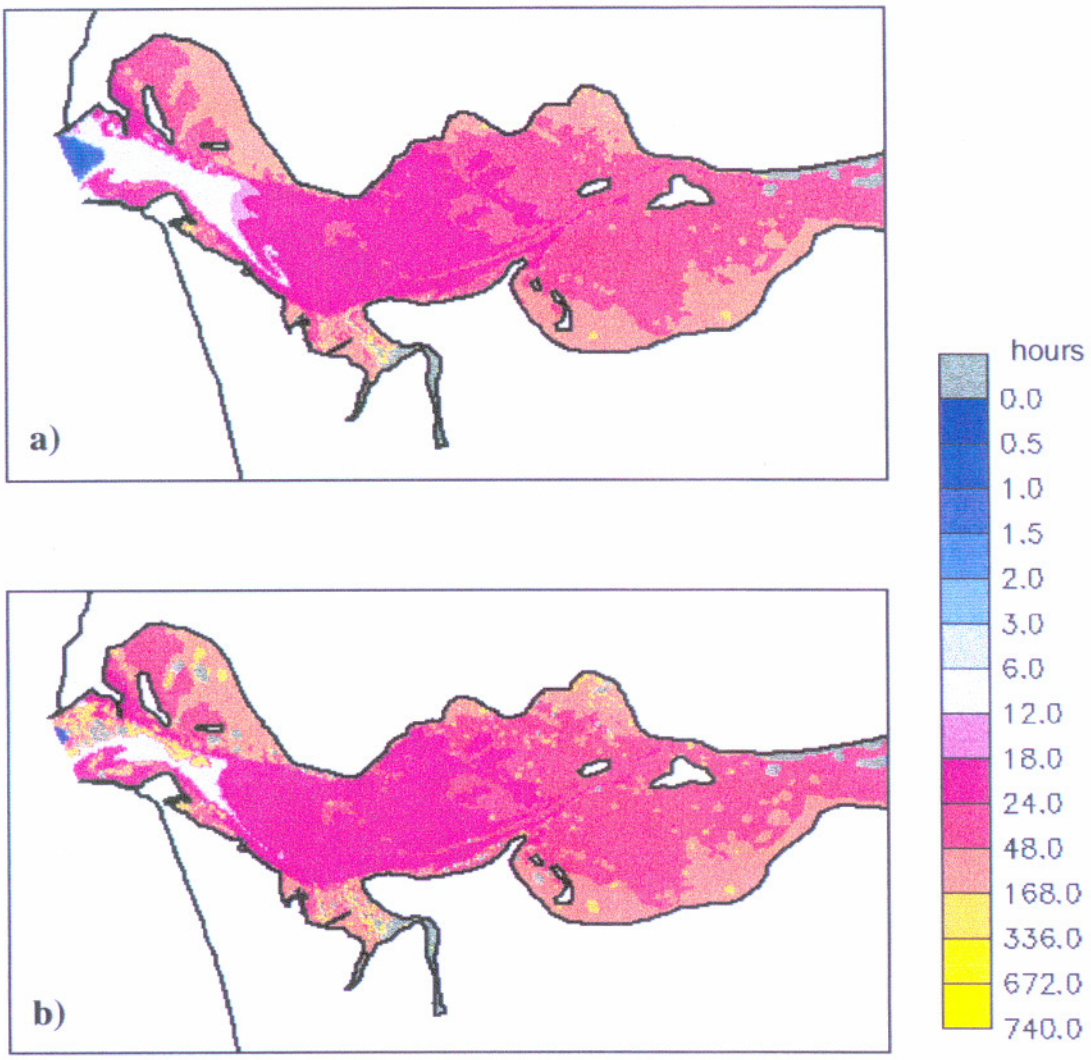

Figure 3.7. Residence times for July 1997 to RM 30 in the estuary. a) once-through scenario; b) re-entrant tracer scenario.

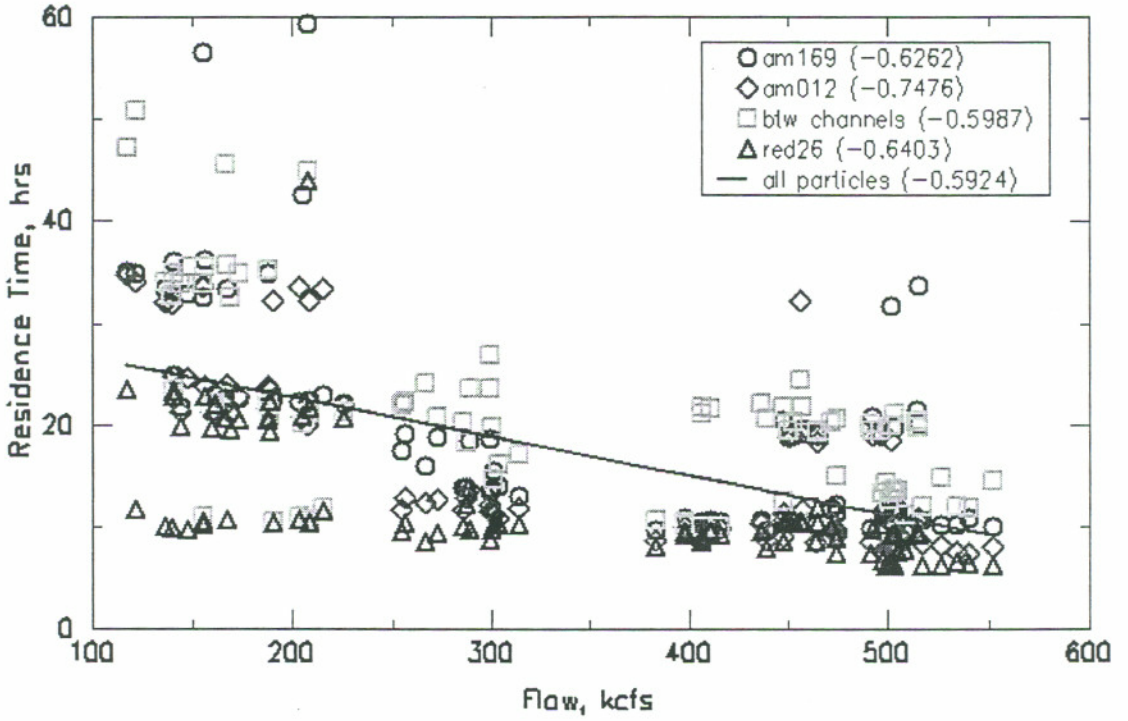

Figure 3.8. Residence times versus river flow for four particles released in the estuary. Value in ( ) is the correlation coefficient for each particle and all particles.

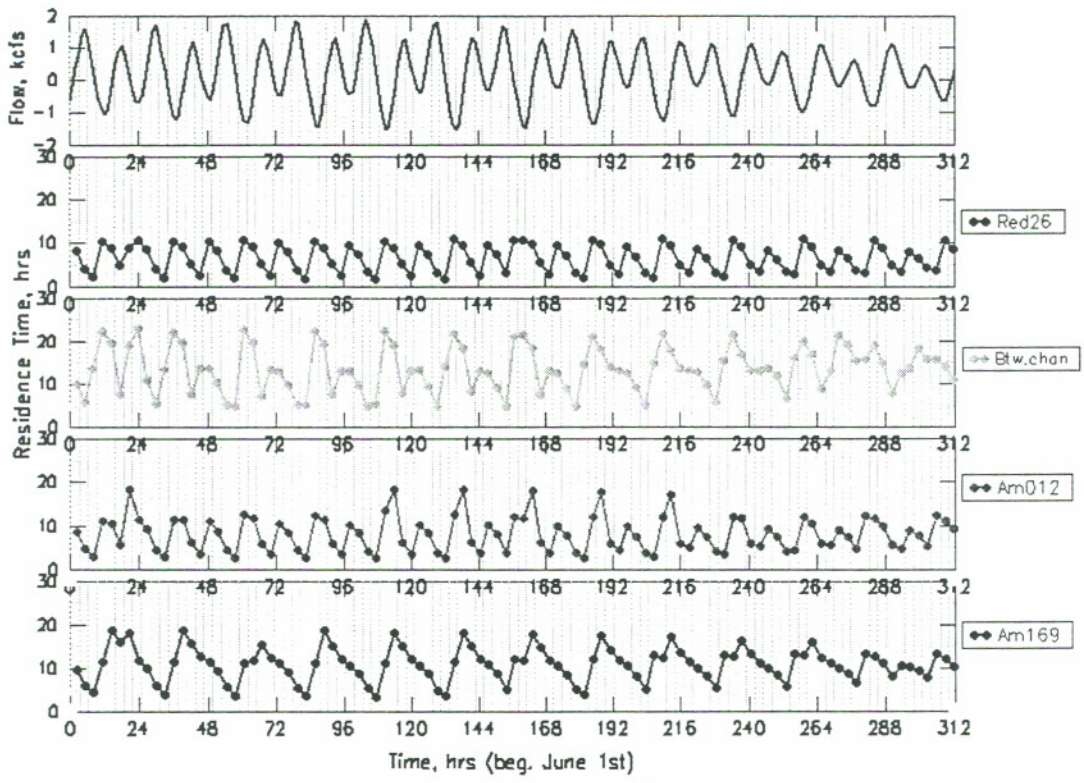

Figure 3.9. Time series of residence times for June 1997. a) modeled surface elevations; b-e) residence times for 4 particles released at locations shown in Figure 3.1. The dotted lines correspond to the particle release time interval of 3.1 hours.

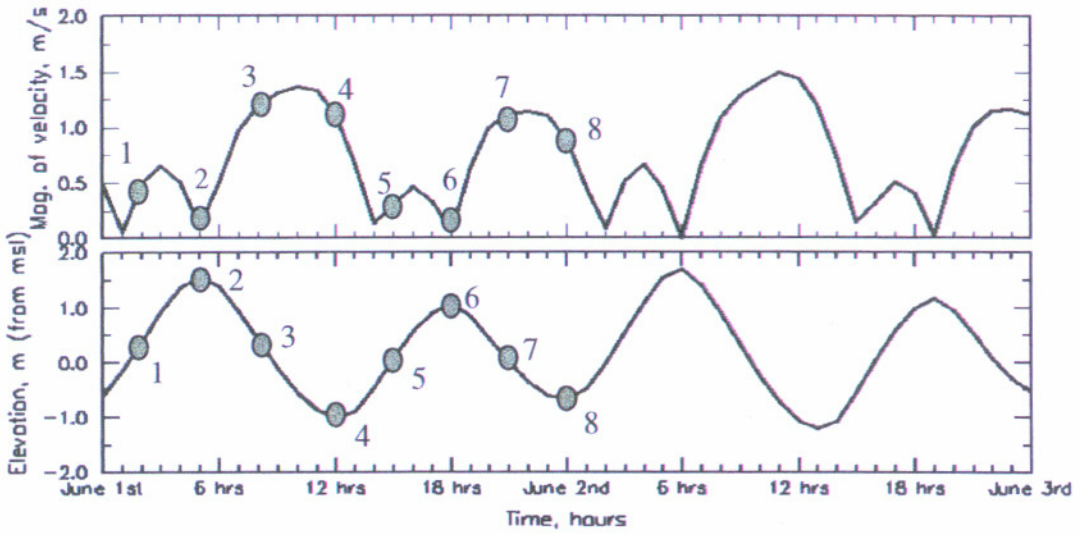

Figure 3.10. Model results for a 2-day period in June. a) magnitudes of depth-averaged velocity; b) surface elevations. Ovals coincide with a particle release time interval of ~3.1 hours.

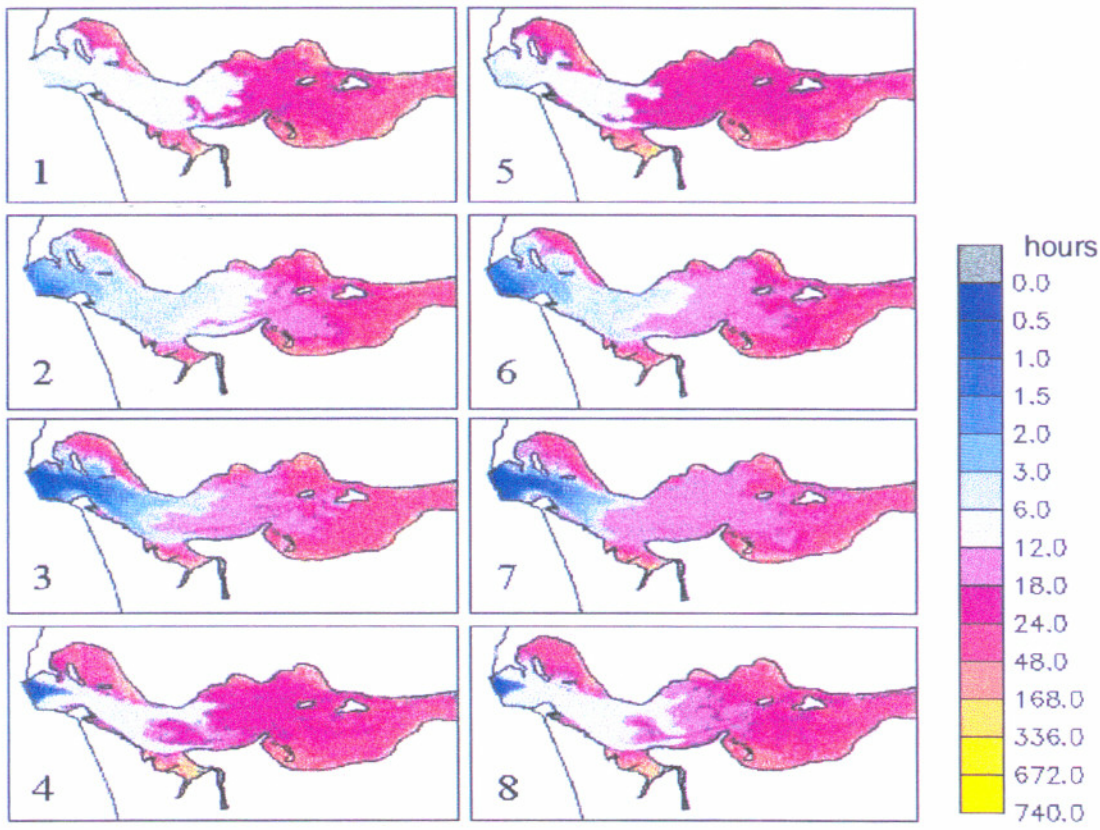

Figure 3.11. Residence times for June 1997 at eight release times. 1-8 correspond to release times identified in Figure 3.10.

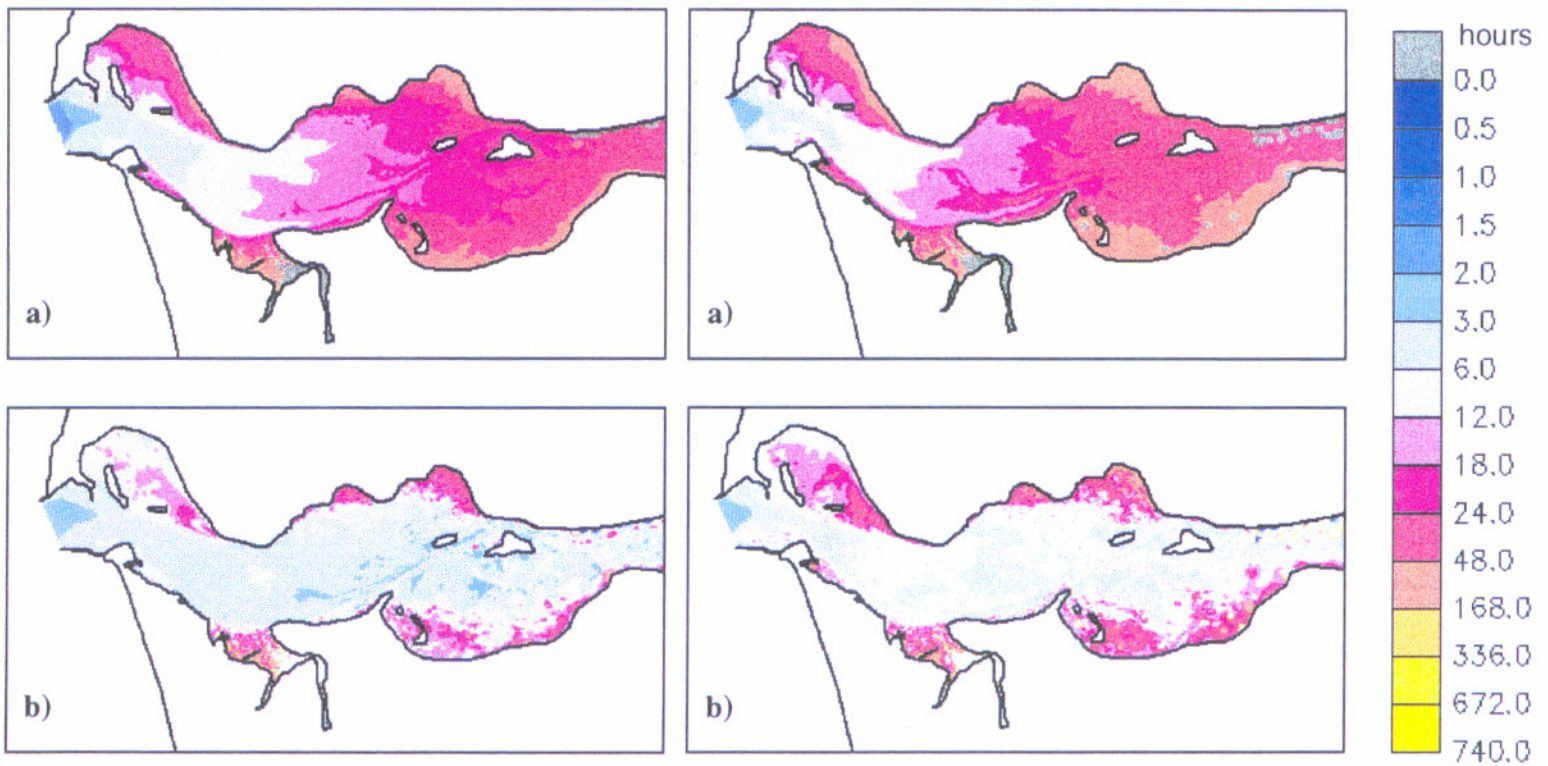

Figure 3.12. Residence times for June 1997. a) mean; b) standard deviation.

Figure 3.13. Residence times for July 1997. a) mean; b) standard deviation.

Drifter Experiment

Drifters have been widely used to enhance understanding of circulation and dispersion in the ocean and coastal regions. Specific designs have been built for good water-following capability, durability and low-cost (Niiler et al., 1987; Sybrandy and Niiler, 1991). Drifter use in estuaries has been more limited, in particular because of logistical difficulties associated with morphological constraints and navigation.

To begin assessing the ability of operational CORIE models to represent lagrangian transport in the estuary, we conducted a pilot drifter experiment. The specific motivation, approach, and results of the experiment are described below.

4.1 Transport Models

As a step of the progressive development of operational modeling capabilities for CORIE, we computed depth-averaged salinity concentrations using the transport component of VELA driven by ADCIRC hindcast simulations of circulation. Simulations showed insufficient upstream salt penetration (Figure 4.1). From work of Das and Baptista, we have determined the problem to have a similar manifestation in a 3D model. QUODDY (Lynch and Werner, 1991) is a 3D baroclinic circulation model based on the shallow water equations. Comparisons of salinity concentrations generated by QUODDY for a period in July 1997 with salinity data at the CORIE stations, showed the model to under-represent upstream transport in the channels (Figure 4.2). Although the model correctly represented the phase of salinity concentrations, not enough salt is transported upstream from the ocean. The results from both models clearly suggest that transport is not fully captured, however, comparisons of velocities for the 2D model in the South channel (Figure 3.4) and the 3D model (Figure 4.3) show that eulerian circulation is generally well represented in the estuary.

We believe that the difficulty of representing the salinity distribution is associated with boundary conditions at the ocean, and is possibly complicated locally by limitations in the representation of turbulence closure under dynamic, stratified conditions. However, we can not discard *a priori* that a more fundamental problem exists in the representation of lagrangian transport from the eulerian circulation field. This latter aspect of the problem can be partially evaluated through drifter experiments. We felt that a pilot drifter experiment was necessary because of the implications on our residence time analysis. Therefore, if the model results of particle tracking compare reasonably well with the field drifter, we gain some measure of confidence in our residence time calculations.

4.2 Drifter Design

The drifter experiment was performed in an exploratory nature as a first attempt at using such a device in the Columbia River estuary. Our objectives were many: evaluate the drifter's design and performance in the estuary, observe the logistics of a moving drifter while daily operations such as fishing and navigation flourish in the channels, and most importantly, collect field data to compare with the particle-tracking model. We constructed one drifter modeled after the WOCE/TOGA Lagrangian Drifter design (Sybrandy and Niiler, 1991). We modified the drogue design for use inside the estuary because wind stress is less important and the shallow region raised concern about beaching the drifter on mud flats in the upper reach of the channel. The primary changes to the drogue design included omitting the "holes" and shortening the length. Our drifter design consisted of a 38 cm fiberglass sphere attached to a sock drogue by a 1.5 m cable (Figure 4.4). The buoy (sphere) housed the GPS receiver and antenna and had a spread spectrum (1Ghz) antenna mounted upright to the outside. The subsurface drogue, made of a polypropylene fabric, was 0.7 meters wide and 1.2 meters long. It extended to a depth of 2.7 m below the water surface. The reference GPS antenna and receiver were placed at a fixed location next to the river where it received positions and stored them on a computer. Both the drifter and base station GPS antennas received satellite information at 1hz frequency. A receiving antenna to download the GPS data from the drifter was

located at a separate station on land because the data logger that was originally housed in the buoy was not functioning properly.

4.3 Model Design

Prior to conducting the field experiment, ADCIRC was run in forecast mode to predict surface elevations and depth-averaged velocities for the day of the experiment (Pearson and Baptista, 1998). The predictions were used to determine a release time that corresponded to the onset of flood at several locations in the North channel. The grid used in ADCIRC was cut at RM 65 (Longview, WA) and this "new" river boundary was forced with observed and predicted river flow data generated by the Northwest River Forecast Center and distributed to us by the Port of Portland. The open ocean boundary was forced with tides generated by global and regional tide models that were forecasted to equilibrium tides. The wind forcing was a constant wind speed of 5 knots (2.6 m/s) from the northwest, which is representative of observed data in the estuary. The simulation was run with the first four days based on observations, and the remaining three days in forecast mode. We used the forecasted velocities to run the particle-tracking model. We tracked particle trajectories of drifters released at different locations in the North channel to predict where we could release a drifter and follow it for a full tidal cycle while avoiding the tidal flats on flood and losing the drifter to the ocean on ebb.

4.4 Results

Based on the model predictions, we released the drifter in the North channel at a location between Sand Island and Chinook Pt. It was released less than an hour after the onset of the flood tide (on a neap tide) at approximately 5:15am (PST), (Figure 4.5) and its movement was tracked with the GPS system for 10 hours. The construction of the buoy allowed it to float slightly more than halfway above the water surface, keeping the antenna out of the water. We were interested in tracking the drifter for the full flood tide because the models were under-predicting transport during this phase of the circulation.

Following the field experiment, we re-ran ADCIRC to compute the flow field in hindcast, using the observations of river flow for the corresponding day. We then ran the particle-tracking model with the latest flow field and released the particle at the exact time and location as our field drifter. Wind measurements suggest that wind drag did not play a major role because wind speeds never surpassed a moderate 8.0 m/s recorded in mid-afternoon (Figure 4.6). As shown in Figure 4.7, the model trajectory is similar to the field data, but upstream transport is not fully captured. On flood tide, the drifter travels 2.5 km farther upstream than the modeled particle (Figure 4.8), and on ebb, both the model results and the drifter show similar locations by the end of the experiment.

The along-channel and cross-channel velocities for both the drifter and modeled particle were computed using the drifter's x, y positions (Figure 4.9). The comparisons for both velocity components indicate that the model is not properly representing the advective processes in the estuary, which affects the particle tracking. The field drifter's overall traveling distance is longer because the along-channel velocities of the field drifter are higher at peak flood and ebb. The paths of the field drifter and the model results diverge at peak flood because the cross-channel velocities in the field are considerably higher (more north) at peak flood. Despite differences between the model and field experiment, the trajectories do follow the same path for the first 2¼ hours, or 6.1 km and then show similar trajectory patterns for the remaining time. The results suggest the model performs well, considering it is forced with a depth-averaged flow field. To identify reasons for the discrepancies after that point in time and space, we repeated the model simulation with the particle released at the time and location of where the results differ.

The trajectory from the second model run (Figures 4.7 - 4.8) follows a closer path to the field drifter and the differences in distance traveled upstream decreased. An explanation for why the first model results are not as good deals with the location of when the field data and first model results began to differ. As discussed in Section 3, since the grid structure at Am012 does not fully represent the bathymetry in the channel,

the direction of velocities at this location do not compare well with CORIE field data (Figure 3.4). The velocity components computed from the modeled drifter show similar effects with the field data, in which the largest differences coincide with drifter locations just upstream of Am012 (Figure 4.7). As a result, the modeled drifter is forced in a direction different from the field data and then is tracked in a different flow regime. The model results demonstrate the cumulative effect of the spatial sensitivity in the flow field. In both the field data and model results, any change to the path would ultimately affect the resulting trajectory. The second model run began upstream of Am012, but differences between the simulations are apparent because the bathymetry is not fully represented for this reach in the channel. The trajectories of the model results suggest that transport is highly sensitive to spatial variability in the flow field.

In addition to the model, there are limitations associated with a field drifter. Slip, or the drogue's movement relative to the water, is a common occurrence of drifters, that is caused by wind and the velocity differences between the buoy and the drogue. The effect is that the drifter cannot accurately measure the currents of the water parcel it is tracking. Drifters have been deployed with velocity current meters attached to the top and bottom of the drogue to assess the amount of slip (Niiler et al., 1987). After much testing, the advanced drifter designs have a slip of 1-2 cm/s in wind speeds of 10 m/s, which were achieved by increasing the size of the drogue to increase the drag coefficient (Niiler et al., 1987). For our exploratory application, we did not measure slip nor assess the drag coefficient for our modified design prior to conducting the experiment. Since wind measurements were small, and wind is much less significant inside the estuary, we do not believe the velocity differences between the model results and field data are strongly influenced by slip. The other limitation of the drifter relates to errors in the drifter positioning. The GPS gives accurate positions within 100 meters. This can be improved with use of a differential GPS in which the errors are reduced to 5 meters. For this experiment, 100-meter accuracy does not greatly affect the differences between the modeled drifter and field data since they are greater than the accuracy limits.

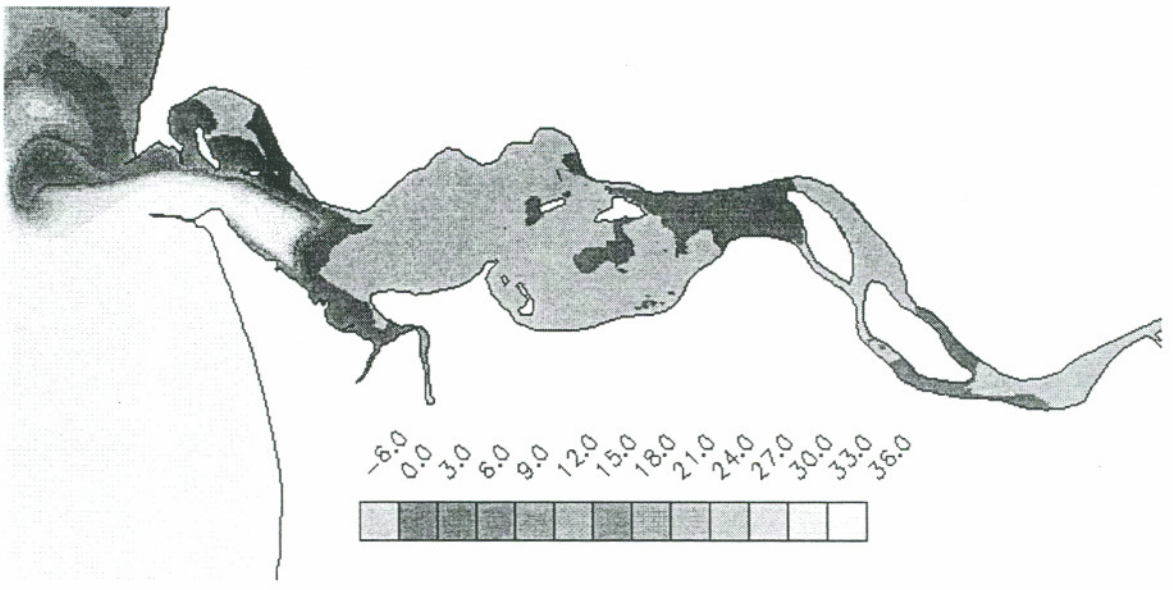

Figure 4.1. Salinity concentrations (ppt) computed using the 2D transport model for March 1998. On flood, the salinity concentrations only extend upstream to RM 10.

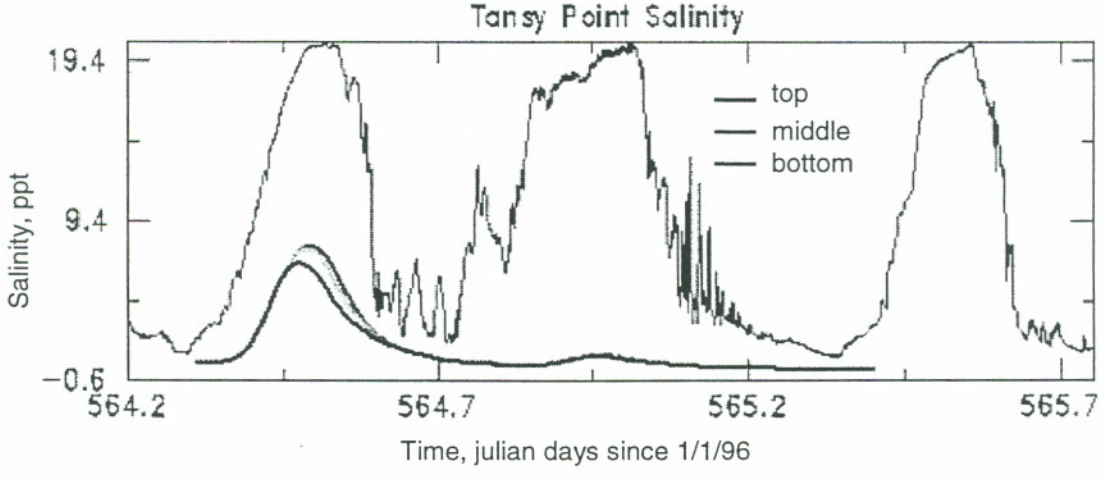

Figure 4.2. Quoddy vs. CORIE field data for salinity concentrations at Tansy for two tidal cycles in July 1997.

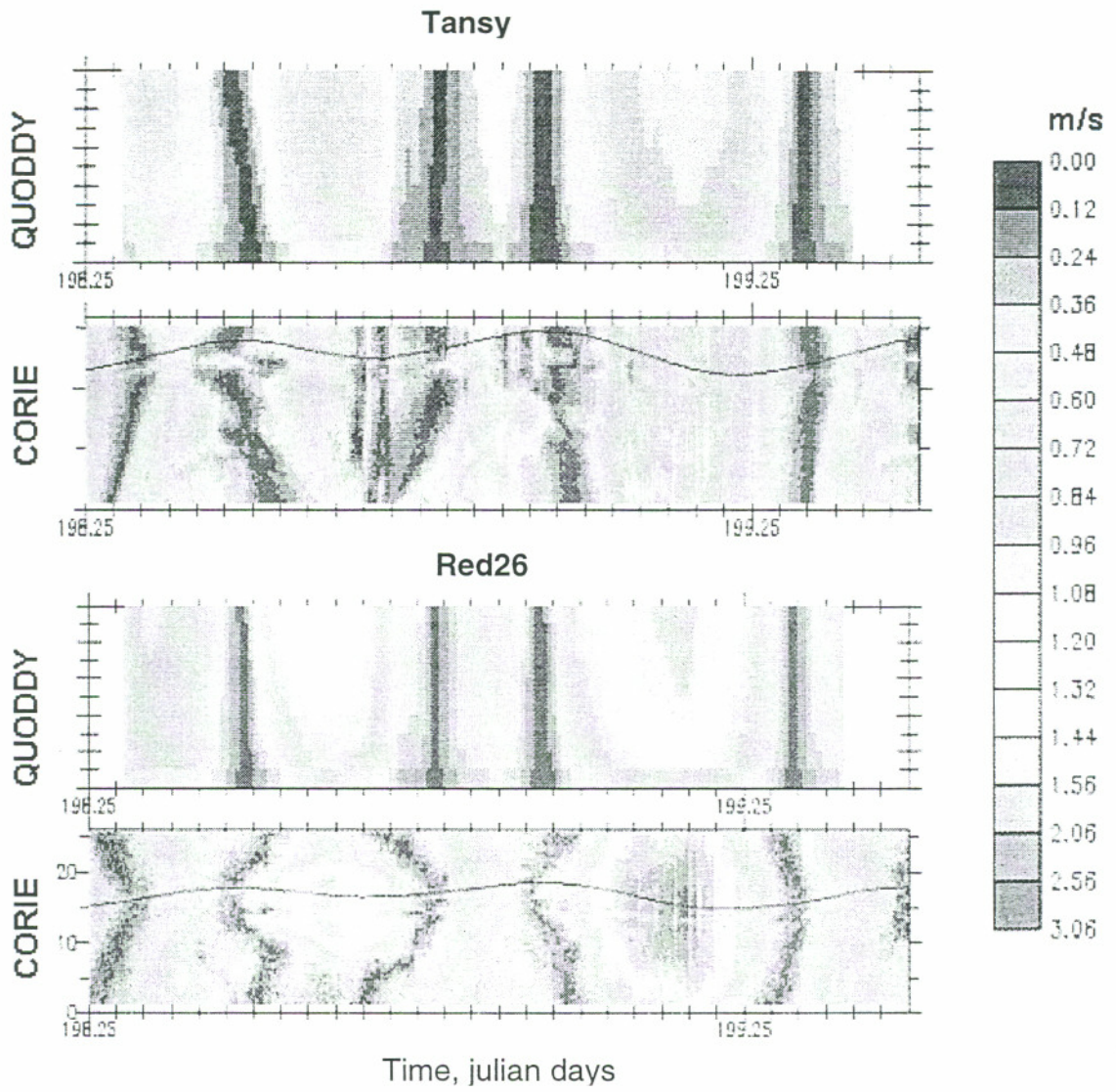

Figure 4.3. Comparison of velocity magnitudes for the 3D model and CORIE data. The model properly represents the magnitudes and phase, but does not capture the heterogeneous vertical structure apparent in the field data. Note: model results are shown in σ-coordinates, while CORIE data are shown in z-coordinates.

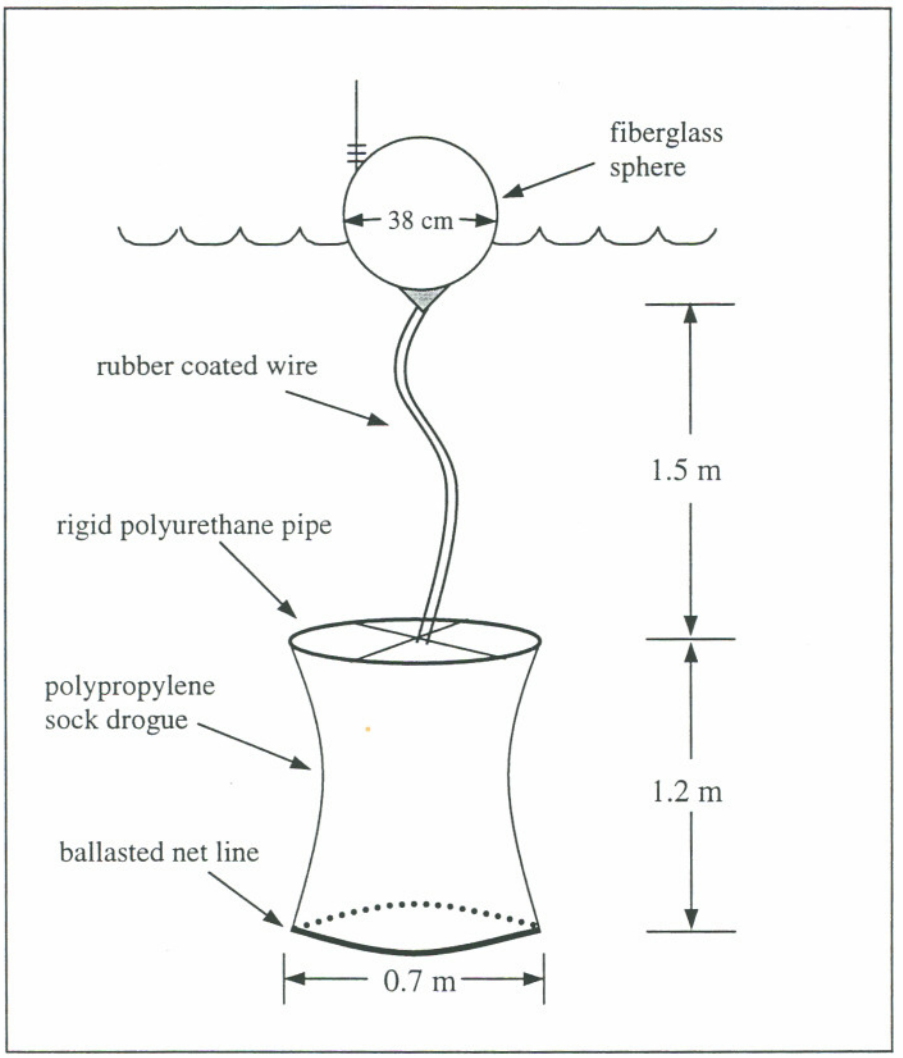

Figure 4.4. Drifter design used in field experiment. Modeled after the WOCE/TOGA Lagrangian Drifter (Sybrandy and Niiler, 1991). Courtesy of M. Wilkin, 1998.

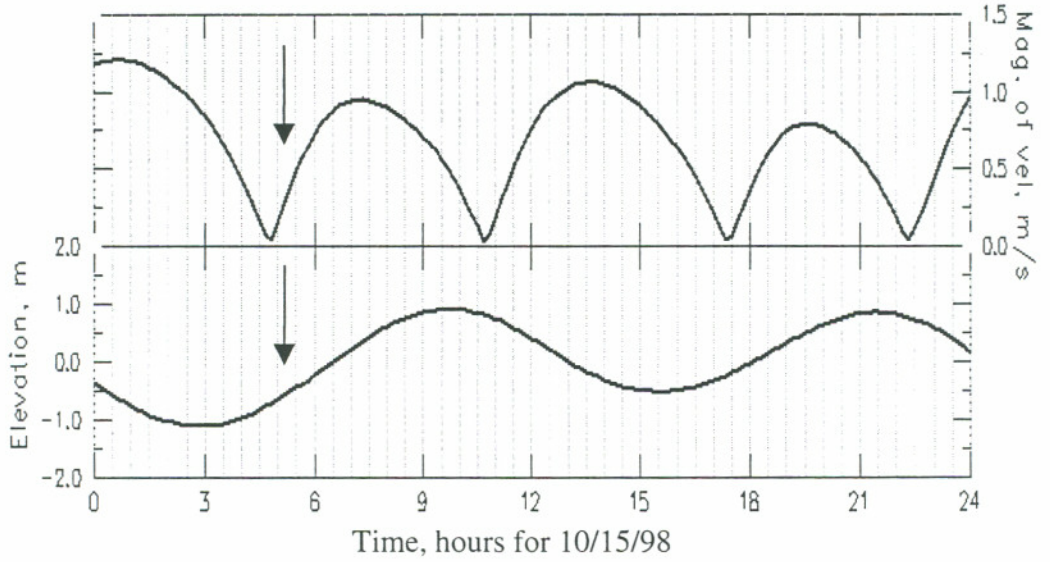

Figure 4.5. Forecast results of depth-averaged velocities and surface elevations used to determine release time of drifter. Arrows indicate release time of 5:15 am PST during a neap tide.

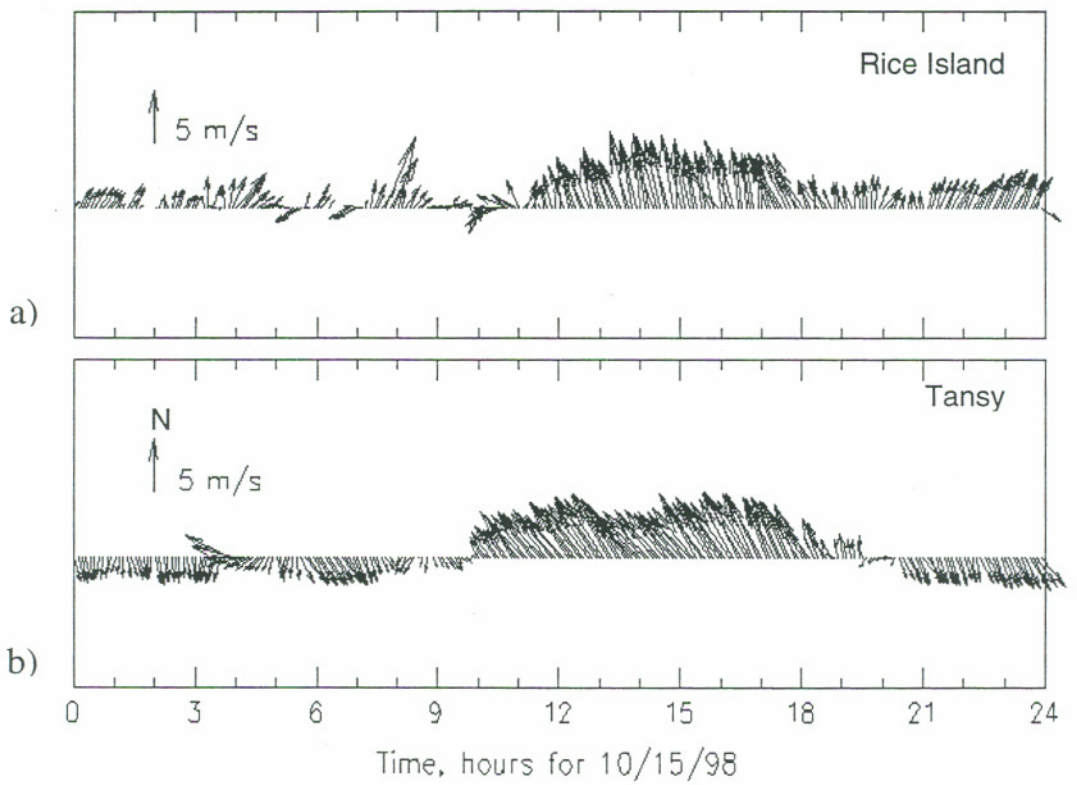

Figure 4.6. Wind speed and direction recorded in the lower Columbia River estuary for the time period corresponding to the drifter experiment. a) Rice Island; b) Tansy. (Station locations in Figure 1.1)

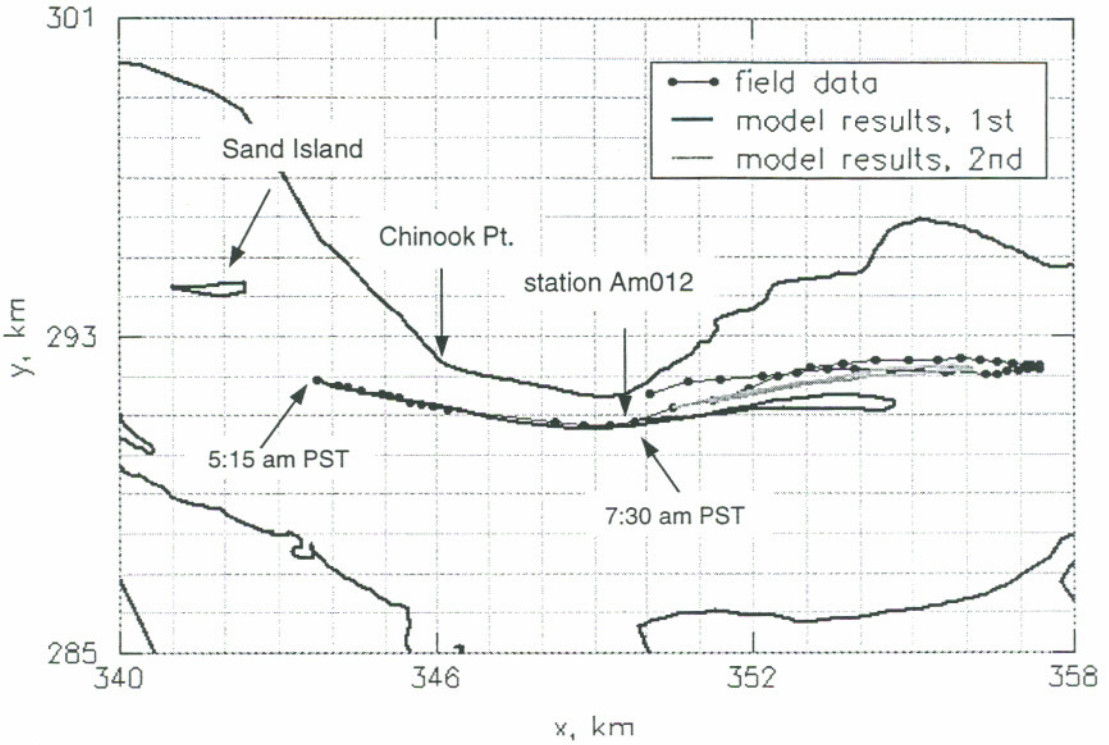

Figure 4.7. Trajectories of the field drifter and modeled drifter. Error of ±100 meters for the field data tracked with the GPS.

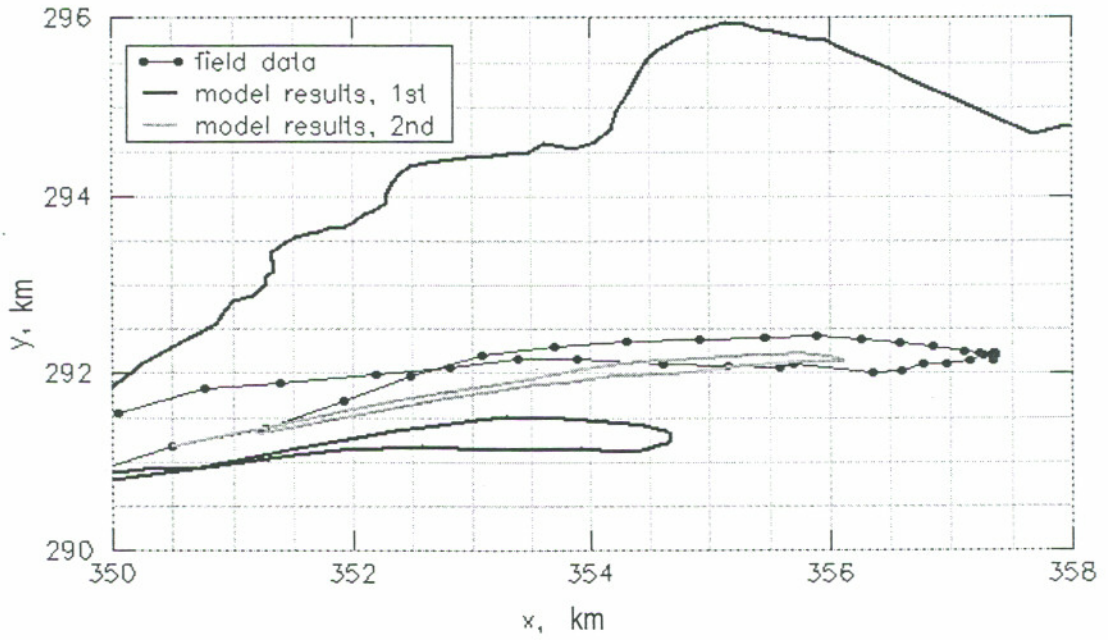

Figure 4.8. Trajectories of the field drifter and modeled drifter expanded from Figure 4.7 Shows extent of upstream transport and the differences between field data and model results. Error of ±100 meters for the field data tracked with the GPS.

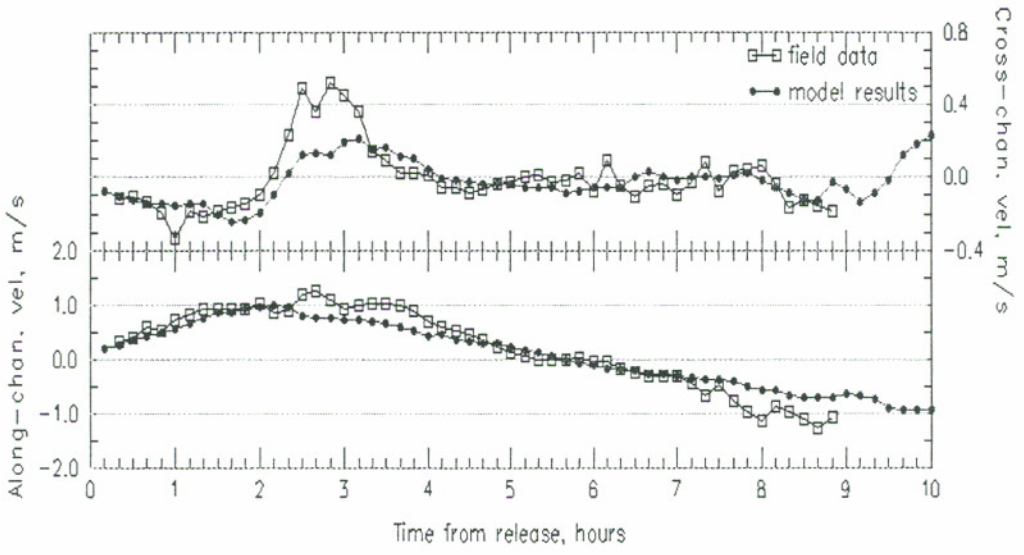

Figure 4.9. Cross-channel and along-channel velocities computed from the field experiment and model results. North-flowing cross-channel velocities and along-channel land-ward and ocean-ward velocities are larger for the field drifter.

CORIE Data Processing

For the residual velocity calculations, we concentrated on four stations in the lower portion of the estuary that are equipped with acoustic doppler profilers (ADP's). The ADP's are mounted in frames deployed in the riverbed and record several physical variables at approximately 5-minute intervals. These include the instrument orientation (heading, pitch, roll), temperature, pressure, (*u, v,* and *w*) velocity components, standard deviation of velocity components and the signal strength (backscatter). User inputs including the averaging interval, pinging rate, cell size and number of bins, also in the data record, define parameters to custom-design the ADP to our specific uses.

The ADP's were initially deployed at Red26 and Tansy in December 1996, at Am169 in January 1997, and at Am012 in May 1997 (station locations in Figure 1.1). Our analysis of ADP data extends from initial deployment through September 1998. The firmware of all instruments was upgraded in early 1998, on different dates for each station. With the original firmware, the velocity profile was computed from a plane that used constant distances along each beam and then the values were corrected for pitch and roll. When the new firmware was installed, the ADP's pitch and roll were accounted for during beam mapping in the averaging interval. This upgrade corrected for velocities being recorded at different bin depths for each transducer head when the instrument is tilted. The archived data did not show any noticeable pattern differences when the new firmware was installed, but we have not analyzed in detail the implications of the firmware change.

Prior to computing residual velocities from the ADP data, we examined the data to identify unreasonable velocity values and missing records due to instrument malfunctions or recovery/deployment activities. This process of quality control involved analyzing all variables simultaneously at each station and as an ensemble of all four stations to determine instrument performance for the length of deployment. When available, we compared ADP pressure data to CTD pressure data at the same stations for

additional assessment. We performed our analysis for each month individually, because we wanted to compare residual velocities at monthly time scales. Our criteria for determining which months were unusable included determining whether there was insufficient data to compute residual velocities, and determining whether unusual trends appeared to be station specific. Many of these trends represented inaccurate measurements that appeared to be caused by ADP instability on the channel bed.

Figures 5.1 through 5.4 show the data measured by the ADP at each station from initial deployment through September 1998. We compared the data at each station with field notes in order to determine whether observed unusual behavior had a physical explanation. As summarized in Tables 5.1 through 5.4, gaps in the data record or sudden shifts and spikes in the variables either had an explanation that pertained to deployment/recovery operations, other diver operations, or instrument instabilities. Some examples are discussed below:

- Red26: March 1998 (Figure 5.1) ADP positioned on its side (Table 5.1)
  - sudden shifts in the pressure
  - sudden shifts in the velocity components and standard deviation
  - sudden shifts in backscatter
  - pitch and roll exceeded sensor limits (±50°)
  - followed by unreasonable values for all parameters

- Am169: November 1997 - February 1998 (Figure 5.2) ADP buried in the sand and on its side; two attempts to recover instrument in January (Table 5.2)
  - temperature shows minimal variability with the tides
  - velocities are unusually large and highly variable
  - spikes in the standard deviation
  - backscatter signal significantly decreased
  - instrument orientation exceeded sensor limits (±50°)

- Tansy: September 1997 - January 1998 (Figure 5.3) ADP unstable
  - gradual increase in pressure
  - gradual decrease in the range of velocities
  - gradual decrease in backscatter
  - spikes in the standard deviation
  - large shifts heading, pitch and roll

For time periods where no reason is given for gaps or spikes in the data, we ascertain that any number of issues such as network or telemetry problems and power losses may be the cause.

In addition to station specific behavior, other trends are observed in the data records that occur at all stations. For example, all stations show a slight increase in mean pressure during certain periods of deployment. A drift in the pressure sensors caused this increase[1], which affects the calculation for elevations, but does not have any impact on the velocity measurements.

In addition, at all four stations, the pressure data showed an abrupt decrease in 1998 that coincided with a re-deployment date for each instrument (Tables 5.1 - 5.4). Comparisons with CTD data at Red26 and Tansy (Figures 5.1 and 5.3, respectively) showed that the pressure shift was not a physical occurrence in the estuary, but rather a consequence of the ADP placed in a shallower location upon re-deployment. At Tansy, another pressure shift occurred on January 22, 1997 when the ADP was situated in a deeper location. We did not observe abnormal behavior in the other variables at each station, indicating the velocity data should not be discounted. However, when comparing residual velocities for pre- and post-redeployment months, there is the possibility that the data records are from different flow regimes. Following the analysis of this data, the ADP frame was modified to remain fixed on the channel bed so that in most re-deployments

[1] SonTek has upgraded the pressure sensors on their new ADP's (SonTek, 1998, personal communication) to eliminate this type of problems.

only the instrument needs to be removed from the frame (1998, Wilkin and Baptista, personal communication).

Another noticeable trend in the data records is the occasional decrease in backscatter at each station for varying lengths of time, typically during summer or fall. This decrease was caused by biological growth on the transducers (SonTek, 1997). When biofouling is naturally reduced with the changing season, the signal strength is restored. In principle, velocity measurements are not affected by biofouling of the sensors because they are computed from phase shifts in the acoustic beams, not intensity. However, the correlation between degradation of velocity and the backscatter signal for Tansy Pt. between September 1997 and January 1998 acoincided with instrument instability.

Table 5.1 summarizes our evaluation of the ADP data between initial deployment and September 1998. For all four stations, several months had to be discounted for insufficient data. Also, specific months were discounted from Red26, Am169 and Tansy for unreasonable velocity values caused by ADP instabilities.

Standard deviations recorded by the ADP are an indication of the uncertainty in the recorded velocities due to water velocity variations in the averaging interval and instrument noise. We calculated the standard deviation as a function of the instrument's operating parameters to determine the amount of instrument noise expected to be expected by the ADP. This value was computed using the equation (SonTek, 1997b):

$$\sigma = \frac{140c}{F\Delta z\sqrt{N}} \tag{4.4}$$

where σ is the standard deviation of horizontal velocity measurement (m/s), c is the speed of sound (nominal value of 1500 m/s), F is acoustic frequency (Hz), Δz is cell size (m) and N is number of samples. N is determined by multiplying the averaging interval (seconds) by the pinging rate (samples/second). Shifts in the expected standard

deviation would occur when the any of the operating parameters are altered during deployment. Similarly, the measured standard deviations would reflect changes to the operating variables.

The differences between the measured and predicted values are most likely caused by water velocity changes, normal for turbulent flow regimes, and the measured values are usually 2-3 times greater in these flow conditions (SonTek, 1998, personal communication). This is consistently the case for all four stations (Figures 5.1-5.4), with the exception of time periods early in the deployment record at Red26, Am169 and Tansy. The large spikes in the measured standard deviations at these three stations (2/97 - 5/1/97) (Figures 5.1 - 5.3) coincide with periods when the velocity profile was computed in beam coordinates (Tables 5.1 - 5.3). The spikes in the standard deviations (and backscatter) at Tansy between 12/97 and 2/97 are most likely caused by the short averaging interval (2 minutes). In addition, ADP instability may affect the measured standard deviations (SonTek, 1997). Sudden changes or spikes in the measured values that were accompanied by unusual behavior in the other variables signified the problematic situations described above (ADP buried in the sand, on its side or shifting orientation).

A limitation with using ADP data is that the instrument's region of measurement does not extend to the surface and bottom of the water column (Figure 5.5). We recognize that residual properties should be computed for the entire column. In order to evaluate whether this limited spatial range of the water column would influence our results, we computed residual velocities (method described in Section 6.1) in both sigma and z-coordinates. We used velocities generated in sigma coordinates by the 3D-circulation model and velocities interpolated to z-coordinates from the model results. We selected sigma coordinates for comparison because they capture the free surface through expansion and compression of the vertical dimension. As shown in Figure 5.6, the differences between the two coordinate systems are on the order of millimeters. Although the model does not have as much vertical structure as the field (Figure 4.2) and the height

of water column is under-represented, the minimal differences indicate the z-coordinate system used by the ADP is sufficient for analysis of residual velocities in the spatial range of measurement.

Since the ADP measures the water column in z-coordinates, the profiling range cannot be adjusted as the water surface fluctuates with the tides. As a result, velocities are recorded above the water surface when the profiling range is not always entirely in the water column. For the residual velocity calculations, it is necessary to decipher where the water surface is relative to the number of bins in the profiling range in order to avoid using data recorded outside the water column. We used pressure data from the ADP to calculate the height of the water column (Fofonoff and Millard, Jr., 1983) above each instrument at every time interval. The surface bin was then determined to be one meter below this height (SonTek, 1997a) at every time interval and only data from bins that remained submerged throughout a given month were used in the residual velocity calculations.

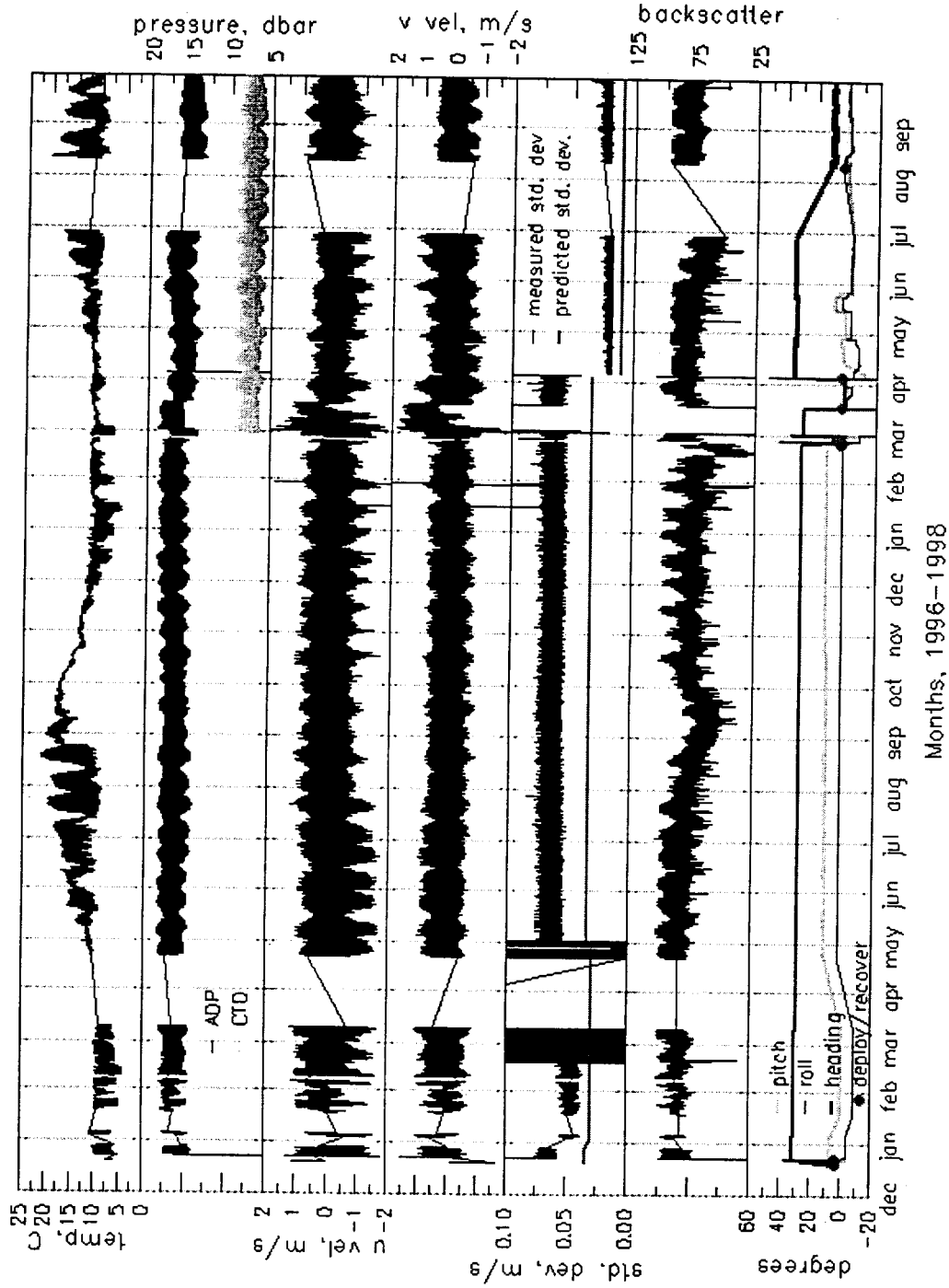

Figure 5.1. Hydrologic and instrument orientation variables recorded by the ADP from December 1996 through September 1998 at station Red26.

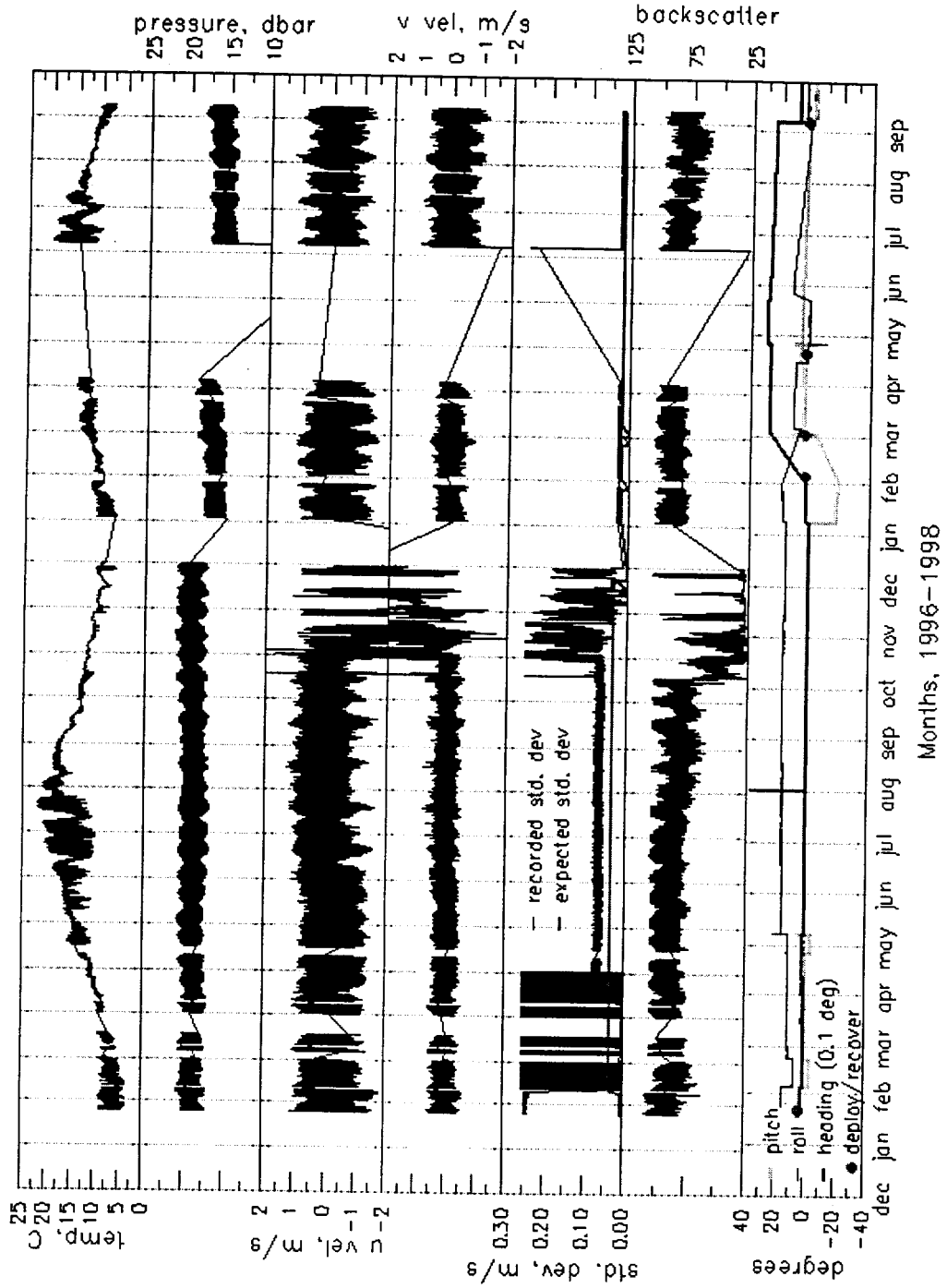

Figure 5.2. Hydrologic and instrument orientation variables recorded by the ADP from January 1997 through September 1998 at station Am169.

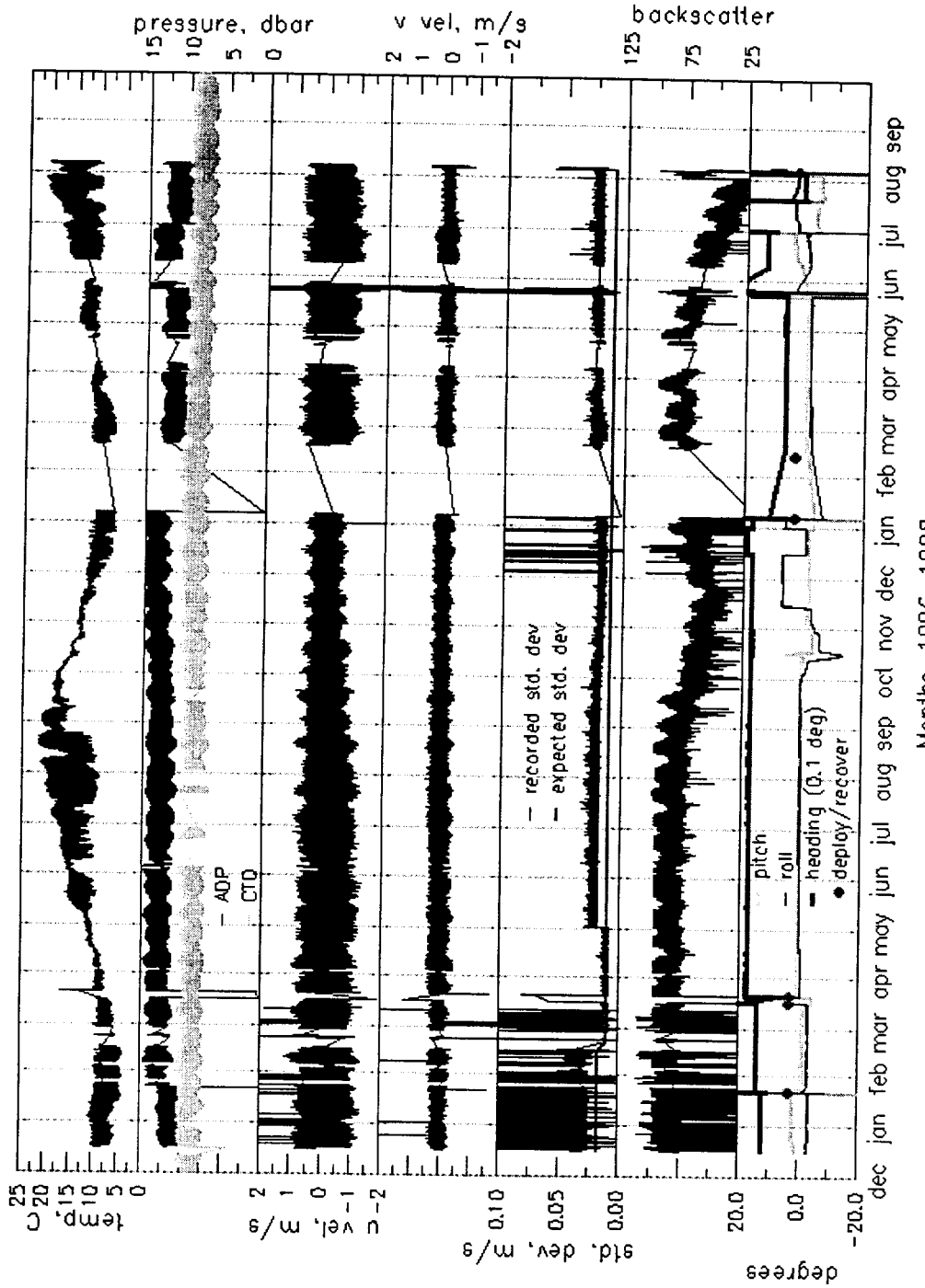

Figure 5.3. Hydrologic and instrument orientation variables recorded by the ADP from December 1996 through September 1998 at station Tansy.

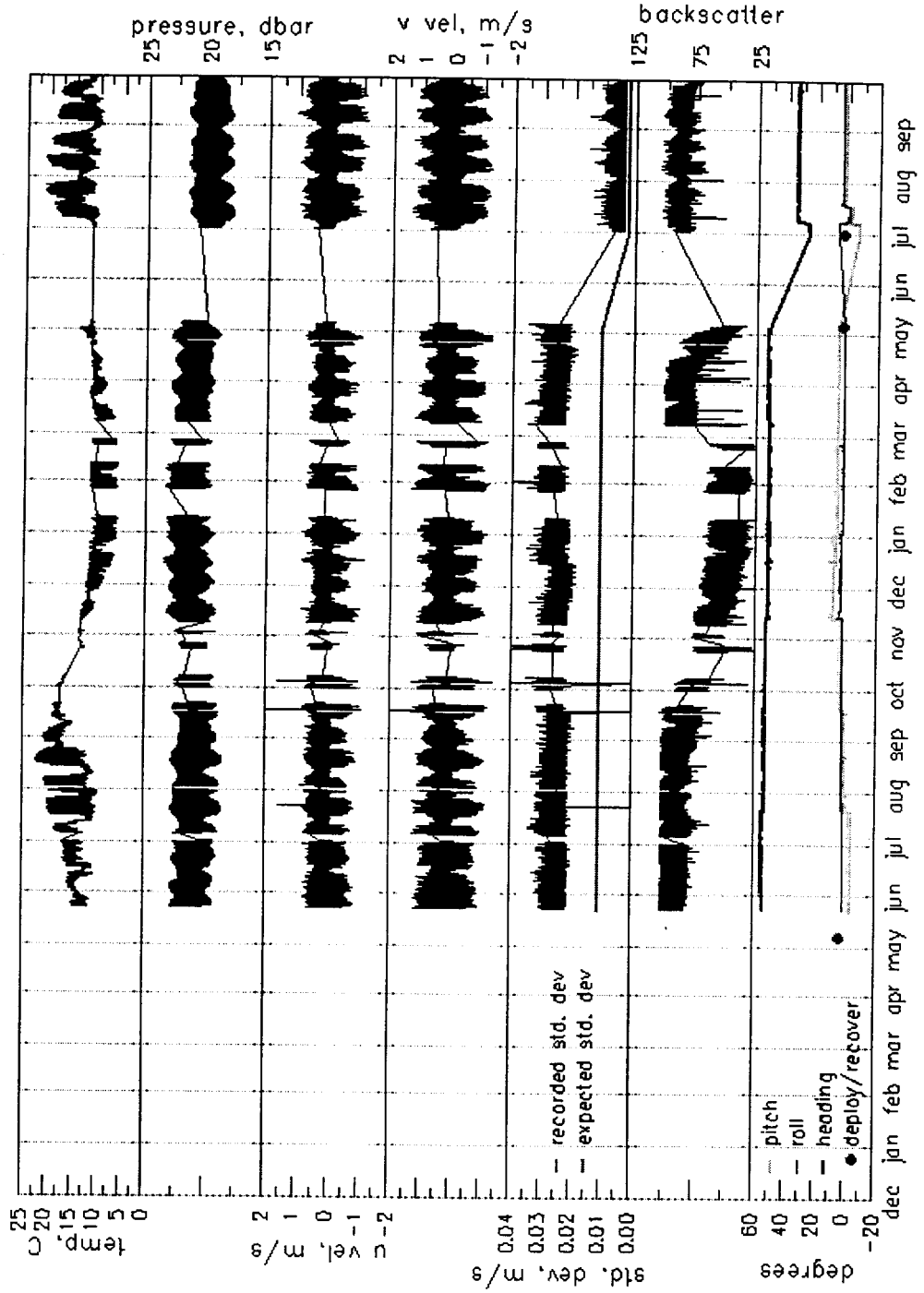

Figure 5.4. Hydrologic and instrument orientation variables recorded by the ADP from May 1997 through September 1998 at station Am012.

Table 5.1. Red26 ADP observations for time periods marked by missing data records or unusual behavior.

DATE	OBSERVATIONS	REASON	COMMENTS
12/23/96		Deployed/ recovered	
12/26/96		Deployed	
12/28 - 1/4/97	Gap in data		
1/4/97	Predicted and measured std. deviations are slightly smaller	Cell size increased from 50 to 60 cm	Larger cell size = smaller std. deviation
1/5 - 1/18/97	Gap in data		
1/18 - 2/6/97	Unusual data for all variables		
2/6 - 2/9/97	Gap in data		
2/18/97		ENU to beam coordinates	
2/18 - 3/10/97	Spiky std. deviation	ENU to beam coordinates	
2/19 - 2/21/97	Drop in backscatter		
3/11 - 4/21/97	Gap in data		
4/21/97	Measured std. deviation is smaller		
4/21 - 5/1/97	Spiky std. deviation		
5/1/97	Spikes end in std. deviation Predicted and measured std. deviations are larger	Beam to ENU coordinates, cell size decreased to 50 cm	Corrected bad idea, smaller cell size = larger std. deviation
8/1 - 9/30/97	Gradual decrease then increase in backscatter data	Biological growth on sensors	Biofouling affects signal strength
2/15 -3/2/98	Drop in backscatter, then sharp increase		
2/24/98		Recovered	
2/26/98	Shifts in pressure, heading, pitch and roll	Deployed	Shallower location
3/2 - 3/18/98	Shifts in all variables, then unusual data	ADP on its side	
3/18/98	Pressure shift	Recovered/deployed	Shallower location
4/5/98	Shifts in pressure, predicted and measured std. deviations are smaller	Recovered/ deployed with new instrument (1500 hz) and new firmware, cell size decreased to 25 cm	Shallower location, larger frequency = smaller std. deviation, has more impact than decrease in cell size
4/23 - 4/25/98	Gap in data	Existing port failed	
6/98	Gradual decrease in backscatter	Biological growth on sensors	Biofouling affects signal strength
6/28- 8/10/98	Gap in data	ADP reset itself, had date problem	
8/10/98		Recovered/deployed	

Table 5.2. Am169 ADP observations for time periods marked by missing data records or unusual behavior.

DATE	OBSERVATIONS	REASON	COMMENTS
1/21/97		Deployed	
1/22/97		Recovered/deployed	
1/24 - 2/8/97	Large velocities and std. deviation	XYZ coordinates, ave interval = 100 seconds	Shorter ave. interval records more noise
2/5/97	Shift in heading, pitch, roll		
2/8 - 2/10/97	Gap in data		
2/10/97	Predicted std. deviation shifts up, measured std. deviation shifts down	Cell size lowered from 400 to 50 cm, ave int. increased to 5 minutes, ENU to beam coordinates,	Smaller cell size = larger std. deviation, but larger averaging interval = smaller std. deviation
2/10-5/1/97	Spiky data for std. deviation	ENU to beam coordinates	
2/18/97	Gap in data		
2/22/97	Shift in pitch and roll		
3/2 - 3/7/97	Gap in data		
3/9 - 3/12/97	Gap in data		
3/18 - 4/1/97	Gap in data		
4/8 - 4/10/97	Gap in data		
4/26/97	Shift in pitch		
5/1/97	Shift up in std. deviation and spiky data ends	Beam to ENU coordinates	Corrected bad idea
5/7/97	Shift in heading, pitch, roll		
5/11 - 5/17/97	Gap in data		
8/1/97	Spike in heading	Attempt to lift ADP	
11/15 - 11/18/97	Unusual backscatter data	Sand covering sensor	
11/18 - 11/20/98	Drop in backscatter, unusual velocities and std. deviation	Sand covering sensor	
11/20/98	Spike in backscatter, velocities and std. deviation	Sand covering sensor	
11/31/97 - 1/31/98	Unusual behavior in all data, but pressure	Tilted and buried in sand	
1/9/98	Shifts in heading and pitch	Attempt to recover ADP	
1/31/98		Attempt to recover ADP	
2/2/98		Recovered	
3/2/98	Shift in pressure data, smaller predicted and measured std. deviation	Deployed with new firmware, cell size increased to 100 cm	Shallower location, larger cell size = smaller std. deviation
3/3 - 3/6/98	Shifts in pitch and roll		
3/28 - 4/2/98	Gap in data		
4/15/98	Shift in pitch		
4/26/98	Shifts in pitch and roll		
5/22 - 5/26/98	Gap in data		
6/5 - 8/2/98	Gap in data	Cable malfunction	
8/2/98		Recovered	
9/6/98	Pressure shift	Deployed instrument with new frame	Shallower location
10/11 - 10/12/98	Gap in data	ADP power cycling	
10/25 - 10/27/98	Gap in data		
12/2 - 12/3/98	Shift in pitch		

Table 5.3. Tansy ADP observations for time periods marked by missing data records or unusual behavior.

DATE	OBSERVATIONS	REASON	COMMENTS
12/16/96		Deployed	
12/96	Spiky backscatter and std. deviation		
1/22/97	Shift in pressure data	Recovered/deployed	Deeper location
1/24 - 1/27/97	Gap in data		
1/97	Spiky backscatter and std. deviation, some spikes in u-vel		
2/4/97	Gap in data		
2/5 - 2/6/97	Gap in data		
2/17 - 2/22/97	Gap in data		
2/21/97	Predicted and measured std. deviation are smaller	Ave interval increased from 2 to 5 min, ENU to beam coordinates	Higher ave interval = smaller std. deviation
2/23 -2/27/97	Gap in data		
3/12/97	Spiky std. deviation and backscatter ends		
3/17/97		Recovered	
3/21/97		Deployed	
4/3 - 4/4/97	Gap in data		
4/20/97	Gap in data		
5/1/97	Shift up in std. deviation	Beam to ENU	Corrected bad idea
6/3 - 6/7/97	Gap in data		
9/1/97 - 1/7/98	Gradual increase in pressure, gradual decrease in velocity range and backscatter	ADP instabilities, possible biological growth on sensors	Biofouling affects signal strength
10/12 - 10/18/97	Pitch and roll variations		
11/12 - 11/14/97	Roll variations		
12/97	Spiky std. deviation and backscatter		
12/16/97	Shift in roll and heading		
12/28 - 1/7/98	Oscillations at every sample in backscatter data		
1/7/98		Recovered	
2/13/98	Shift in pressure data	Deployed	Shallower location
3/20/98		New firmware upgrade	
4/1 - 4/2/98	Gap in data		
4/7 - 4/19/98	Gap in data		
4/19 - 4/22/98	Gap in data		
4/24 - 4/26/98	Gap in data		
5/1 - 8/1/98	Gradual decrease	Biological growth on sensors	Biofouling affects signal strength
5/22 - 5/25/98	Shifts in pressure, heading, pitch and roll, unusual velocity		
5/26/98	Gap in data		
5/27 - 6/8/98	Gap in data		
6/8 - 8/31/98	Gradual decrease in backscatter, variations in instrument orientation	Biological growth on sensors	Biofouling affects signal strength ADP shifts may affect velocities
6/30/98	Shift down in pressure		
8/1/98	Shift up in backscatter		
8/4 - 8/6/98	Shifts in all data	Diver operations on 8/4	
8/6/98		Recovered/deployed ADCP	

Table 5.4. Am012 ADP observations for time periods marked by missing data records or unusual behavior.

DATE	OBSERVATIONS	REASON	COMMENTS
5/7/97		Deployed	
7/1 - 7/6/97	Gap in data		
7/31 - 8/3/97	Gap in data		
9/16 - 9/17/97	Gap in data	Network problem	
9/21 - 9/30/97	Gap in data		
10/1/97 -3/8/98	Gradual decrease in backscatter	Biological growth on sensors	Biofouling affects signal strength
10/3 - 10/4/97	Gap in data		
10/8-10/23/97	Gap in data	Power outage/date problem; reset on 10/23	
10/27-11/2/97	Gap in data	Problem with radio link	
11/3 - 11/9/97	Gap in data	Problem with radio link	
12/15/97	Shift up in std. deviation		
1/11 - 1/27/98	Gap in data	Computer not operative, box removed 1/20, replaced 1/27	
2/11 - 2/22/98	Gap in data		
2/26 - 3/8/98	Gap in data		
4/24 - 4/26/98	Gap in data		
4/16 - 5/6/98	Backscatter sharply decreasing	Biological growth on sensors	Biofouling affects signal strength
5/6/98		Recovered; heavily fouled	
7/1/98	Predicted and measured std. deviations are smaller	Deployed with new firmware & antifouling, cell size increased from 25 to 100 cm	Possible shift in pressure, larger cell size = smaller std. deviation
10/4 - 11/5/98	Backscatter drops off		
10/7-10/18/98	Gap in data		
10/8-10/12/98	Gap in data	Power interruption	
11/25-11/28/98	Gap in data	Power interruption	

Table 5.5. Summary of the evaluation of ADP data the four reference stations. Data is evaluated in terms of usable (good), unusable (bad), and insufficient(lack of) for computing residual velocities.

		Red26			Am169			Tansy			Am012	
	Good	Bad	Lack of	Good	Bad	Lack of	Good	Bad	Lack of	Good	Bad	Lack of
Dec			X			X	X					X
Jan			X			X	X					X
Feb	X			X			X					X
Mar	X			X			X					X
Apr	X			X			X					X
May	X			X			X			X		
Jun	X			X			X			X		
Jul	X			X			X			X		
Aug	X			X			X			X		
Sep	X			X			X			X		
Oct	X			X				3				X
Nov	X				2			3		X		
Dec	X				2			3		X		
Jan	X				1,2				X			X
Feb		1							X			X
Mar		1		X			X			X		
Apr	X			X					X	X		
May	X			X			X					X
Jun	X					X		3				X
Jul			X			X		3		X		
Aug			X			X			X	X		
Sep			X	X					X	X		

Legend:
1 ADP on its side
2 ADP buried in the sand
3 ADP unstable

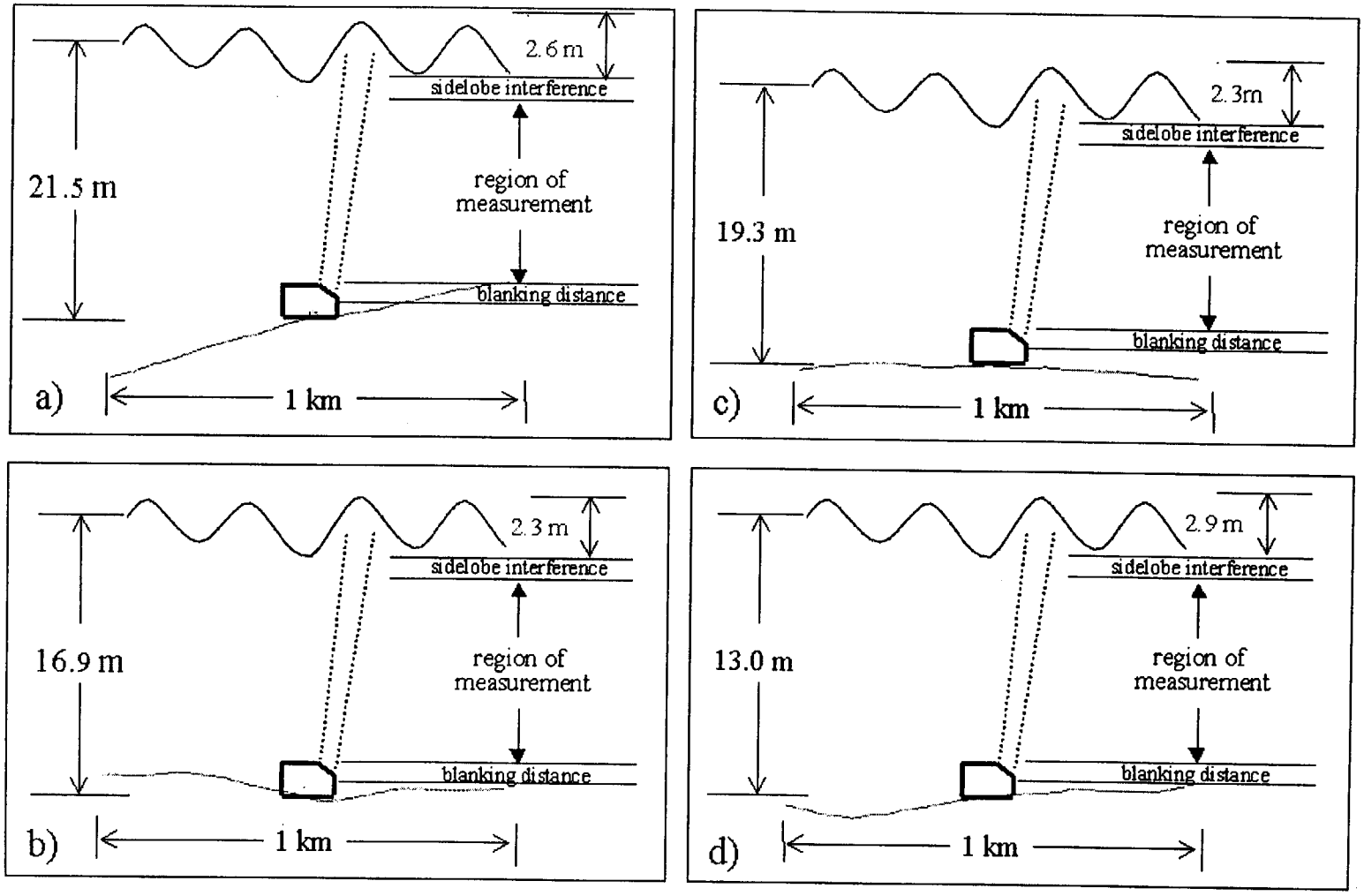

Figure 5.5. Vertical profile of ADP's situated on the channel bed at each station. a) Am012. b) Red26, c) Am169, d) Tansy. (Scale applies to bed topography only.)Schematic based on SonTek, 1997.

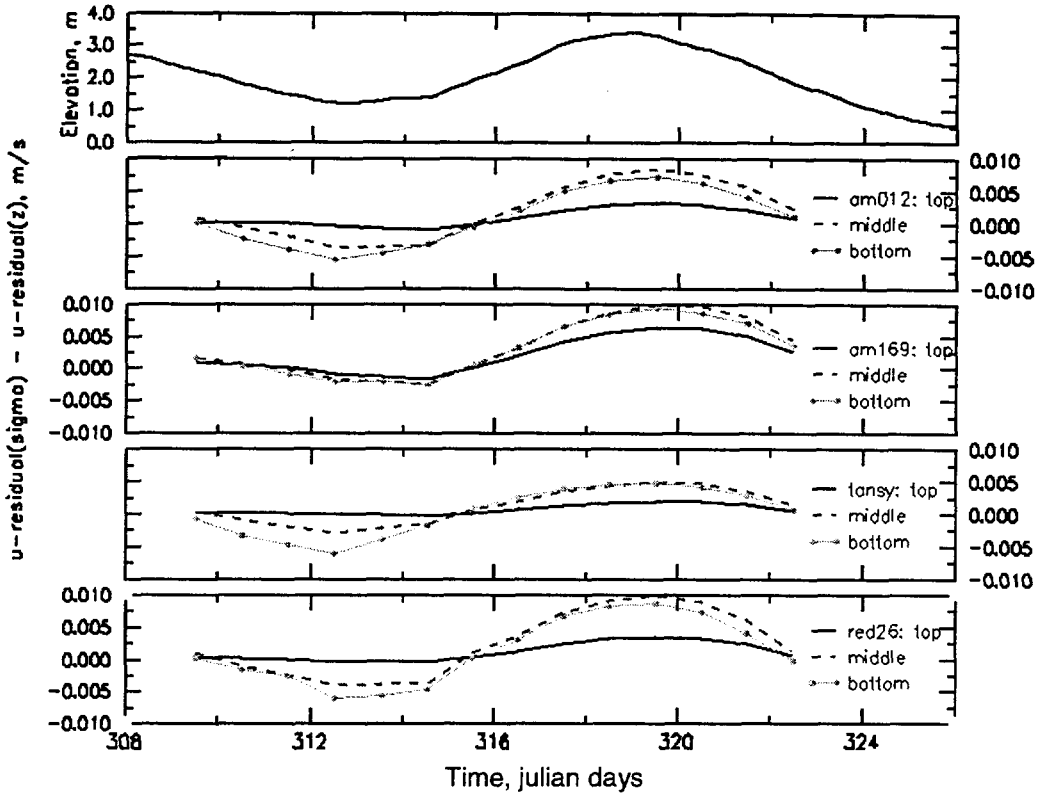

Figure 5.6. Differences in along-channel residual velocities computed in sigma and z-coordinates. The residual velocities were calculated over a 1-tidal cycle averaging period for July 1997 using the results of the 3D-circulation model (QUODDY). The residual velocities were downstream (negative) for the time period shown, which means the values computed in sigma-coordinates are higher in the downstream direction on ebb and smaller in the downstream direction on flood.

Residual Circulation

Residual circulation inside the Columbia River estuary is mainly caused by the interaction between tidal forcing and river flow, with wind having a less significant role. Therefore, variability of residual currents is largely attributed to variability of both tides and river flow. Theoretical analysis of the generation of residual circulation in the Columbia River estuary has been performed using both analytical (Jay and Smith, 1990a,b) and numerical models (Hamilton, 1990). Jay and Smith (1990a,b) explored the role of ebb-flood asymmetry in the generation of residual circulation and their analysis showed that the character of residual circulation varies with the degree of stratification in the estuary, a direct indication of the variability of tides and river flow.

Tidal variability at the monthly scale was further explored in Jay and Smith (1990c) by computing mean flow and salt transport for spring and neap tides using data collected from two field programs in the Columbia River estuary. Model simulations performed by Hamilton (1990) confirmed the results of Jay and Smith (1990c) and provided insight into the spatial variability of net flow in the channels. We will compare the results of Jay and Smith (1990c) and Hamilton (1990) with our daily time scale analysis to show both similarities and differences in observed trends (Section 6.2.1.3)

Our analysis of residual circulation will be substantially more empirical and oriented towards a broader range of scales of variability. The analysis will be based on CORIE ADP observations between December 1996 and September 1998 at four reference stations (Figure 1.1) and on 2D depth-averaged flow simulations. Because this represents the first systematic use of the CORIE ADP data set, an evaluation of the data quality was necessary (Section 5).

6.1 Evaluation of Residual Velocities

The eulerian residual current is defined here as the net excursion over the integration period divided by the integration period. Mathematically, the eulerian residual current is defined by the equation (Heaps, 1978; Alfrink and Vreugdenhil, 1981):

$$\vec{V}_{er} = \frac{1}{T}\int_{t_o}^{t_o+T} \vec{V}\left(\vec{X}_o, t'\right)dt' \tag{6.1}$$

where T is the integration period, $\vec{V}\left(\vec{X}_o, t'\right)$ is the velocity at position $\vec{X}_o$, and t′ varies from t_0 to $t_0 + T$. A discrete version of equation (6.1) was used in our calculations of residual velocities using the equation (Cheng, 1988):

$$\vec{V}_{er} = \frac{1}{T}\sum_{i=0}^{N} \vec{V}\left(\vec{X}_o, t_i\right)\Delta t \tag{6.2}$$

where Δt =300 seconds, $t_i = t_o + i\Delta t$ and $N = T/\Delta t$. We computed along-channel residual velocities to explore the variability of net flow in the upstream and downstream directions. We did not concentrate on cross-channel residual velocities because the estuary is long and narrow relative to its width, and consequently cross-channel circulation is relatively small compared to along channel circulation. To adjust for the along-channel direction we multiplied equation (6.2) by cosine (θ); where

$$\theta = \tan^{-1}\left(\frac{V_{er_y}}{V_{er_x}}\right) - \alpha\left(\vec{X}_o\right) \tag{6.3}$$

and $\alpha\left(\vec{X}_o\right)$ is the angle of the channel at each station location.

In order to explore multiple time scales, different integration periods (T) were used: 24.8 hours (~1 day), 173.6 hours (~7 days) and 719.2 (~30 days). We used a running residual to compute residual velocities by advancing the integration period (integration window) in one-hour increments. We then recorded the residual velocity at the middle of the window. For the 1-day and 7-day averaging periods, we set a 5% and 10% limit, respectively, over the integration period to avoid averaging data over large time gaps. Therefore, if the time between the first and last data record in the integration period was greater than 5(10)% of the integration period, the residual velocity for that window was discounted. Although this approach allowed for better residual velocity calculations, it caused gaps in the results (to be shown in the Section 6.2). For the 1-month averaging period, the number of sets (N) was reduced by the number of data records that were discounted for too large or too small Δt's and T was recomputed with the modified N value.

Numerical residual velocities were calculated using equations (6.2) and (6.3) from the flow fields generated by the 2D circulation model that were used for the residence time calculations. Residual velocities were computed at every node in the finite-element grid. In order to evaluate the numerical results with the field data, we selected residual velocities computed at the nearest node in the finite-element grid that coincide with the four ADP reference stations. Since the model results are depth-averaged, our goal was not to make quantitative comparisons, but to assess whether the model yielded similar trends at different spatial and temporal scales.

6.2 Results

We calculated residual velocities for all months not discounted during the data selection stage. However, we will focus our analysis here on June and July of 1997 because these months have contrasting flow conditions and usable data at all four stations (Table 5.1). Consequently, residual velocities were analyzed for both temporal and spatial variability. Using the along-channel direction for reference, positive residual velocities

represent upstream (land-ward) flow and negative residual velocities represent downstream (ocean-ward) flow.

6.2.1 Analysis Based on ADP Data

6.2.1.1 Seasonal Time Scale

Residual velocities averaged over a 1-month period provide insight into the overall contribution of river flow and tides to the net flow. The results for June of 1997 indicate the contribution is highly channel specific. In the South channel, (Red26, Tansy, Am169) the magnitude of downstream velocities ranges between 0.2 - 0.8 m/s in the water column, whereas in the North channel, the magnitude of downstream velocities ranges from 0.0 - 0.35 m/s and the magnitude of upstream residual velocities ranges from 0.0 to 0.2 m/s in the upper three-quarters and bottom one-quarter of the water column (measured from the ADP), respectively (Figure 6.1a). The differences between the channels are primarily caused by more river flow conveyed through the South channel. As a result, the South channel is more river dominated, thereby inhibiting contribution of upstream tidal advection. The North channel is less river dominated, therefore, the contribution of upstream tidal advection to the residual flow is stronger.

Although river flow averages $200x10^3$ cfs less in July than in June of 1997 (Figures 6.2a and 6.3a), the South channel remains primarily river dominated. Downstream residual velocities occur throughout most of the water column and only Red26 and Am169 have any upstream bottom flow (Figure 6.1b). Tansy is mostly uniform throughout the water column and does not respond to changes in river flow conditions because its shallow location (just outside the main channel) is less influenced by tides and river flow. The North channel is strongly affected by the decreased river flow since upstream bottom flow is larger and extends to one-half of the water column. Although the downstream residual velocities in both channels are smaller during the lower river flow conditions of July, the results indicate the North channel is more

sensitive to seasonal variability in river discharge. This may seem less intuitive, because one might expect that the magnitude of variability should scale with the magnitude of river influence. The seasonal effect of river discharge is more pronounced in the North channel in the sense that decreased river flow leads to higher neap-spring variability. During spring tides, strong tidal currents on flood and ebb cause a well-mixed vertical structure, whereas during neap tides, weaker tidal currents lead to stratified conditions. Therefore, the vertical profile of long-term residual flow computed over neap and spring tides reflects both the stratified and mixed conditions that occur in over the monthly tidal cycle.

Since the region of measurement by the ADP does not extend to the riverbed or to the free surface, therefore, the values in the ADP's "blind-spots" may not be fully represented in our results. Specifically, the regions outside the limits may have higher downstream velocities at the surface, and higher upstream velocities along the channel bottom. However, the contrasts between the two channels are clearly captured in the region of the water column shown in Figure 6.1, indicating the available data provides a good representation of the water column at each station.

6.2.1.2 Monthly Time Scale

Residual velocities calculated over a 7-day averaging time period afford more insight into the stability of net flow than the 1-month averaging period. Histograms were selected to provide quantitative analysis about the stability of residual velocities. We used four bins in our analysis to represent the lowest depth recorded by the ADP, ¼ and ¾ of the depth away from the instrument, and the uppermost submerged bin for the given month.

The 7-day averaging period for June 1997 (Figure 6.4) indicates net flow in the South channel is strongly controlled by river flow since all South channel stations have

land-ward velocities throughout the water column, and the values are mostly stable. In the upper depths, more than fifty percent of the residual velocities at these stations are centered on one value. In contrast, the North channel is affected by both tides and river flow since the histograms show residual velocities at Am012 are both positive and negative and are not concentrated around any particular value throughout the water column. Although the stability of residual velocities may be greater at the free surface and at the channel bottom, where data is not available, the residual velocities in the region of measurement clearly illustrate that uniformity is spatially sensitive in both the vertical direction of the water column and horizontally in the domain.

The histograms for July 1997 also capture the unequal distribution of river flow in the channels (Figure 6.5) observed for the high flow conditions. The South channel exhibits uniformity near the surface whereas the North channel is not stable. In addition, the residual velocities remain negative in the South channel except for the bottom-most bin and the residual velocities remain positive in the North channel for both lower bins. The results indicate that tidal variability is mostly dampened in the South channel over a long averaging period under both high and low flow conditions, whereas tidal variability is evident in the North channel under both flow conditions.

6.2.1.3 Daily Time Scale

Residual velocities averaged over a 1-day period (24.8 hours) capture changes associated with river flow and tides that were not apparent for the longer averaging periods. For example, both channels show response to variable river discharge into the estuary. The increases in river flow in June (Figure 6.2a) cause magnified downstream flows in the upper depths of the water column at Am012, Am169 and Red26 (Figure 6.6a), with the exception of Tansy. Similarly, decreases in river flow cause diminished downstream flows in the upper depths at the same stations.

The 1-day residual velocities also capture neap-spring variability. The variability is more pronounced in the North channel and is more pronounced in both channels during the lower river flow conditions of July. During a high flow month, conditions are weakly stratified on neap tides in the South channel. There is no upstream net flow, but the weakest downstream residual velocities (Figure 6.6a) coincide with neap tides (Figure 6.2a). In the North channel, however, stratification is apparent during neap tides with strong land-ward velocities (0.2 - 0.3 m/s) occurring in the lower layers of the water column (Figure 6.6a). High river flow and increased mixing during spring tides causes the stratification to break down and the along-channel circulation is ocean-ward throughout the water column for both channels.

During the lower river flow conditions of July, the residual velocities are approximately half as large in the upper depths for Red26, Am169 and Am012 (Figure 6.6b). The South channel experiences land-ward residual velocities in the lower layers during neap tides and ocean-ward residual velocities throughout the water column during spring tides. Variability is similar for the North channel, but land-ward residual velocities are present throughout the month with the strongest values (0.1 - 0.4 ms/s) during neap tides. The upstream residual velocities extend higher into the water column and are present throughout the month because less river flow is directed into the North channel, thereby causing even less mixing during a low flow month. The variability of the 1-day residual velocities in the South channel compare with 50-hour averages computed by Jay and Smith (1990) and Hamilton (1990) at South channel stations for a low flow month. As listed in Table 1 (Jay and Smith, 1990), upstream bottom flow was present near the mouth and upstream of Am169 during a neap tidal period and downstream flow was predominant during a spring tidal period. Similarly, Hamilton's results show upstream residual flow near the locations of Am012 and Am169 on neap tides and downstream residual flow near Red26 on spring tides.

Our results for July 1997 also show differences between the South channel stations of Am169 and Red26. Land-ward residual velocities persist throughout the

month at Am169 and not at Red26, and land-ward residual velocities are higher during neap tides at Am169 (Figure 6.2b). The residual velocities computed for the remaining low flow months of 1997 (August - November) consistently show these differences between the two stations. The differences were also observed in Hamilton's (1990) model results (Figure 8). For the low flow month of October 1980, upstream residual flow was present on both spring and neap tides at a location similar to Am169, and was not present on spring tides at a location similar to Red26. As shown in Figure 5.5, Am169 is located in a deeper section of the channel. Whereas tidal flow causes vertical variations of residual velocities, topography, bottom friction, stratification and pressure gradients influence the spatial variability of residual velocities (Jay and Smith, 1990).

In terms of seasonal variability of neap-spring transitions, our results contrast the analysis presented by Jay and Smith (1990). Our computations of residual velocities for both channels indicate higher and more extensive land-ward residual flow is apparent during low river flow conditions, whereas their analysis indicates upstream residual flow is more apparent during the high flow season when conditions are stratified over the month. Our comparison of high and low flow months was based on average river flows of 500 and 275x103 cfs, respectively, while the analysis of Jay and Smith (1990) was based on 1980 and 1981 conditions which had much less average flows (Figure 2.1). We verified our conclusions are representative of seasonal variability for the length of ADP deployment by comparing residual velocities calculated for other flow conditions. Again, our results indicated land-ward residual velocities are more pronounced on neap tides during low flow months.

6.2.1.4 Interannual Time Scale

The 1997-98 El Niño has significantly impacted the Pacific Northwest, as marked by increased sea-surface temperatures, warmer air temperatures, less precipitation and decreased snowpack in the winter. These effects are evident in the spring of 1998, in which the maximum river flow was $125x10^3$ cfs lower than the previous year (Figure

2.2). To explore how El Niño influenced the Columbia River estuary we compared residual velocities computed with a 1-day averaging period for May of 1997 and 1998. As discussed earlier, the ADP's were situated in slightly different locations upon re-deployment, prior to May 1998. Although the other variables recorded by the ADP's did not seem affected by the location change, we considered it another difference between the two time periods.

As shown in Figure 6.7, May of 1997 represents a high flow month and May of 1998 represents a low flow month. Therefore, El Niño effects in the South channel mirror the decrease in flow conditions observed from June to July 1997. The residual velocities are smaller in the downstream direction in May of 1998, but the South channel remains river dominated. The only upstream residual velocities in May of 1998 occur at Red26 (Figure 6.7b), because its location is more tidally influenced. The shallower ADP locations in 1998 do not show any patterns in the residual velocities not observed in the low flow month of July 1997, which verifies that location did not influence the comparisons. The results illustrate how the South channel is always river dominated even when the spring following an El Niño winter (warm and dry) yields decreased snowmelt and much less runoff. CORIE has therefore proven to be a useful tool in both strengthening and enhancing our knowledge of how the Columbia River estuary responds to climate effects.

6.2.2 Analysis Based on Model Results

We calculated residual velocities using hindcast flow fields based on the 2D-circulation model ADCIRC, with the same time averaging periods used in the analysis of ADP data. As mentioned earlier, flow patterns are strongly affected by the physical features in the estuary. This is clearly illustrated in the depth-averaged residual velocities (Figure 6.8a) in which the main navigation South channel and North channel have the highest residual velocities (0.5 - 0.7 m/s), the lateral bays and tidal flats have the lowest values (0.0 - 0.1 m/s) and the lateral channels fall in between. The model also captures

the sensitivity of net flow to seasonal variability in which the residual velocities are approximately half as large for a low flow month (Figure 6.8b).

We compared the simulated depth-averaged residual velocities with CORIE data for the 1-month and 7-day averaging periods. At the seasonal scale, the modeled values show the same contrasts between the two channels (to a lesser degree) and the same trend of decreased downstream residual velocities for a low flow month (Figures 6.1a-b). Similarly, the histograms for June and July of 1997 show a distinction between the two channels and a similar trend between high and low months (Figures 6.4a and 6.5a), but again to a lesser degree. The model weakens the strong contrasts between the two channels that is depicted in the field data largely because the lack of a vertical structure in the model. However, the depth-averaged residual velocities are both qualitatively and quantitatively similar to the field data, for both averaging periods and for the four reference stations.

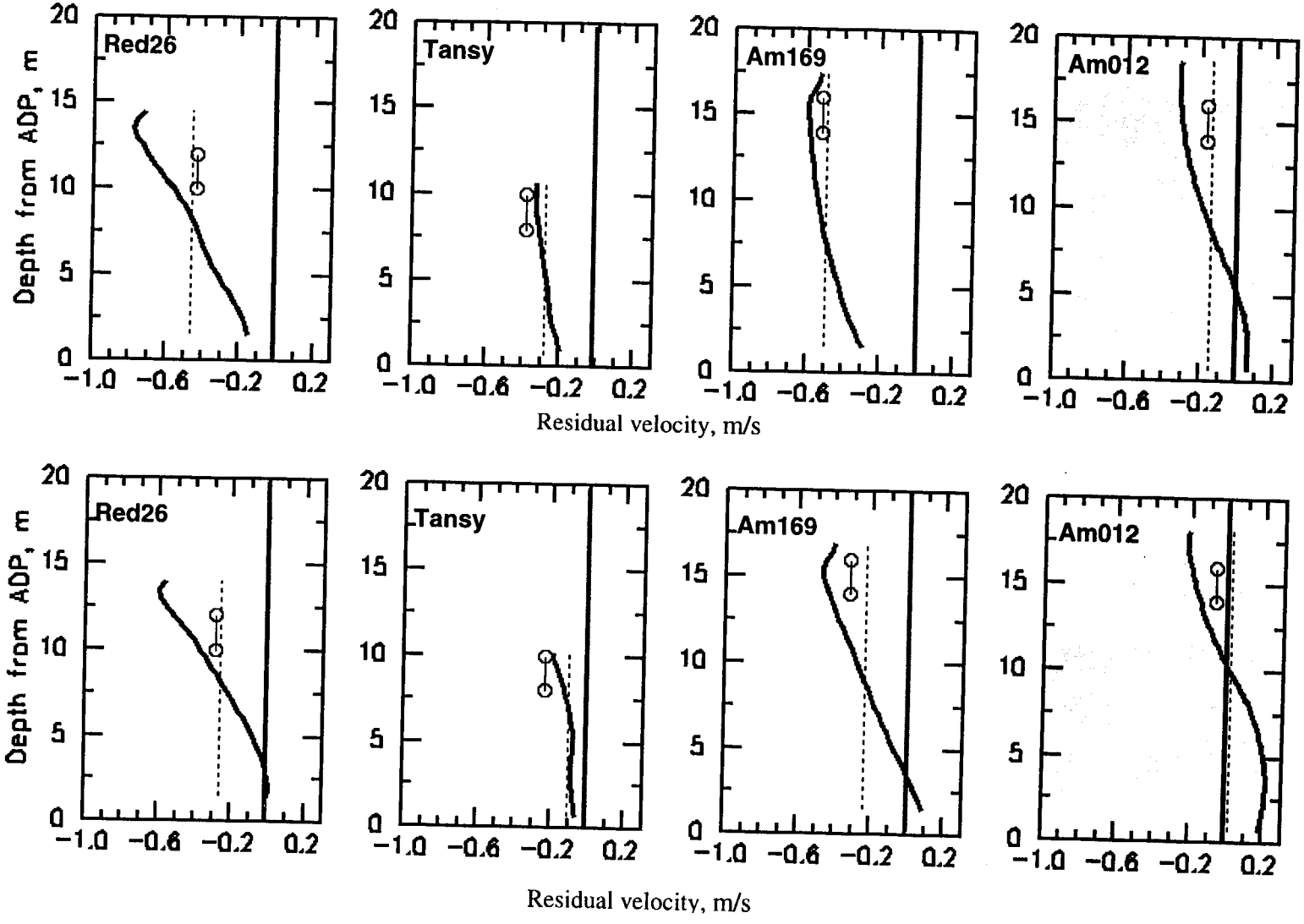

Figure 6.1. Along channel residual velocities over a 1-month period at the 4 reference stations. a) June 1997, b) July 1997. The lines symbolize: — ADP data; --- average ADP data; o—o model. The mean residual velocity computed from the field data is shown to compare with the depth-averaged model results

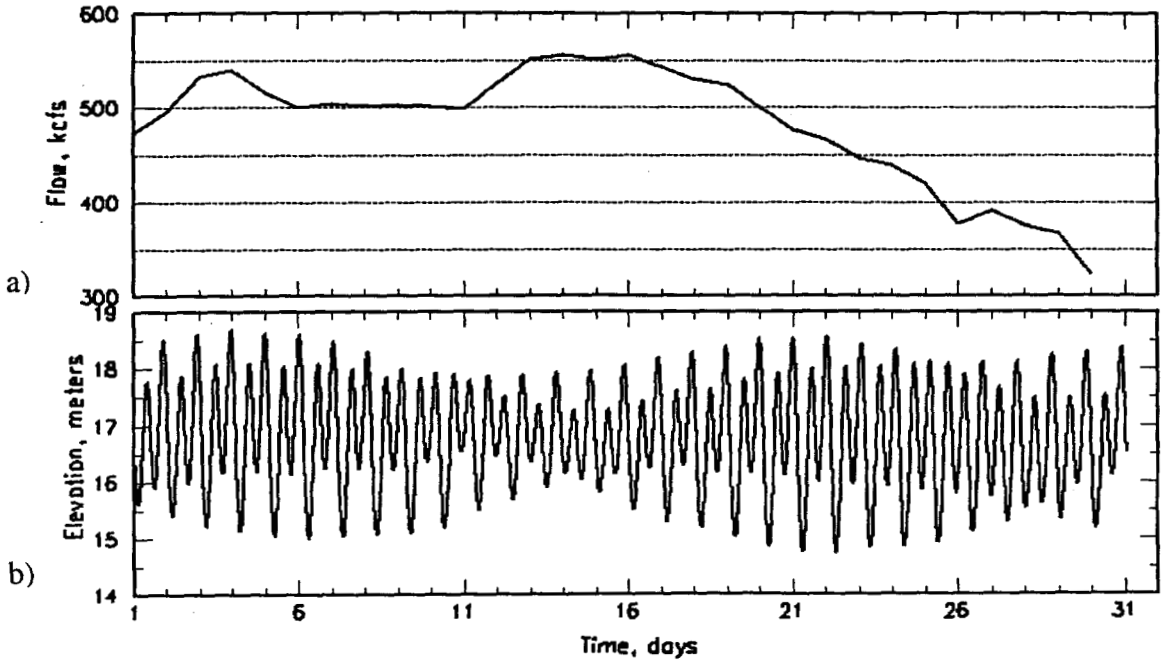

Figure 6.2. River flow (a) and tidal elevations (b) for June 1997. River flow extracted from Figure 2.2; elevations recorded at Am169.

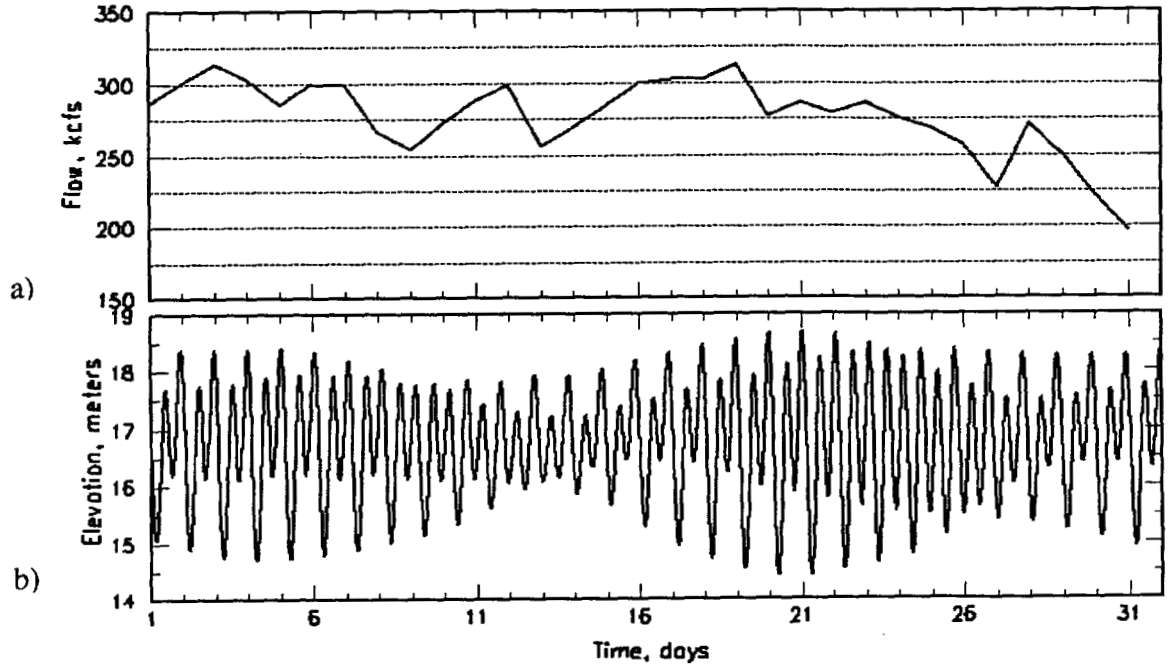

Figure 6.3. River flow (a) and tidal elevations (b) for July 1997. River flow extracted from Figure 2.2; elevations recorded at Am169.

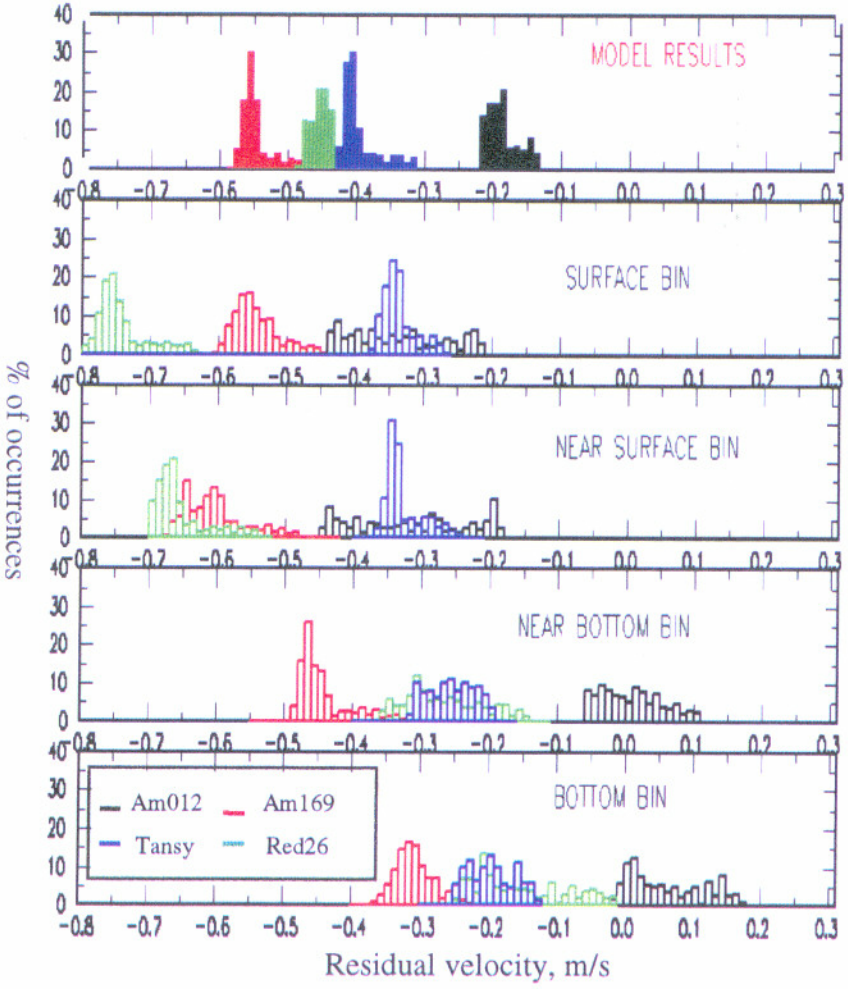

Figure 6.4. Along channel residual velocities over a 7-day period at the four reference stations for June 1997. a) model results; b-e) ADP stations at four depths in the water column.

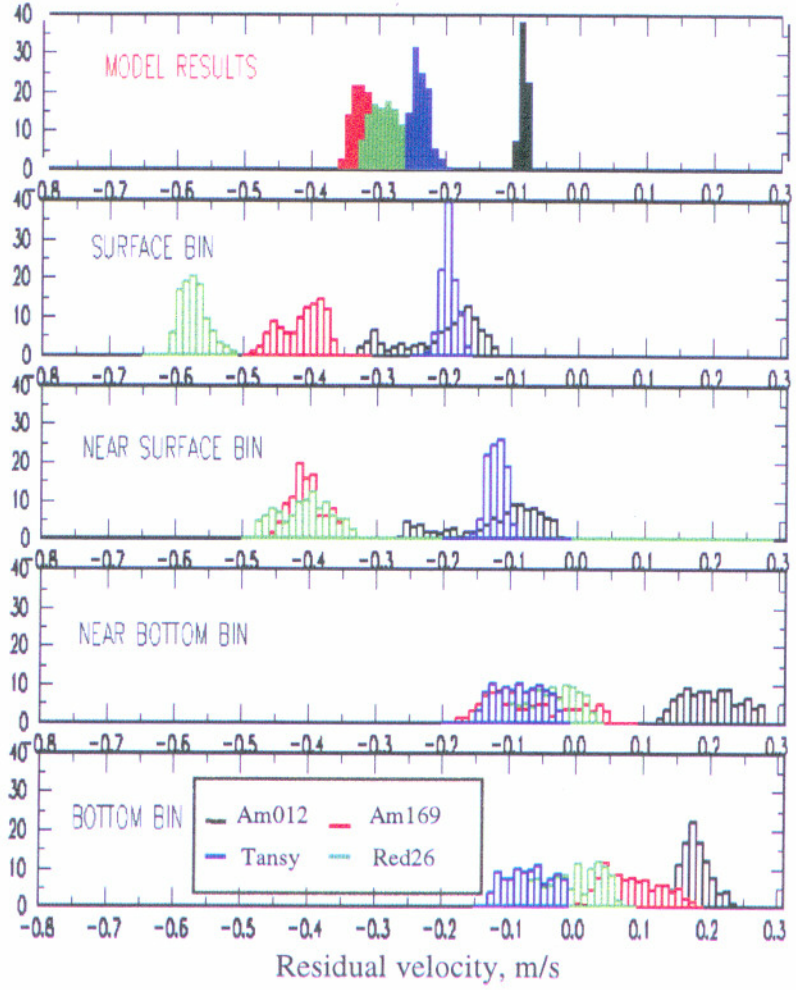

Figure 6.5. Along channel residual velocities over a 7-day period at the four reference stations for July 1997. a) model results; b-e) ADP stations at four depths in the water column.

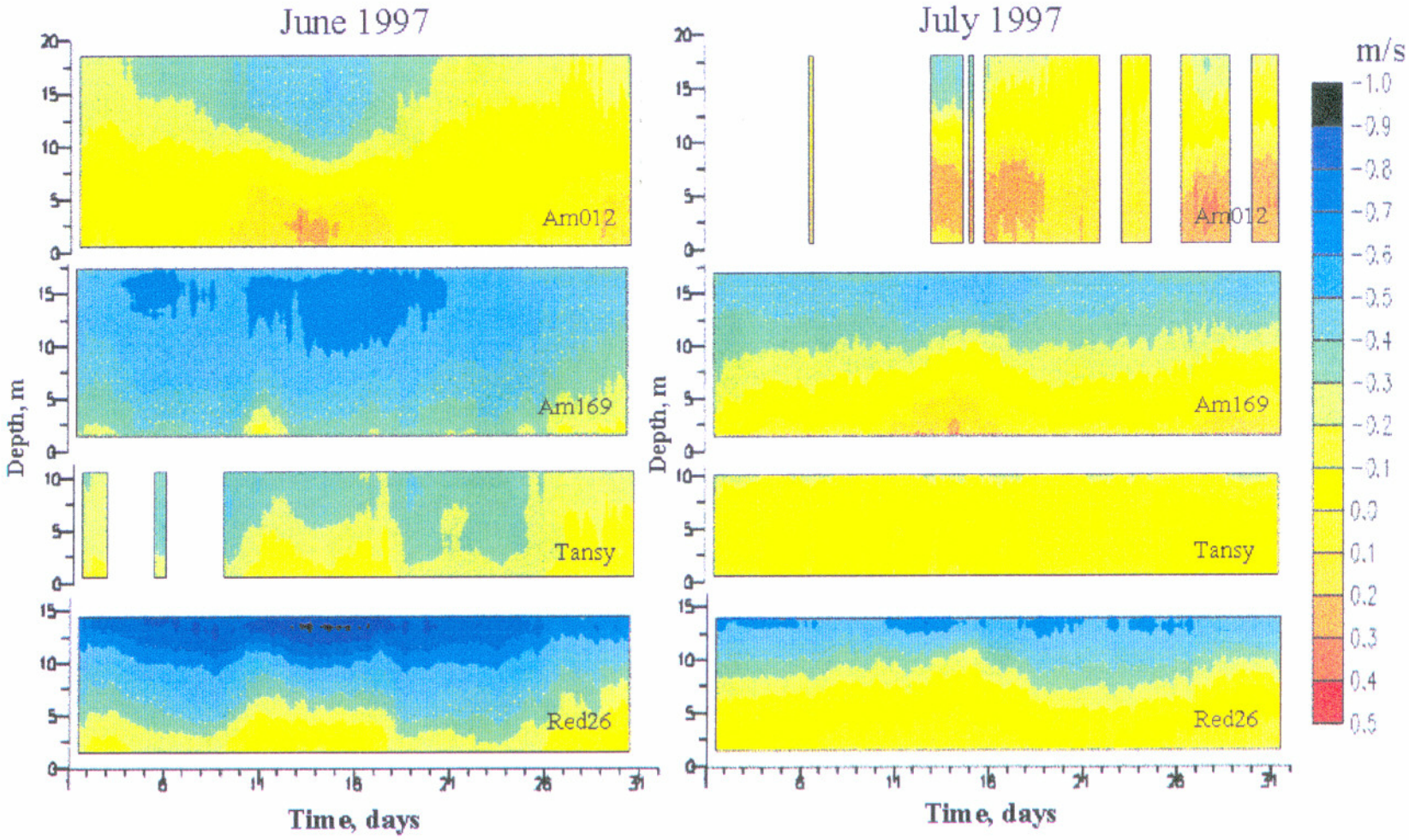

Figure 6.6. Along channel residual velocities over a 1-day averaging period at the four reference stations. a) June 1997, b) July 1997. The spaces in the plots are times in the months where not enough data was available in the 1 day averaging period.

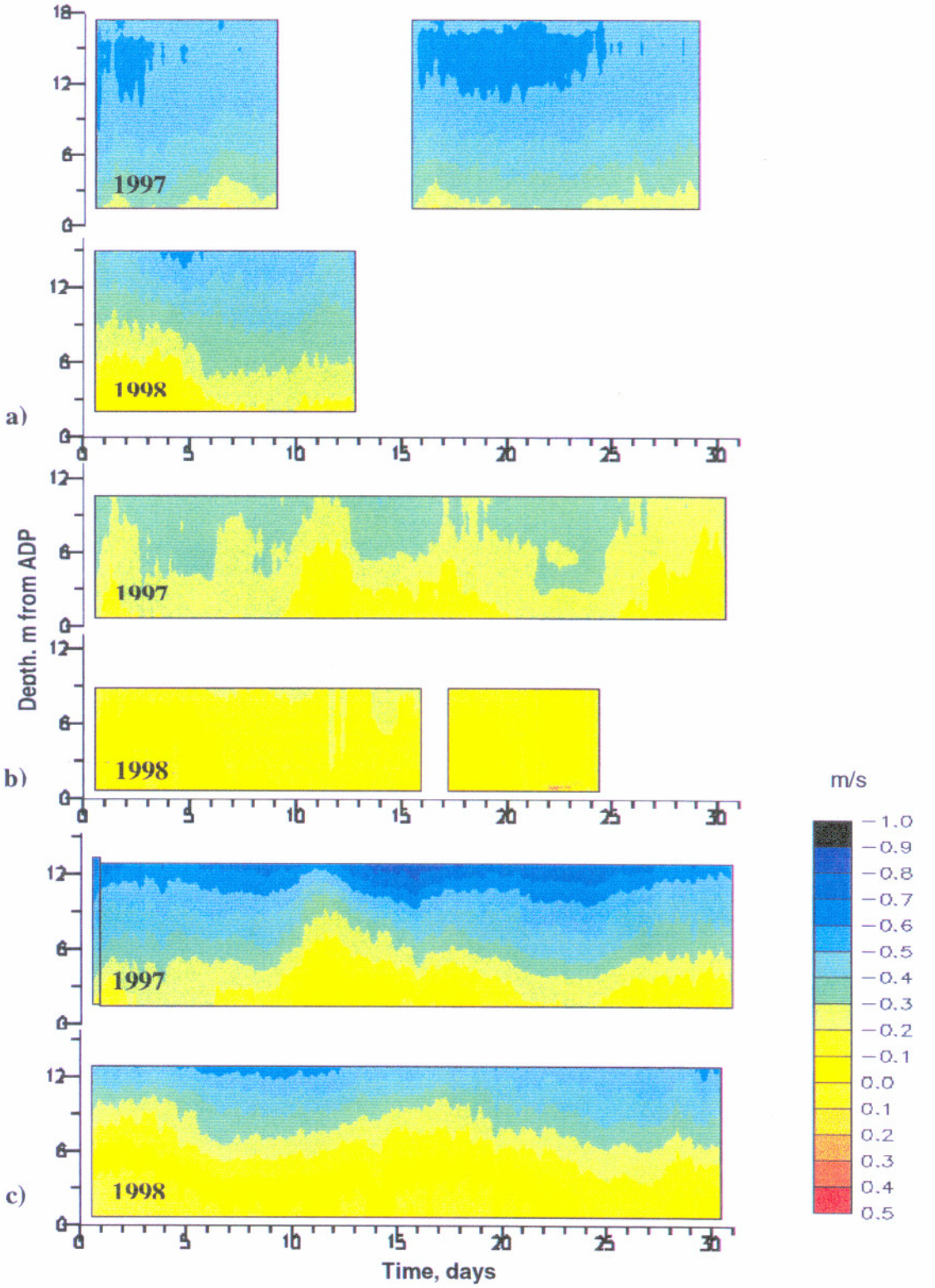

Figure 6.7. Along channel residual velocities over a 1-day averaging period for May 1997 and May 1998 to observe El Niño effects. a) Am169; b) Tansy; c) Red26.

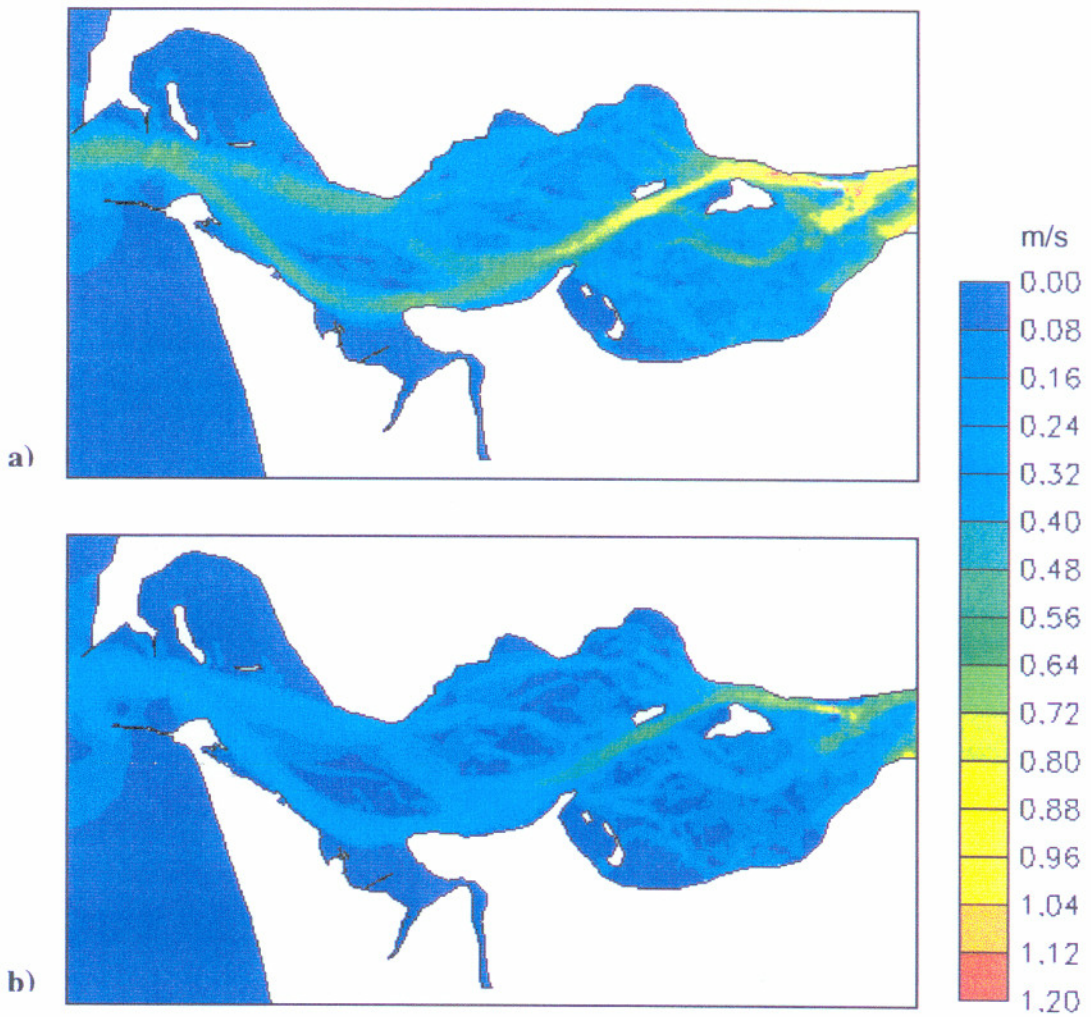

Figure 6.8. Magnitude of simulated depth-averaged residual velocities over a 1-month averaging period. a) June 1997; b) July 1997.

Conclusions and Future Considerations

We analyzed multiple scales of spatial and temporal variability of residual properties in the Columbia River estuary, with emphasis on residence times and residual velocities. Our goals were to assess emerging technologies in their ability to enhance our understanding of estuarine processes. The results from this study provided both qualitative and quantitative analyses that led to useful insights on variability of physical processes at seasonal and tidal time scales and on contrasts between the North and South channels. Our work suggests, but in no way fully explores, the value of the long-term data archival and numerical modeling components of CORIE in advancing the understanding of complex processes in the Columbia River estuary. Our work also illustrates the value of the real-time capabilities of CORIE to design targeted field surveys in support of model validation and of interpretation of the physical and ecological dynamics of the estuary.

With the significant caveat of still not including baroclinic effects, our residence time analysis illustrates the use of diagnostic numerical modeling to understand the interplay of complex processes and the variability of these processes at multiple temporal and spatial scales. The maps of residence times for June and July of 1997 indicated residence times are on the order of hours to a few days downstream of RM 30, and clarified the effects of major topological features and distance from the mouth on transport at seasonal and tidal time scales. Channels tend to have the shortest residence times and lateral bays and intertidal flats the longest residence times. Within a same type of environment, distance to the mouth tends to increase both the residence times and their seasonal variability and to decrease sensitivity to the time of release within the tidal cycle. Variability of residence times could not be reliably described in Young's Bay and perhaps other lateral bays because of lack of appropriate data on local freshwater inputs.

While residence times strongly depend on (a) river discharge and associated variability, (b) tides and release time, and (c) spatial location including distance from the

mouth, neither relationship is simple. A number of scientific and management applications may be able to benefit from the descriptive detail of our approach to describe variability of residence times as a function of tides, spatial attributes, and river discharge.

Our residual velocity analysis provides additional information about variability of physical processes and residual properties in the estuary. By using both field data (at four reference stations) and model simulations, we were in particular able to quantify aspects of the contrasting residual dynamics in the South and North channels. The South channel, to where the system topology mainly diverts upstream freshwater inputs, has primarily ocean-ward month-averaged residual velocities, while the North channel shows a distinct lower layer (with seasonally-varying thickness) with land-ward residual velocities. For shorter (7-day) averaging periods the same holds true, indicating river-dominated flow in the South channel dampens the spring-neap tidal variability that is observed in the North channel.

Using even shorter averaging periods, the CORIE field data provides more insight into the contribution of tides to the net flow in the channels. Residual velocities computed over a 1-day averaging period strongly capture effects associated with spring-neap tidal variability. At lower layers in the water column, the largest land-ward residual velocities in the North channel coincide with neap tides for both high and low flow months. In the South channel, net upstream flow is only present during the low flow month (at neap tides) because there is less river input to contend with. The shorter averaging period further illustrates that the channels have very different residual flows. The residual velocities computed over the three averaging periods suggest that estuarine processes including dispersion of salt and nutrients, transport of suspended sediment and pollutants and the presence of estuarine turbidity maximum (ETM) may also be sensitive to the contrasting residual dynamics of the North and South channels.

Both residence times and residual circulation have been investigated before for the Columbia River. Contrast with historical and often more formal analyses was not

thoroughly explored here, and is an area that invites substantial further work. While our work suggests that CORIE enables an unprecedented degree of spatial and temporal resolution, it is important to stress that CORIE is not an alternative but rather a key complement to formal tools of estuarine analysis. Indeed, the wealth of information generated by models and observations is most useful if put in context by conceptual abstractions of system behavior validated by that same information.

Although our work concentrated on archived CORIE data and model results, similar analyses of residual circulation and residence times can be performed in real-time and forecast modes. We expect that this study will motivate new or modified scientific CORIE products along these lines, some of which will be used to assist the Summer 1999 field survey of the CRETM project.

The drifter experiment was a first attempt of evaluating the actual (rather than numerical, an aspect dealt with extensively by Oliveira and Baptista, 1997) accuracy of the particle tracking simulations used as a basis for computation of residence times. While a more systematic field program is necessary with drifter releases in both the North and the South channel for various conditions of stratification, preliminary results are encouraging. Indeed, not only were simulated and observed trajectories similar in general, but observed divergences appear to confirm our earlier, independent identification of a local weakness of the circulation model in the region around Am012. There are intriguing implications from the above. First, there appears to be a promising degree of robustness, at least during weakly stratified periods, in lagrangian simulations based on even the two-dimensional barotropic models now operationally available. This implies that we may, at least under certain circumstances, be closer to having useful tools for search and rescue or oil spill response than anticipated prior to this work. Second, synoptic drifter experiments may perhaps be used to identify local weaknesses of models in areas where there is no CORIE instrumentation, thus guiding the design of future vessel-based oceanographic surveys or specialized bathymetric surveys.

To advance the understanding of the (often contrasting) dynamics of the North and South channels was an important goal of this work. We feel that the objective was accomplished through our residual velocity analysis, both coarsely through depth-averaged simulations and more finely though the analysis of vertical profiles of residual velocities computed from ADP data. For residence times, we contributed mostly to the coarse picture, and see the need for re-visiting our work when operational 3D baroclinic circulation models become available in CORIE. Indeed, the vertical structure of residual velocities suggests a complex vertical structure of residence times, which drifters alone will have difficulty capturing.

Residence times and residual velocities provide unique but complementary insights on the complex residual processes in the estuary. A similar duality exists between the analysis of field data and modeling results. CORIE and estuarine nowcast-forecast in general are evolving technologies that enable a much more iterative type of science to be developed. To take full advantage of these technologies, we will need to learn to effectively blend tools (e.g., monitoring and modeling, lagrangian and eulerian observations, etc.) and approaches (e.g., analyses of residence times and residual velocities). By operating at the edge of the capabilities of these systems, we expect to contribute to the cultural adoption of "virtual estuaries", half-monitoring half-modeling entities which we interrogate progressively more critically as we better understand and reproduce the real estuary. This thesis is a modest step in that direction.

References

Alfrink, B.J. and C.B. Vreugdenhil, 1981. *Residual Currents*, R1469-11, Delft Hydraulic Laboratory, Delft.

Baptista, A.M., M. Wilkin, P. Pearson, P. Turner, C. McCandlish, P. Barrett, S. Das, W. Sommerfield, M. Qi, N. Nangia, D. Jay, D. Long, C. Pu, J. Hunt, Z. Yang, E. Myers, J. Darland and A. Farrenkopf, 1998. Towards a multi-purpose forecast system for the Columbia River estuary. *Ocean Community Conference, Marine Technology Society*, Baltimore, MD, 6pp.

Barnes, C.A., A.C. Duxbury and B.A. Morse, 1972. Circulation and selected properties of the Columbia River effluent at sea. In *Bioenvironmental Studies of the Columbia River Estuary and Adjacent Ocean Regions*, D.L. Alverson and A.L. Prutter, eds. University of Washington Press, Seattle, WA, 41-80.

Cheng, R.T, 1988. Eulerian and Lagrangian modeling of estuarine hydrodynamics. In *Hydrodynamics of Estuaries: Estuarine Physics, Vol. 1*. B. Kjerfve, ed. CRC Press Inc, Boca Raton, FL, 150-159.

Cheng, R.T., and W.L. Wilmot, 1997. A nowcast model for tides and tidal currents in San Francisco Bay, California, (abstract). *Conference Proceedings of the 5th International Conference on Estuarine and Coastal Modeling*, Alexandria, Virginia. (http://www.oce.uri.edu/ecm5/paper11.html) Viewed Dec. 15, 1998.

CREDDP, 1984. The Columbia River Estuary. Atlas of Physical and Biological Characteristics. Northwest Cartography, Inc, Seattle, WA, 1-87.

Das, S.K., and A.M. Baptista, 1998. Personal communication, Oregon Graduate Institute of Science and Technology.

Fofonoff, N.P. and R.C. Millard, Jr., 1983. Algorithms for computation of fundamental properties of seawater. *UNESCO Technical Papers in Marine Science*, No. 44, 53 pp.

Forman, M.G.G., 1977. Manual for tidal heights and prediction. *IOS Report 77-10.* Institute of Ocean Sciences, Victoria, B.C., 101 pp.

Garratt, J.R., 1977. Review of drag coefficients over oceans and continents. *Monthly Weather Review*, 105: 915-929.

Giese, B.S. and D.A. Jay, 1989. Modelling tidal energetics of the Columbia River Estuary. *Estuarine, Coastal and Shelf Science*, 29: 549-571.

Godin, G., 1972. *The analysis of tides*. University of Toronto Press, Toronto, 264 pp.

Hamilton, P., 1990. Modelling salinity and circulation for the Columbia River Estuary. *Progress in Oceanography*, 25(1-4): 113-156.

Heaps, N.S., 1978. Linearized vertically-integrated equations for residual circulation in coastal seas. *Deutsche Hydrographische Zeitshrift*, 31:147.

Hickey, B.M., 1998. Coastal oceanography of western North America from the tip of Baja California to Vancouver Island. In *The Sea*, A.R. Robinson and K.H. Brink, eds. John Wiley and Sons, New York, 345-393.

Jay, D.A., 1994. Residence times, box models and shear fluxed in tidal channel flows. In *Changes in Fluxes in Estuaries,* K.R. Dyer and R.J. Orth, eds. Olsen and Olsen, Fredensborg, Denmark, 3-12.

Jay, D.A. and E.P. Flinchem, 1997. Interaction of fluctuating river flow with a barotropic tide: A demonstration of wavelet tidal analysis methods. *Journal of Geophysical Research*, 102(C3): 5705-5720.

Jay, D.A. and J.D. Smith, 1990a. Residual circulation in shallow estuaries. 1. Highly stratified, narrow estuaries. *Journal of Geophysical Research*, 95(C1): 711-731.

Jay, D.A. and J.D. Smith, 1990b. Residual circulation in shallow estuaries. 2. Weakly stratified and partially mixed, narrow estuaries. *Journal of Geophysical Research*, 95(C1): 733-748.

Jay, D.A. and J.D. Smith, 1990c. Circulation, density distribution and neap-spring transitions in the Columbia River Estuary. *Progress in Oceanography*, 25(1-4): 81-112.

Luettich, R.A., J.J. Westerlink, 1995. Implementation and testing of elemental flooding and drying in the ADCIRC hydrodynamic model. *Final Contractors Report, Contract No. DACW39-94-M-5869.* Coast. Engrg. Res. Ctr., US Army Engrs. Wtrways. Experiment Station, Vicksburg, Miss.

Luettich, R.A., J.J. Westerlink, and N.W. Scheffner, 1991. *ADCRIC: An advanced three-dimensional model for shelves, coasts and estuaries. Report 1: Theory and methodology of ADCRIC-2DI and ADCIRC-3DL, Dredging Research Program Technical Report DRP-92-6*, Coast. Engrg. Res. Ctr., US Army Engrs. Wtrways. Experiment Station, Vicksburg, Miss.

Lynch, D.R. and F.E. Werner, 1991. Three-dimensional hydrodynamics on finite elements. Part II: Non-linear time-stepping model. *International Journal for Numerical Methods in Fluids*, 12: 507-533.

Mantua, N.J., 1996. Relationships between the ENSO and PDO and PNW regional temperatures, precipitation, snowpack and streamflow. In *Year 1 reports to NOAA/OGP for the integrated assessment of the dynamics of climate variability, impacts, and policy response strategies in the Pacific Northwest.*

Mantua, N.J., S.R. Hare, Y. Zhang, J.M. Wallace, and R.C. Francis, 1997. A Pacific interdecadal climate oscillation with impacts on salmon production. *Bulletin of the American Meteorological Society*, 78(6): 1069-1079.

Myers, E.P., and A.M. Baptista, 1998. Inversion for tides in the Eastern North Pacific Ocean. *Advances in Water Resources*, (submitted).

Officer, C.B. 1980. Box models revisited. In *Estuarine and Wetland Processes*, Hamilton and MacDonald, eds. Penum Press, New York, 65-114.

Oliveira, A. and A.M. Baptista, 1997. Diagnostic modeling of residence times. *Water Resources Research*, 33(8): 1935-1946.

Orem, H.M., 1968. Discharge in the lower Columbia River basin, 1928-65. *U.S. Geological Survey Circulation*, 550, 24 pp.

Pearson, P., and A.M. Baptista, 1998. Personal communication, Oregon Graduate Institute of Science and Technology.

Neal, V.T., 1972. Physical aspects of the Columbia River and its estuary. In *The Columbia River Estuary and Adjacent Ocean Waters.* A.T. Pruter and D.L. Alverson, eds. University of Washington Press, Seattle, WA, 19-40.

Niiler, P.P., R.E. Davis and H.J. White, 1987. Water following characteristics of a mixed layer drifter. *Deep-Sea Research*, 34: 1867-1881.

Pilson, M.E.,1985. On the residence time of water in Narraganset Bay. *Estuaries*, 8(1): 2-14.

Sherwood,C.R., D.A. Jay, R.B. Harvey, P. Hamilton, and C.D. Simenstad, 1990. Historical changes in the Columbia River estuary. *Progress in Oceanography*, 25(1-4): 299-352.

SonTek, 1997a. *ADP (Acoustic Doppler Profiler) Operation Manual*, Firmware Version 4.4, SonTek, Inc., San Diego, CA. 79 pp.

SonTek, 1997b. *ADP (Acoustic Doppler Profiler) Principles of operation*, SonTek, Inc., San Diego, CA. 12 pp.

SonTek, San Diego, 1998. Personal communication.

Sybrandy, A.L., and P.P. Niiler, 1991. *WOCE/TOGA Lagrangian drifter construction manual, SIO Reference 91/6, World Ocean Circulation Experiment Report Number 63.* Scripps Institution of Oceanography, La Jolla, CA.

Wilkin, M., 1998. Personal communication, Oregon Graduate Institute of Science and Technology.

Yang, Z., 1998. Personal communication, Oregon Graduate Institute of Science and Technology.

Vincent, M., D. Burwell, B. Galperin, and M. Luther, 1997. An operational real-time data acquisition and circulation modeling system in Tampa Bay, Florida, (abstract). *Conference Proceedings of the 5th International Conference on Estuarine and Coastal Modeling*, Alexandria, Virginia.
(http://www.oce.uri.edu/ecm5/paper83.html) Viewed Dec. 15, 1998.

Zimmerman, J.T.F., 1988. Estuarine Residence Times. In *Hydrodynamics of Estuaries: Estuarine Physics, Vol. 1.* B. Kjerfve, ed. CRC Press Inc, Boca Raton, FL, 76-84.

Biographical Sketch

I was born on June 24, 1972 in Queens, NY. I graduated from Pennsylvania State University in May 1994 with a Bachelor of Science degree in Civil Engineering and a minor in Environmental Engineering. After reaching California for the first time in the summer of 1994, I moved to Santa Fe, NM and worked as an Engineer Assistant for the City of Santa Fe.

In September 1996, I entered into the master's program at the Oregon Graduate Institute of Science & Technology and was awarded a Master of Science degree in Environmental Science and Engineering in January 1999.